Control and estimation of wall bounded flow systems

by

Jérôme Hœpffner

Typsatt i $\mathcal{A}_{\mathcal{M}}\mathcal{S}$-LaTeX.

Control and estimation of wall bounded flow systems

Jérôme Hœpffner 2004
KTH Mechanics
SE-100 44 Stockholm, Sweden.

Abstract

This thesis focuses on the application of linear feedback control and estimation to channel flow. Both the initial stage of the transition and the low Reynolds number turbulent cases are studied. From sensors at the wall, the state of the flow is estimated, using a stochastic description of the flow disturbances. The estimated state is in turn fed back to the flow system in order to achieve a control objective. This model based scheme uses the linearised Navier–Stokes equations as a dynamic model for the flow evolution. The emphasis is here put on the estimation procedure, that was so far the limiting factor for the overall control performance. We show that the estimation performance rely on a correct description of the flow disturbances. We apply model reduction on the controller, and show that we can maintain the control performance even with a highly truncated system. We then introduce a representation of the feedback by means of transfer functions, and discuss the implication of the transfer function for the interpretation of the feedback, and for possible implementation of the control loop.

Descriptors: Control, estimation, transient growth, optimisation, feedback, transition to turbulence, model reduction.

Preface

This thesis considers the application of linear feedback control to wall bounded flow systems. The first part is a summary of the research presented in the second part.

Paper 1. HŒPFFNER, J., CHEVALIER, M., BEWLEY, T., & HENNINGSON, D. S. 2003 State estimation in wall-bounded flow systems. Part I : laminar flow. *Submitted to Journal of Fluid Mechanics (with minor modifications).*

Paper 2. CHEVALIER, M., HŒPFFNER, J., BEWLEY, T., & HENNINGSON, D. S. 2004 State estimation in wall-bounded flow systems. Part II : turbulent flow. *To be submitted.*

Paper 3. HŒPFFNER, J., & HENNINGSON, D. S. 2004 Model reduction applied to control of wall-bounded flow systems. *Internal report.*

Paper 4. HŒPFFNER, J., & HENNINGSON, D. S. 2004 Coupling sensors to actuator in flow control. *Internal report.*

Division of work between authors

The control and estimation kernels were computed with a numerical code developed by Jérôme Hœpffner (JH), initially based on a code from Markus Högberg. The direct numerical simulations (DNS) in paper 2 were performed by Mattias Chevalier (MC) using a pseudo-spectral code developed by Thomas Bewley (TB). The writing of paper 1 was done by JH, Thomas Bewley and Dan Henningson, with feedback from Mattias Chevalier. The writing of paper 2 was done by MC, with collaboration with Dan Henningson (DH) and feedback from JH. Paper 3 and 4 are the work of JH, with feedback from DH.

Contents

Part 1

Summary

CHAPTER 1

Introduction

1.1. Background

As the traditional field of transition in fluid mechanics aims at understanding and model the evolution of flow systems, flow control aims at using this knowledge to affect the evolution of a flow. For example postpone the transition to turbulence on an aeroplane wing to reduce the friction drag, prevent the separation in an air intake to increase the flux, or trigger turbulence to increase the mixing in a chemical reaction. In this work we focus on hindering the growth or sustainment of flow fluctuations.

The field of control became prominent in engineering applications as fast computers became available and efficient theory were developed. Most of the effort in control theory converged to the formulation of the LQG feedback control, also known as $\mathcal{H}_2$ control. It embraces and unites the apparently disconnected fields of dynamical systems, filtering, control, and optimisation. The name LQG stands for Linear, Quadratic, Gaussian, meaning that the dynamic model is a linear system, that the disturbances to the state are Gaussian, and that the control objective is quadratic. Gaussian disturbances can be completely described by their mean and covariance, so that the disturbance model will be formulated in terms of covariance, and energy is a typical objective that takes the form of a quadratic function of the state. The feedback law is then optimised to accommodate flow disturbances and sensor noise on one hand, and control objective and control cost[1] on the other hand.

It is common practice in the fields of transition and turbulence to decompose the flow into mean and fluctuating parts. In transition typically, the stability of the laminar mean flow will affect the potential for growth of small fluctuations. Minute external disturbances are thus fed from the kinetic energy stored in the mean flow profile. For instance, a boundary layer with an inflection point can be unstable to a range of waves that will grow and possibly disrupt the mean profile. In a turbulent flow the picture is different. The mean profile is not a solution to the Navier–Stokes equations, and cannot be sustained without the mixing effect of large amplitude fluctuations. Linear growth and nonlinear recycling of the energy is operated through the interaction of the fluctuating and mean components of the flow.

---

[1]The cost of the control is the energy spent for the actuation, it should be low compared to the energy gained when the control is applied.

There are two basic strategies for flow control. The first one is to act on the mean flow. For instance the wall suction in the asymptotic suction boundary layer affects the shape factor that further stabilises the flow. This goal can as well be sought by fluctuating devices as periodic blowing and suction. Another strategy is to affect the dynamics of the perturbations themselves by use of a reactive, or feedback control scheme. In a transitional flow case, If we can hinder the growth of small perturbations, we can prevent them from disrupting the mean flow. In a turbulent flow, the opposition to the energy feeding mechanism by action on the perturbation to the mean flow can also lead to mean flow changes (relaminarisation for instance).

This work aims at a control effect orders of magnitudes greater than the control effort. In the case of transition from a laminar flow, we thus target the fluctuations and disturbances at the early stages of growth, just when they emerge from the background noise. If the flow is already turbulent, we aim to target the energy feeding and sustaining mechanisms. We thus use a feedback scheme.

By the word disturbances we mean all the processes that affects the evolution of the system once modelled. It includes the initial condition, the volume forcing due to external sources, and volume forcing due to model error. Indeed the initial condition is assumed to be unknown, also there may be incoming waves from out of the system, and the modeling (use of linear equations, etc ...) induces an error in the dynamics that can be seen as a forcing to the state.

The method of investigation and experimentation is the numerical tool. Many fundamental issues about modeling and formulation should be understood before it become meaningful or even feasible to test this type of control in a wind tunnel.

In §1.2 we present the previous research that lead to the present thesis. In §1.3 and §1.4 we briefly recall the main ideas of transition to turbulence in shear flows and the control technique. In chapter two, we see how we can use the knowledge from the physical system in the framework of the optimal control.

1.2. Flow control using feedback

The first steps towards feedback control schemes using the knowledge from control theory in flow control were made by Hu & Bau (1994), Joshi *et al.* (1995) and Joslin *et al.* (1997). In these works the eigenvalues of the closed loop transition problem are stabilised in a closed loop framework. The technique used were a proportional controller, where the measurement is directly fed back to the actuation through a gain, as well as proportional-integral controller (i.e. a controller with both proportional and integral term) and also LQG. Joshi *et al.* (1995) already apply model reduction by truncating the problem to the nine least stable modes. Bewley & Liu (1998) studied separately the control and estimation in a $\mathcal{H}_2$ and $\mathcal{H}_\infty$ (robust) procedure, and introduced transfer functions to assess the performance of the controller for isolated Fourier modes.

A review of the challenges of feedback control can be found in Bewley (2001). A formal treatment of the distributed nature of the present problem is given in Bamieh (1997).

The control was then applied to larger problem through direct numerical simulation (DNS), in Högberg *et al.* (2003) where threshold for transition are examined with control and estimation. It was applied to relaminarisation of a turbulent channel flow by Högberg *et al.* (2003*a*) using full state information. It was as well extended to non-parallel flow in Högberg & Henningson (2002) by a spatial windowing method, leveraging the spatial localisation of the feedback law. A further application to non-parallel flow can be found in Cathalifaud & Bewley (2004*a*) and Cathalifaud & Bewley (2004*b*) where a non-causal framework is used in the spatial direction (instead of the temporal) with use of the Parabolized stability equations (PSE). At the same time, further effort were made towards the reduction of skin friction in turbulent channel flow. A review of such efforts can be found in Kim (2003).

Much useful understanding was gathered in numerical simulations where full state information is assumed to be known. The estimation part on the other hand remains the limiting factor of the overall closed loop performance. This may be a consequence of the underlying stochastic framework, not familiar to the fluid mechanics community.

1.3. Knowledge from fluid mechanics

Understanding of the mechanisms of transition and turbulence is central to tune the controller to its applications. This is done through the choice of the dynamic model, the design of the disturbance model and the choice of the objective function. The knowledge of the flow is also useful to assess a performance measure for the controller. For further details, see e.g Schmid & Henningson (2001).

The transition process in shear flows begins with the receptivity stage in which external disturbances interact with the system. Depending on the type of disturbances present in the environment, and the way they are filtered when penetrating the system, the actual disturbance that will further evolve can be of a variety of types. Then follow different routes, depending on the type of instability triggered by the disturbances. Typical external disturbances in a shear flow can be acoustic waves, free stream turbulence or wall roughness.

In the case of wall-bounded flows (boundary layer, channel flow, etc...), if the system is linearly unstable, exponentially growing waves may appear. This is the modal instability mechanism, and appear for Reynolds numbers above the critical value, or flows with inflectional profile as separated and nearly separated boundary layers, or Falkner–Skan–Cooke boundary layers. In the case of shear flows, initial disturbances in the shape of streamwise elongated vortices may lift up low momentum fluid from the wall, thus generating streamwise elongated streaks that grow algebraically. This is the nonmodal mechanism, related to the nonnormal nature of the governing operator, and is of importance in flows
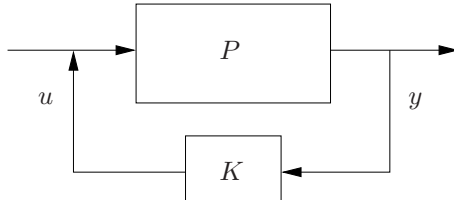
FIGURE 1.1. The plant P and the closed loop controller K, with measurement y and control u.

subjected to high amplitude disturbances as in the boundary layers subject to free-stream turbulence.

When the disturbances reach an amplitude of the order of magnitude of the free stream velocity, nonlinear interactions occur and harmonics of the growing waves are generated. This may lead to a new saturated state, that is a more complex, but still laminar flow. Eventually, instability of the new flow, will trigger the growth of high frequency waves evolving to turbulent spots, merging further to turbulence.

Turbulence is then sustained by extraction of energy from the mean profile in the near wall region. Coherent structures in the form of streamwise elongated streaks and their instabilities play a central role in this process.

1.4. Optimal feedback control

In this section, we discuss the main features of the feedback method, introducing the plant and the estimator.

There is only a limited amount of information one can extract from the system (or the plant), this is the measurement vector y. If $q(t)$ is the state, and C is the measurement operator, then $y = Cq$. Similarly, one is restricted in the action on the system. The control signal u is input in the system through the input operator B_2.

The plant can be written in state space form

$$\begin{cases} \dot{q} = Aq + B_1 f + B_2 u, & q(0) = q_0, \\ y = Cq + g. \end{cases} \tag{1.1}$$

The state q follows the dynamics due to the linear operator A, and is forced by external disturbance f through B_1 and can be regulated by a control u through B_2. The measurement y is extracted from the state by the measurement operator C, and affected by the sensor noise g. The disturbances q_0, f and g are assumed to be stochastic quantities and can be described by their covariance

$$\text{cov}(q_0) = S_0, \quad \text{cov}(f) = R, \quad \text{cov}(g) = G.$$

1.4.1. *Linear response*

We seek a controller, that by use of all the available information (the measurement history), will give the best control towards an objective. See figure 1.1

for the diagram of the closed loop. The control is linear in the sense that the control signal is a linear mapping of the measurement history. Such a linear operator can be represented in state space

$$\begin{cases} \dot{\hat{q}} = M_1\hat{q} + M_2 y, \\ u = M_3\hat{q}, \end{cases} \qquad (1.2)$$

where $\hat{q}$ is the state of the controller and M_j are operators to be constructed. Such a linear mapping can equivalently be represented as a transfer function (see e.g. Kailath (1980))

$$u(t) = \int_0^\infty \underbrace{M_3 e^{M_1\tau} M_2}_{G(\tau)} \, y(t-\tau)\mathrm{d}\tau. \qquad (1.3)$$

Note that in (1.3), $u(t)$ is explicitly dependent on all the measurement history, whereas this dependence is implicit in (1.2).

1.4.2. *Control and estimation*

The general optimisation problem formulated as above is complicated and has many local minima. An easier path is to consider it as the union of a filtering problem and a control problem. If the system is subject to state disturbances and sensor noise, how can we optimally estimate the state? This estimation problem, solved in Kalman & Bucy (1960) is the celebrated Kalman filter. We build an estimator system analogous to the plant (1.1)

$$\begin{cases} \dot{\hat{q}} = A\hat{q} + B_2 u - v, \quad \hat{q}_0 = 0, \\ \hat{y} = C\hat{q}, \\ v = L(y - \hat{y}). \end{cases} \qquad (1.4)$$

The estimator state $\hat{q}$ follow the same dynamics A as the flow state q and is forced by a feedback v of the measurement error $\tilde{y} = y - \hat{y}$. The measurement error is better known as the innovation process. The modeled dynamics of the system is used as a filter for the measurement noise. Since the estimator should deal with uncertainty, it is a stochastic problem and the optimisation is done in the stochastic framework. The second problem is a deterministic one: how can we apply control in order to minimise a chosen performance index, using full state information. The control u is obtained by feedback of the flow state

$$u = K\hat{q}, \qquad (1.5)$$

through the control feedback gain K. The controller that assumes the state to be known is called full information controller, or LQR for Linear Quadratic Regulator. If only the measurement is known, the state has to be estimated, this is the measurement feedback controller, also known as compensator. In the following, we use the measurement feedback controller.

The separation principle (Green & Limebeer (1995)) formally proves that the optimal measurement feedback controller is the optimal full information controller that uses the state estimate from the Kalman filter.

1.4.3. *Optimality*

The optimal estimation problem without sensor noise is ill posed. If an exact measurement is available, and if all the eigenmodes of the system are detectable from the measurement (the system is observable) then the estimator can converge arbitrarily fast, with corresponding arbitrary high amplitude estimation gains. The optimality comes from the balance of sensor signal and sensor noise. This ratio defines the quality of the signal, and a useful signal (relatively low sensor noise) will lead to high gain and rapid convergence due to the confidence in the provided information. Similarly the control problem without introduction of a control cost is ill-posed. Indeed, if all the eigenmodes of the system can be affected by the actuation (the system is controllable) then the objective can be reached arbitrarily fast, with control gains of arbitrarily high amplitude. But the optimisation seeks to minimise a weighted sum of the objective and the cost. The relative weighting of objective and cost will thus determine the allowed amplitude range for the control signal.

CHAPTER 2

From the mathematical framework to the physical system

The mathematical formulation of the LQG controller leaves many degrees of freedom for the application to a specific physical problem. We will see in this chapter how fluid mechanics knowledge can be input to the optimisation problem.

2.1. Linear dynamics

The dynamic model is the Navier–Stokes equations, Fourier transformed in the two homogeneous directions. We lump both the nonlinear terms and the external disturbance into an external forcing function, thereby restricting the flow model to the linear terms. The dynamic model is thus the Orr–Sommerfeld/Squire equation for each wave number pair (k_x, k_z), where k_x stand for the streamwise wave number and k_z for the spanwise wave number.

If the amplitude of the disturbances is small, nonlinear effects can be neglected altogether. For higher amplitude, the nonlinear effects redistribute the energy in Fourier space (introducing a coupling between Fourier modes). For intermediate amplitudes of the disturbances, we can consider this effect to be slower than the reaction of the controller, thus accounting for the nonlinear effect as a stochastic forcing can be justified. When new instabilities appear due to the deformation of the mean flow, we cannot claim that the stochastic term captures the effect of the nonlinearity. In this case, encountered in the estimation of turbulent flow and of the late stages of transition, our hope relies on the linearity of the driving energy processes, with the main role of the nonlinearity seen as the recycling of a linearly generated energy (for a discussion on this topic, see Waleffe (1995), Henningson (1996) and references therein).

2.2. Sensing and actuation

We measure at the wall the two components of the skin friction and the pressure. The streamwise component of the skin friction will be a good measurement for flow cases associated with the transient growth. Indeed, streamwise elongated vortices generate strong streamwise elongated streaks on the streamwise velocity component by interaction with the mean shear. Those structures have a clear wall footprint of streamwise skin friction. Equivalently, the spanwise component of the skin friction gives information on spanwise elongated

structures. There is no central mechanism involving such structures, so that this measurement will play a minor role in the control performance. The pressure measurement gives information on fluctuations further away from the walls (Bewley & Protas (2003)). It is seen that an initial disturbance that is located in the centre of the channel will be detected early at the wall from pressure fluctuations.

The actuation is done by zero-net flux blowing and suction at the wall. The wall normal velocity can interact with the mean shear to have a large effect on the flow. For example in a context of streaks generated by streamwise vortices, the wall normal component of the velocity can directly counteract the vortices.

We assume here that we have a continuous distribution of sensors and actuators, to be able to decouple the problem in Fourier space.

2.3. Model reduction

Computational time and closed loop complexity depend on the number of degrees of freedom in the controller. In order to lighten this burden, one can chose to reduce the order (size of the matrices) of the dynamic model. The optimal feedback gains should be computed using the full dynamic operator since an optimisation carried on this operator with a small reduction error could lead to a large error in the gains themselves. Nevertheless, we can use a reduced version of the dynamic operator for the estimation.

The model reduction method used here is based on truncation of eigenmodes of the flow model, i.e. modal truncation. An eigenmode that does not appear at the measurement is said to be unobservable. Equivalently, an eigenmode that is not accessible to the actuation is said to be uncontrollable. Those eigenmodes will be immaterial to the closed loop performance. Poorly observable and controllable eigenmodes can be progressively discarded with progressive degradation of the closed loop performance.

We apply here a simple model reduction technique on the controller once computed, i.e. we do not take the closed loop performance into account when reducing. Method for controller reduction are being developed (see e.g. Obinata & Anderson (2001)), that explicitly account for the complete closed loop system. Such method seek to maintain closed loop performance, and can provide guarantees on closed loop stability.

2.4. Quadratic objective

In the present work we seek to minimise the energy density of the disturbance to the mean flow. For the optimisation problem to be well posed, and to have a knob on the desired amplitude range of the feedback, we add to the objective function a term accounting for the cost of the control.

Postponing the transition to turbulence is a common control objective. Such a general objective is however out of the scope of a linear controller. Indeed a disturbance with higher energy may be potentially less destructive

than another disturbance, so that the quadratic function described above fails to seek the optimal controller. Insight into transition in specific flow cases should be used in the future to design quadratic objective that target the central destabilisation mechanisms. Even though the destabilisation mechanism itself may be nonlinear, there is possibility for correctly targeted linear controller to prevent transition, beyond the short-sighted goal of keeping the disturbances low.

2.5. Gaussian disturbances

Both transitional and turbulent flows are composed of a mean and fluctuating part. The energy of the fluctuations that we want to estimate originates from initial condition and forcing from external sources. We account for both of them as disturbances. The better the knowledge about those sources, the better we can follow the evolution of the resulting flow.

We represent the disturbances by their covariance, and assume a zero mean. The model for the disturbances used in previous work reflected little of the real flow processes that trigger the instability mechanisms. Previously used model assumed zero correlation in space and time for the disturbances. By introducing a finite correlation length scale, we had a model that would converge upon grid refinement. Furthermore, the zero correlation in space introduced singularities in the optimisation so that the wall measurements using derivatives of the flow states would not lead to well resolved gains.

The forcing on two points in the flow will be as uncorrelated as they are far from each other. We still assume that the disturbances are uncorrelated in time. Introducing a correlation in time can be done by a noise colouring method (see e.g. Lewis & Syrmos (1995)), but we did not find this necessary. We deal with each wavenumber pair separately, so that the forcing on two different wave number pairs is uncorrelated by construction. We then distribute the disturbance energy in the Fourier plane. This way, we can specify the type of flow disturbances by locating energy peaks in the power spectra of the disturbances.

Introduction of the covariance for the initial conditions implies that the flow statistics evolve in time before reaching a steady state where the flow is exclusively driven by the disturbances. Thus, the optimal estimation gains are time-varying and eventually reach a steady state.

In the case of estimation of a turbulent flow, the main disturbance on the modeled system comes from the neglection of the nonlinear dynamic effects. In this case too, we can build a covariance model. We run a DNS of the full Navier–Stokes equations and store statistics of the spatial covariance of the nonlinear term for each wave number pair, and use it for R in the computation of the estimator.

The more specific the real flow disturbances and initial conditions are, the better the estimation performance if those disturbances are accounted for in the covariance model. For instance one may expect Tollmien–Schlichting waves

to arise from linear instability of the boundary layer over an aeroplane wing. The shape of those disturbance is known, only their phase and amplitude has to be recovered by the estimator. The covariance model is a way to target flow cases, and the specificity of the central flow mechanism is thus a great advantage for the estimation.

2.6. Optimisation

Once the stochastic input to the system are defined, one can derive the equation for the covariance of the resulting flow. This is the Lyapunov equation. Equivalently, one can write a Lyapunov equation for the estimation error with an arbitrary estimation gain. A Lagrange multiplier technique is then used to find the gain that minimises this error. The result of this optimisation can be extracted from the solution of a Riccati equation. Similarly, one can use a Lagrange multiplier technique to derive the control gain that minimises the objective function for arbitrary disturbances. Once again, the optimal control gain is to be extracted from the solution of a Riccati equation.

CHAPTER 3

Summary of the papers

Paper 1
This paper is devoted to the estimation problem. We introduce the covariance model for both initial conditions and volume forcing due to external sources. We compute time varying estimation kernels for the estimation of localised perturbations in channel flow. It is shown that by using a spatially correlated covariance model for the disturbance, we can compute well resolved estimation kernels for all the desired wall measurement, i.e. the streamwise and spanwise skin friction and the pressure. We show that a proper description of the disturbance can help to improve the estimator's performance.

Paper 2
We apply here the ideas from paper 1 to a low Reynolds number turbulent channel flow. The covariance model for the volume forcing is obtained through a DNS of a turbulent flow. This covariance data is in turn used for the computation of the optimal linear estimator. We show here that the performance of the estimation can be improved when using the proper covariance model. The turbulent flow is well estimated close to the walls.

Paper 3
In this paper we investigate the performance of a reduced order controller in a laminar channel flow. The reduction technique is modal truncation. The adjoint of the controller's dynamic operator is used for the projection of the controller on the basis of its eigenmodes, in which states are truncated. It is shown that a controller with moderate strength can be highly truncated with retained performance.

Paper 4
The state space formulation of the controller used in the previous papers do not show explicitly the relation between sensors and actuators in the closed loop setting. We introduce a transfer function representation, mapping the sensor signal history over the walls and the actuation over the walls.

CHAPTER 4

Conclusion and outlook

In the discussion of the thesis of Markus Högberg (Högberg (2001)), it is said "If the flow near the wall can be estimated with faster convergence, the compensator performance could be improved. Also further development by incorporation of more measurements and knowledge about flow properties could improve the present results". The first result of the present thesis was to obtain estimation feedback kernels for additional measurements: the two components of skin friction and pressure. This was possible by introducing a spatially correlated stochastic model for the external disturbances. We showed that this model is the place where to input the "knowledge about flow properties". We developed this idea in a laminar flow case, and applied it in a low Reynolds turbulent flow.

The idea of knowledge about flow properties should be applied in a systematic study on objective functions as well. The model for the external disturbances accounts for flow behaviours that cannot be incorporated in a dynamical description of the system. For instance, incoming acoustic waves cannot be included in the dynamic model, since we would need a larger computational domain to account for their generation and propagation, wall roughness would induce complex boundary conditions, nonlinear effects would require a nonlinear optimisation, a spatially developing base flow would increase the dimension of the system, rendering the control problem intractable in the present formulation etc... Similarly, the exact mechanisms of transition to turbulence cannot be accounted for in a quadratic norm and decoupled in Fourier space. We thus have to use the field of knowledge from stability, transition, and turbulence to design proper objectives for a linear controller. That way, it is possible to think the controller design as a well defined linear "brick" in the design of a controller for complex systems.

A large amount of data has to be treated while controlling the flow in the present formulation. This is a result of the large number of degree of freedom of the flow systems at hand. Firstly, we use all the wall information, using dense arrays of sensor and actuators. Secondly, estimating requires a linear flow simulation on the side of the flow system during the control. The assumption of linearity of the dynamics may be thought as a strong limitation for this control method. The amount of data to be treated prevents even more strongly from a real implementation in wind tunnel and further industrial applications. On the other hand, many complex flows exhibit low-dimensionality, and the typical

mechanisms do not necessarily involve all the degrees of freedom of the system. This means that we do not necessarily need sensors everywhere to detect the waves that may trigger the transition. This comment holds as well for the actuation, and we showed in paper 3 an equivalent result for the dynamic model. Our understanding from the idealised setting in this thesis should help us to achieve this reduction, being thus able to reduce a most general controller (sensing, actuation and feedback computation) to specific cases of application, making use of the specificity (low dimensionality) of the involved processes. The controller once fit to a particular case could be broken down to a simple feedback scheme without significant loss of performance.

Acknowledgement

First of all, much respect is due to my supervisor Dan Henningson for his guidance. Most of the research done in this thesis was the natural follow-up of the PhD thesis of Markus Högberg, who helped me to get started in the field of flow control. I am grateful to Luca Brandt and Jan Pralits for numerous advises and discussions, as well as a warm welcome at the beginning of my stay in Sweden.

Mattias Chevalier is mostly responsible for the great time spent together in San Diego during fall 2002, and continued cooperation. In California, we could work with Thomas Bewley at the University of California San Diego, this was the occasion to seriously get into the bulk of this work. Thomas Bewley strongly contributed to the advance of the research and our scientific excitement by his constant enthusiasm. Laura Cerviño, Haoxiang Luo, Patricia Cathalifaud, Bartosz Protas, and finally the "spanish gang" made our everyday life there smooth and enjoyable.

Later, I could refine my scientific thoughts as well as enjoy Stockholm's life together with Junichiro Shiomi.

My fellow graduate students Ori Levin, Astrid Herbst, Erik Stålberg, and the other students and friends at the department deserve many thanks for the everyday life at KTH.

Bibliography

BAMIEH, B. 1997 The structure of the optimal controller of spatially invariant ditributed parameter systems. In *Proc. 36th IEEE Conf. on Decision and Control*.

BEWLEY, T. R. 2001 Flow control: new challenges for a new renaissance. *Progress in Aerospace Sciences* **37**, 21–58.

BEWLEY, T. R. & LIU, S. 1998 Optimal and robust control and estimation of linear paths to transition. *J. Fluid Mech.* **365**, 305–349.

BEWLEY, T. R. & PROTAS, B. 2003 Skin friction and pressure: the "footprints" of turbulence. *Physica D* In press.

CATHALIFAUD, P. & BEWLEY, T. 2004a A noncausal framework for model-based feedback control of spatially-developing perturbations in boundary-layer flow systems. part 1: Formulation. *Systems and Control Letters* **51** (1), 1–13.

CATHALIFAUD, P. & BEWLEY, T. 2004b A noncausal framework for model-based feedback control of spatially-developing perturbations in boundary-layer flow systems. part 2: Numerical simulations using state feedback. *Systems and Control Letters* **51** (1), 15–22.

GREEN, M. & LIMEBEER, D. J. N. 1995 *Linear robust control*. Prentice Hall.

HENNINGSON, D. 1996 Coment on "transition in shear flows. nonlinear normality versus nonnormal linearity. *Phys. Fluids* **8** (8), 2257.

HU, H. & BAU, H. 1994 Feedback control to delay or advance linear loss of stability in planar poiseuille flow. In *Proc. R. Soc. Lond. A*, , vol. 447, pp. 299–312.

HÖGBERG, M. 2001 Optimal Control of Boundary Layer Transition. PhD thesis, Royal Institute of Technology, Department of Mechanics, Stockholm, Sweden.

HÖGBERG, M., BEWLEY, T. & HENNINGSON, D. 2003a Relaminarization of Re_τ=100 turbulence using gain scheduling and linear state-feedback control. *Physics of fluids* **15**, 3572–3575.

HÖGBERG, M., BEWLEY, T. R. & HENNINGSON, D. S. 2003b Linear feedback control and estimation of transition in plane channel flow. *J. Fluid Mech.* **481**, 149–175.

HÖGBERG, M. & HENNINGSON, D. S. 2002 Linear optimal control applied to instabilities in spatially developing boundary layers. *J. Fluid Mech.* **470**, 151–179.

JOSHI, S. S., SPEYER, J. L. & KIM, J. 1995 Modeling and control of two dimensional poiseuille flow. *34th IEEE Conf on Decision and Control* pp. 921–927.

JOSLIN, R. D., GUNZBURGER, M. D., NICOLAIDES, R. A., ERLEBACHER, G. &

HUSSAINI, M. Y. 1997 A Self-contained, Automated Methodology for Optimal Flow Control Validated for Transition Delay. *AIAA Journal* **35** (5), 816–824.

KAILATH, T. 1980 *Linear systems*. Prentice hall.

KALMAN, R. & BUCY, R. 1960 New results in linear filtering and prediction theory. *ASME Transactions, Series D: Journal of basic Engineering* **83**, 95–108.

KIM, J. 2003 Control of turbulent boundary layers. *Physics of fluids* **15** (5).

LEWIS, F. L. & SYRMOS, V. L. 1995 *Optimal control*. Wiley-Interscience.

OBINATA, G. & ANDERSON, B. D. 2001 *Model reduction for control system design*. Springer.

SCHMID, P. J. & HENNINGSON, D. S. 2001 *Stability and transition in shear flows*. Springer.

WALEFFE, F. 1995 Transition in shear flows. nonlinear normality versus nonnormal linearity. *Phys. Fluids* **7** (12), 3060.

Bibliography

BAMIEH, B. 1997 The structure of the optimal controller of spatially invariant ditributed parameter systems. In *Proc. 36th IEEE Conf. on Decision and Control*.

BEWLEY, T. R. 2001 Flow control: new challenges for a new renaissance. *Progress in Aerospace Sciences* **37**, 21–58.

BEWLEY, T. R. & LIU, S. 1998 Optimal and robust control and estimation of linear paths to transition. *J. Fluid Mech.* **365**, 305–349.

BEWLEY, T. R. & PROTAS, B. 2003 Skin friction and pressure: the "footprints" of turbulence. *Physica D* In press.

CATHALIFAUD, P. & BEWLEY, T. 2004a A noncausal framework for model-based feedback control of spatially-developing perturbations in boundary-layer flow systems. part 1: Formulation. *Systems and Control Letters* **51** (1), 1–13.

CATHALIFAUD, P. & BEWLEY, T. 2004b A noncausal framework for model-based feedback control of spatially-developing perturbations in boundary-layer flow systems. part 2: Numerical simulations using state feedback. *Systems and Control Letters* **51** (1), 15–22.

GREEN, M. & LIMEBEER, D. J. N. 1995 *Linear robust control*. Prentice Hall.

HENNINGSON, D. 1996 Coment on "transition in shear flows. nonlinear normality versus nonnormal linearity. *Phys. Fluids* **8** (8), 2257.

HU, H. & BAU, H. 1994 Feedback control to delay or advance linear loss of stability in planar poiseuille flow. In *Proc. R. Soc. Lond. A*, , vol. 447, pp. 299–312.

HÖGBERG, M. 2001 Optimal Control of Boundary Layer Transition. PhD thesis, Royal Institute of Technology, Department of Mechanics, Stockholm, Sweden.

HÖGBERG, M., BEWLEY, T. & HENNINGSON, D. 2003a Relaminarization of Re_τ=100 turbulence using gain scheduling and linear state-feedback control. *Physics of fluids* **15**, 3572–3575.

HÖGBERG, M., BEWLEY, T. R. & HENNINGSON, D. S. 2003b Linear feedback control and estimation of transition in plane channel flow. *J. Fluid Mech.* **481**, 149–175.

HÖGBERG, M. & HENNINGSON, D. S. 2002 Linear optimal control applied to instabilities in spatially developing boundary layers. *J. Fluid Mech.* **470**, 151–179.

JOSHI, S. S., SPEYER, J. L. & KIM, J. 1995 Modeling and control of two dimensional poiseuille flow. *34th IEEE Conf on Decision and Control* pp. 921–927.

JOSLIN, R. D., GUNZBURGER, M. D., NICOLAIDES, R. A., ERLEBACHER, G. &

HUSSAINI, M. Y. 1997 A Self-contained, Automated Methodology for Optimal Flow Control Validated for Transition Delay. *AIAA Journal* **35** (5), 816–824.

KAILATH, T. 1980 *Linear systems*. Prentice hall.

KALMAN, R. & BUCY, R. 1960 New results in linear filtering and prediction theory. *ASME Transactions, Series D: Journal of basic Engineering* **83**, 95–108.

KIM, J. 2003 Control of turbulent boundary layers. *Physics of fluids* **15** (5).

LEWIS, F. L. & SYRMOS, V. L. 1995 *Optimal control*. Wiley-Interscience.

OBINATA, G. & ANDERSON, B. D. 2001 *Model reduction for control system design*. Springer.

SCHMID, P. J. & HENNINGSON, D. S. 2001 *Stability and transition in shear flows*. Springer.

WALEFFE, F. 1995 Transition in shear flows. nonlinear normality versus nonnormal linearity. *Phys. Fluids* **7** (12), 3060.

Part 2

Papers

1

Paper 1

State estimation in wall-bounded flow systems. Part I : laminar flow

By J. Hœpffner[1], M. Chevalier[1,2], T. R. Bewley[3] and D. S. Henningson[1,2]

[1]Department of Mechanics, Royal Institute of Technology (KTH), S-100 44 Stockholm, Sweden
[2]The Swedish Defense Research Agency (FOI), SE-172 90, Stockholm, Sweden
[3]Flow Control Lab, Department of MAE, UC San Diego, La Jolla, CA 92093-0411, USA

In applications involving the model-based control of transitional wall-bounded flow systems, one often desires to estimate the interior flow state based on a history of noisy measurements from an array of flush-mounted sensors on the wall. This paper considers this estimation problem, using a Kalman filter based on the linearised Navier–Stokes equations and appropriate stochastic models for the relevant statistics of the initial conditions, sensor noise, and external disturbances acting on the system. We show that a physically relevant parameterisation of these statistics is key to obtaining effective, well resolved feedback kernels with appropriate spatial extent. The consideration of time-varying feedback kernels is shown to be particularly advantageous to accelerate the convergence of the estimator from unknown initial conditions. The resulting Kalman filter is tested on the problem of reconstruction of localized disturbances in a laminar channel flow.

1. Introduction

The feedback control of fluid flow systems is a problem that has received growing attention in recent years and has been approached in a number of different manners. One approach is to design controls based on physical insight of dominant flow mechanisms, as by the wave superposition principle (see, e.g., Thomas (1990)). Another approach is to use adaptive or genetic techniques to attempt to learn an effective control strategy by trial and error (see, e.g., Lee *et al.* (1997)). It is also possible to leverage linear control theory, basing the control algorithm on the linearised Navier–Stokes equations governing small perturbations to the flow system, a mathematical statement of the control objective, and a mathematical model of the relevant statistical properties of the unknown initial conditions, sensor noise, and external disturbances acting on the system. The present paper follows this latter approach. Recent reviews of related flow

control efforts can be found in, for instance, Bewley (2001), Gunzberger (1996), Kim (2003), and the introduction of Högberg, Bewley & Henningson (2003).

The classical problem of linear model-based feedback control based on noisy measurements can be decomposed into two independent subproblems: first, the state-feedback (a.k.a. full-information) control problem, in which full state information is used to determine effective control feedback, and, second, the state estimation problem, in which measurements are continuously used to "nudge" a real-time calculation of the flow system in an appropriate manner such that the calculated flow state eventually approximates the actual flow state.

Once both subproblems are solved, one can synthesize them to control a flow based on limited noisy measurements of the flow system. The overall performance of the resulting linear feedback control scheme is limited by the individual performance of the two subproblems upon which it is based. For the application of linear control theory to wall-bounded flows, though encouraging results have been obtained previously on the state-feedback control problem (see, for example, Bewley & Liu (1998) and Högberg *et al.* (2003)), the development of effective state estimation strategies remains largely an open problem. In the present paper, we therefore focus on the state estimation problem exclusively.

One of the primary challenges of the state estimation problem is that its framing is based centrally on quantities which are challenging to model, namely, the expected statistics of the initial conditions, the sensor noise, and the external disturbances acting on the system. The state estimation problem may actually be thought of as a *filtering* problem; that is, the estimator uses the governing equation itself as a filter to extract, from the noisy measurements of a small portion of the dynamic system, that component of the measurements which is most consistent with the dynamic equation itself. In other words, the estimator uses the governing equation to extract the signal from the noise, and in the process builds up an estimate of the entire state of the system. The purpose of the estimator at time t is to filter the measurements gathered prior to time t to estimate the instantaneous state of the flow field. The purpose of the state-feedback controller at time t, on the other hand, is to apply forcing to the flow such that the subsequent evolution of the flow, after time t, exhibits favourable characteristics. Thus, the controller is based on a metric defining these favourable characteristics (the objective function), whereas the estimator is based on a model describing, to the extent that they are known, the statistical properties of the unknown quantities affecting the system.

Some attention has been paid in the literature to the creative choice of objective functions for the control problem. Kim & Lim (2000), for example, performed an numerical experiment which applied body forcing via linear feedback everywhere on the interior of a turbulent channel flow. This linear feedback was constructed to exactly cancel the linear coupling term [$\mathcal{C}$ in (2)]

in the nonlinear simulation, with the result that the turbulent flow relaminarized. This result lends credibility to the idea of using a more sophisticated objective function which targets this linear coupling (that is, one which targets the non-normality of the system eigenvectors) rather than using an objective function which simply targets the disturbance energy directly. The appropriate selection of the objective function is thus seen to be not a trivial problem, and is closely linked to our understanding of the relevant flow physics. The problem of disturbance modeling for the state estimation problem, which is also inherently linked to our understanding of the relevant flow physics, is perhaps even more subtle.

The importance of this issue was understood by Jovanovìc & Bamieh (2001), where a stochastic disturbance model is sought, that recreates second order satististics of a turbulent chanel flow through the linearized Navier–Stokes equations. Nevertheless, little has been accomplished in terms of application of an appropriate disturbance models for flow estimation and control in the published literature. Bewley & Liu (1998), Joshi, Speyer & Kim (1999), and Högberg *et al.* (2003) modeled the covariance of the external disturbances at a single wavenumber pair by a simple identity matrix, implying a constant variance of disturbances distributed in the wall-normal direction and zero correlation of the disturbances at different heights above the wall. This model restricted the effectiveness of the resulting estimators in our previous work, and also led to realization problems that required us to limit the types of wall measurements that we could consider while still obtaining convergence of the feedback kernels upon refinement of the numerical grid. In the present paper, we propose an improved stochastic model for the external disturbances (that is, random volume forcing on the interior of the flow domain) that may be used to account for wall roughness, acoustic waves, and neglected dynamics, as well as appropriate stochastic models for the unknown initial conditions and sensor noise.

In previous studies, only time-constant feedback kernels have been considered in the estimator. By introducing time-varying feedback kernels into the estimator, the present paper incorporates plausible models of the statistics of the unknown initial conditions on the flow in order to maximize the speed of convergence of the estimator from unknown initial conditions. As a consequence, the initial transients in the estimator are shown to be greatly diminished.

In the present paper, we will design and test an estimator for 3D plane channel flow. After describing the system of interest, we propose a stochastic model for the flow's initial conditions, external disturbances, and sensor noise in §2.4. An appropriate Kalman filter is designed in §2.5 in order to determine suitable estimator feedback. After a discussion of the numerical methods employed, we test the estimator in numerical simulations at isolated wavenumber pairs in §3. We then inverse Fourier transform the estimator feedback rules determined on a large array of wavenumber pairs to obtain well resolved feedback

convolution kernels in physical space for all of the measured quantities on the wall, as discussed in §4.2. The resulting estimator for the entire 3D channel is tested in numerical simulations in §4.3.

2. Formulation

2.1. *Flow configuration and governing equations*

This paper considers the 3D flow between two infinite flat plates (at $y = \pm 1$) driven by a pressure gradient in the streamwise (x) direction. Scaling the time variable appropriately, the mean velocity profile is given by $U(y) = 1 - y^2$. For computational efficiency, we model the flow as being periodic in the horizontal directions x and z, using a computational domain of sufficient extent in these directions that this nonphysical assumption does not significantly affect the statistics of the flow. This approach allows all variables with spatial variation to be expanded in Fourier series. Thus, the state vector describing the wall-normal velocity $v_{mn}(y, t)$ and wall-normal vorticity $\eta_{mn}(y, t)$ on the interior of the domain at each wavenumber pair $\{k_x, k_z\}_{mn}$ may be denoted by

$$q_{mn}(y, t) = \begin{pmatrix} v_{mn}(y, t) \\ \eta_{mn}(y, t) \end{pmatrix}.$$

The evolution of the flow can then be written with the linear terms, M and L, on the left-hand side and the nonlinear terms, N, on the right-hand side, in addition to an external forcing term e_{mn} to account for unmodeled effects. This yields

$$\underbrace{\frac{\mathrm{d}}{\mathrm{d}t} M q_{mn} + L q_{mn}}_{Linear\ dynamics} = \underbrace{\sum_{\substack{k+i=m \\ l+j=n}} N(q_{kl}, q_{ij})}_{Nonlinear\ coupling} + \underbrace{e_{mn}(y, t)}_{External\ forcing}, \tag{1}$$

where

$$M = \begin{pmatrix} -\Delta & 0 \\ 0 & I \end{pmatrix} \text{ and } L = \begin{pmatrix} \mathcal{L} & 0 \\ \mathcal{C} & \mathcal{S} \end{pmatrix}. \tag{2}$$

The operators $\mathcal{L}$, $\mathcal{S}$, and $\mathcal{C}$ relate to the Orr–Sommerfeld/Squire equations and are defined as

$$\begin{cases} \mathcal{L} = -ik_x U \Delta + ik_x U'' + \Delta^2/Re, \\ \mathcal{S} = ik_x U - \Delta/Re, \\ \mathcal{C} = ik_z U'. \end{cases}$$

The Laplacian operator is denoted $\Delta = D^2 - k^2$, where D and D^2 represent first- and second-order differentiation operators in the wall-normal direction, and $k^2 = k_x^2 + k_z^2$. The Reynolds number Re is based on the centreline velocity and channel half-width. The double convolution sum in (1) represents the nonlinear "triad" interactions. For an explicit form of the nonlinear operator, see, e.g., Henningson & Schmid (1992). The boundary conditions on v and η correspond to no-slip solid walls

$$v = Dv = \eta = 0 \quad \text{at} \quad y = \pm 1.$$

In the following, the right hand side of (1) will be lumped into a forcing function $f_{mn}(y,t)$, thereby restricting the flow model to the linear terms, accounting for both the nonlinear terms and the external disturbances with a stochastic model. Suppressing the $\{\}_{mn}$ subscript for clarity, the resulting flow model can be written as

$$\frac{\mathrm{d}}{\mathrm{d}t}Mq + Lq = Tf(y,t), \tag{3}$$

where the operator

$$T = \begin{pmatrix} ik_x D & k^2 & ik_z D \\ ik_z & 0 & -ik_x \end{pmatrix},$$

transforms the forcing $f = (f_1, f_2, f_3)^T$ on the evolution equation for the velocity vector $(u, v, w)^T$ into an equivalent forcing on the $(v, \eta)^T$ system (see Jovanovič & Bamieh (2001) for a carefull derivation of this transformation).

2.2. *Measurements*

The choice of the measurements to be taken in order to obtain the state estimate (without knowledge of the initial conditions of the flow) is ultimately a matter of practicality. In the present work, we will consider an idealised problem in which the continuous distributions of streamwise and spanwise skin friction and pressure on the wall are available as measurements in order to estimate the state of the flow away from the wall. This information is mathematically complete in the following sense: if this information is uncorrupted by noise and the external forcing on the system is known exactly, the entire state of the flow (even in the fully turbulent regime, and at any Reynolds number) is uniquely determined by these measurements at the wall in an arbitrarily small neighbourhood of time t (*without* knowledge of the initial conditions), as discussed in Bewley & Protas (2003). However, in any practical problem, the measurements are corrupted by noise, the modeling of the system is not precise, and there are external disturbances on the system which are not accounted for. Thus, in the practical setting, it is essential to filter the measurements appropriately to reconcile the noisy measurements of the system with the approximate dynamic model of the system. The Kalman filter used in the present paper is a mathematically-rigorous tool to achieve this reconciliation.

In our previous formulations of the estimator problem, as discussed in Högberg *et al.* (2003), only the feedback gains using the measurement η_y, the first wall-normal derivative of η, were used. In §2.4, we develop an improved formulation based on a more realistic model of the statistics of the external disturbances such that we may now compute well-behaved feedback kernels that converge upon grid refinement for any measurement constructed as a linear combination of the state variables and their derivatives. In particular, the three available measurements at the wall, the streamwise and spanwise wall skin friction and the wall pressure, are related to the quantities v and η in the

state model as follows

$$
\begin{cases}
\tau_x = \tau_{xy}|_{wall} = \mu \dfrac{\partial u}{\partial y}\bigg|_{wall} = \dfrac{i\mu}{k2}(k_x D^2 v - k_z D\eta)|_{wall}\,, \\[2ex]
\tau_z = \tau_{zy}|_{wall} = \mu \dfrac{\partial w}{\partial y}\bigg|_{wall} = \dfrac{i\mu}{k2}(k_z D^2 v + k_x D\eta)|_{wall}\,, \\[2ex]
p = p|_{wall} = \dfrac{\mu}{k2} D^3 v|_{wall}\,.
\end{cases}
$$

In the formulation shown in the remainder of §2, for clarity, we focus on the feedback rules related to measurements made at the lower wall only. The extension of this formulation to the case in which measurements are taken at both walls of the channel, as considered in the simulations reported in §3 and §4, is straightforward.

2.3. *Stochastic setting*

As described earlier, the modeling of the statistical properties of the stochastic forcing function f in (3), which accounts for the effects of both the nonlinear terms and the external forcing, is one of the key steps in the framing of the present estimation problem.

In the present stochastic framework, the mean of any quantity of interest may be obtained using the expectation operator $E[\cdot]$, defined as the average over all possible realizations of the stochastic inputs. In particular, the mean of f is modeled as zero, that is, $E[f] = 0$.

In the present formulation, it is the *covariance* of f that needs to be modeled carefully. Since f is a continuous function of the spatial coordinate y, the appropriate definition of the covariance in this problem is somewhat abstract, as discussed in detail Balakrishnan (1976). As shown in Balakrishnan (1976), once this abstraction is made, the resulting Kalman filter equations in this spatially-continuous formulation are found to be analogous to their counterparts in the classical finite-dimensional setting. In order to proceed with the modeling of the statistics of f, it is necessary to have a clear understanding of what the covariance means.

In the spatially-discrete setting, if *u* and *v* are two zero-mean, random vectors of length n_1 and n_2 respectively, their covariance R_{uv} is defined as a matrix of size $n_1 \times n_2$ such that $R_{uv} = E[uv^*]$. The covariance of a zero-mean random vector *u* is defined as $R_{uu} = E[uu^*]$.

To extrapolate this definition to the spatially-continuous setting (see, e.g., Balakrishnan 1976, p. 267), we make use of inner products with arbitrary test functions chosen from the same Hilbert spaces as the random functions we are considering. That is, if ξ and η are two zero-mean random functions in the Hilbert spaces H_1 and H_2, then their covariance $R_{\xi\eta}$ is defined such that

$$
\forall (x,y) \in H_1 \times H_2, \quad \langle x, R_{\xi\eta} y \rangle_1 = E[\langle x, \xi \rangle_1 \langle y, \eta \rangle_2^*], \tag{4}
$$

where $\langle \cdot, \cdot \rangle_1$ and $\langle \cdot, \cdot \rangle_2$ denote appropriate inner products in the Hilbert spaces H_1 and H_2 respectively. Thus, the covariance $R_{\xi\eta}$ is seen to be a linear operator

from H_2 to H_1; this is analogous to the spatially-discrete setting, in which the covariance is a matrix which when multiplied by a rank n_2 vector results in a rank n_1 vector. Further, if ξ and η are taken to be simple vectors u and v in the above expression, the inner products reduce to the simple form $\langle x, y \rangle = x^* y$, and the spatially-continuous definition of the covariance reduces immediately to the definition given in the spatially-discrete setting.

We will subsequently need to express the covariance of a linear transformation of a random process of known covariance. Letting $g = \mathcal{H}f$ where $\mathcal{H}$ is a linear differential operator and f a random variable, the following relation can easily be deduced from (4)

$$R_{gg} = \mathcal{H}R_{ff}\mathcal{H}^*, \tag{5}$$

where $\mathcal{H}^*$ denotes the adjoint operator of $\mathcal{H}$; note that the adjoint of a linear operator $\mathcal{H} : H_1 \to H_2$ with inner products $\langle \cdot, \cdot \rangle_1$ and $\langle \cdot, \cdot \rangle_2$ on H_1 and H_2 respectively is defined by the equality

$$\forall (x, y) \in H_1 \times H_2, \quad \langle y, \mathcal{H}x \rangle_2 = \langle \mathcal{H}^* y, x \rangle_1.$$

A significant feature of the definition of the covariance is its relation to the expected value of the energy. Taking the trace of (4) with $\eta = \xi$ and simplifying, choosing the inner product related to the energy, it follows that the expected value of the mean energy $E[\mathcal{E}(\xi)] = \text{Tr}(R_{\xi\xi})$.

2.4. *Models for the stochastic inputs*

The flow disturbances that we desire to estimate are affected by the unknown initial conditions and the external disturbances acting to disrupt the system. Since the estimator is intended to converge effectively over a large number of different realizations, a statistical description (mean and covariance) of these unknown quantities, in addition to a statistical description of the sensor noise corrupting the measurements, may be used to tune the feedback in the estimator design. The estimator which we will design, also known as a Kalman filter, will be optimal in the sense of obtaining the most accurate estimate possible over a large set of realizations of the system in which the initial conditions, external disturbances, and sensor noise have the assumed statistical properties.

2.4.1. *Modeling of the initial conditions*

For the purpose of the present work, we will model the mean of the unknown initial condition as zero (that is, we assume there is no preferred phase in the initial flow structures) and its covariance as S_0. Since the initial condition in the estimator is always zero, S_0 also represents the covariance of the state estimation error at $t = 0$.

We want to design an estimator that performs well over a large range of possible initial conditions. It is natural to assume that the initial conditions are completely "random", however, we know from our understanding of the flow physics that there is a tendency for some specific types of flow disturbances to

be present in any given flow. For example, Tollmien–Schlichting (TS) waves are likely to be present if the environment is characterised by acoustic waves, streaks are likely to be present if the environment is characterised by high levels of free-stream turbulence, and streamwise vortices are likely to be present if the environment is characterised by wall roughness. The specific initial conditions which we expect to see at each wavenumber pair in a particular problem (though at an unknown phase and amplitude), and for which we would like to tune the estimator to be particularly efficient at capturing, will be denoted here by $s = s_{mn}(y)$.

We will model the initial conditions q_0 at each wavenumber pair as a linear combination of a component q_s of a specified profile s (but with random magnitude and phase) and a component q_r constructed by a random linear combination of the first p eigenmodes $\xi^j = \xi_{mn}^j(y)$, normalised to unit energy, of the system matrix $M^{-1}L$ in (3) such that

$$q_s = \theta_0\, s\,, \quad q_r = \frac{1}{p}\sum_{j=1}^{p}\theta_j \xi^j,$$

where the coefficients $\theta_j, j \in \{0,\ldots,p\}$ are uncorrelated complex scalar random variables with zero mean and unit variance. The initial condition q_0 is then modeled as a linear combination of these two components such that

$$q_0 = \lambda_1\left(\lambda_2 q_s + (1-\lambda_2)q_r\right).$$

The design parameter $\lambda_1 > 0$ is used to specify the expected amplitude of the initial conditions at this wavenumber pair, and the design parameter $\lambda_2 \in [0,1]$ is used to specify the relative importance of the components q_s and q_r in the initial conditions. The corresponding covariance of the unknown inital conditions is given by

$$S_0 = R_{q_0 q_0} = \lambda_1\left(\lambda_2 R_{ss} + (1-\lambda_2)\sum_{j=1}^{p}R_{\xi^j \xi^j}\right). \tag{6}$$

Note that we expect the energy of the initial conditions at both large wavenumber pairs and small wavenumber pairs to be small. We may account for this in the present model of the initial conditions by allowing λ_1 to vary in a wavenumber-dependent fashion. In the present work, we will model this dependence with the function

$$\lambda_1(k_x, k_z) = v_\lambda k\, e^{-s_\lambda k^2/2},$$

where the design parameter s_λ specifies the exponential decay rate of the expected energy of the initial condition with the amplitude of the wavenumber pair, and the design parameter v_λ scales the overall amplitude of the initial conditions. Other forms for $\lambda_1(k_x, k_z)$ are also possible, and may be experimented with in future work.

2.4.2. *Modeling of the external disturbances*

We will assume the external disturbance forcing f in (3) to be a stationary white Gaussian process (a signal that is uncorrelated in time), with autocorrelation

$$E[f_j(x,y,z,t)f_k(x+r_x,y',z+r_z,t')] = \underbrace{\delta(t-t')}_{Temporal}\underbrace{Q_{f_jf_k}(y,y',r_x,r_z)}_{Spatial},$$

where $\delta(\cdot)$ is the Dirac δ-function. The assumption of zero time correlation eases the derivation of the equations for the covariance of the state, and is appropriate when the characteristic time scales of the external disturbances are short as compared with the characteristic time scales of the flow system. When this is not the case, the approach developed herein is easily extended to incorporate an additional filter in order to "colour" the external disturbances with appropriate self-correlation time scales (see, e.g., Lewis & Syrmos (1995)). We will assume a zero mean disturbance forcing

$$E[f_j(x,y,z,t)] = 0.$$

The remaining property to be described is the spatial extent of the two-point, one-time, auto-correlation of f over the whole domain

$$Q_{f_jf_k}(y,y',r_x,r_z) = E[f_j(x,y,z,t)f_k(x+r_x,y',z+r_z,t)].$$

The corresponding quantity in Fourier space is a covariance operator of the form discussed in §2.3, obtained for any wavenumber pair $\{k_x,k_z\}$ via the following integration over the homogeneous directions

$$R_{f_jf_k}(y,y') = \int\int Q_{f_jf_k}(y,y',r_x,r_z)\mathrm{e}^{-i(k_xr_x+k_zr_z)}\mathrm{d}r_x\,\mathrm{d}r_z.$$

Our model for the autocorrelation of f assumes that the disturbance has a localised structure, i.e., the two-point correlation of the disturbance decays with distance, and that the correlations between forcing terms on different velocity components are zero. These arguments lead to a model of the following form:

$$Q_{f_jf_k}(y,y',r_x,r_z) = v_f\,\delta_{jk}\,\mathcal{M}^x(r_x)\mathcal{M}^z(r_z)\mathcal{M}^y(y,y'), \tag{7}$$

where

$$\begin{cases} \mathcal{M}^x(r_x) = \dfrac{1}{(2\pi s_x)^{1/2}}\mathrm{e}^{-r_x^2/2s_x}, \\[2mm] \mathcal{M}^z(r_z) = \dfrac{1}{(2\pi s_z)^{1/2}}\mathrm{e}^{-r_z^2/2s_z}, \\[2mm] \mathcal{M}^y(y,y') = \dfrac{1}{(2\pi s_y)^{1/2}}\mathrm{e}^{-(y-y')^2/2s_y}. \end{cases} \tag{8}$$

The design parameters s_x and s_z in this model for the statistics of f govern the width of the two-point correlation of the disturbance forcing in the horizontal directions, thus characterising the localised nature of the structure of the disturbances. The corresponding design parameter in the wall normal direction is s_y. The design parameter v_f scales the overall amplitude of the forcing.

In Fourier space, the covariance $R_{f_j f_k}$ at any wavenumber pair $\{k_x, k_z\}$ in this model may be written as

$$R_{f_j f_k}(y, y') = v_f \, \delta_{jk} \, \mathcal{FM}^x(k_x) \mathcal{FM}^z(k_z) \mathcal{M}^y(y, y'),$$

where

$$\begin{cases} \mathcal{FM}^x(k_x) = \mathrm{e}^{-s_x k_x^2 / 2}, \\ \mathcal{FM}^z(k_z) = \mathrm{e}^{-s_z k_z^2 / 2} \end{cases}$$

are the Fourier transform of $\mathcal{M}^x$ and $\mathcal{M}^z$. We will denote $R = R_{ff} = \mathrm{diag}(R_{f_1 f_1}, R_{f_2 f_2}, R_{f_3 f_3})$ in the sections that follow.

2.4.3. *Modeling of the sensor noise*

Each of the three measurements is assumed to be corrupted by sensor noise, modeled as independent white random processes the amplitude of which is determined by the assumed quality of the sensors. The covariance of the sensor noise vector g can thus be described in Fourier space by a diagonal 3×3 matrix G whose diagonal elements α_ι^2 are the variances of the sensor noise assumed to be associated with each individual sensor

$$R_{g_\iota(t), g_\kappa(t')} = \delta_{\iota\kappa} \delta(t - t') \alpha_\iota^2,$$

where $\delta_{\iota\kappa}$ is the Kronecker delta. Thus, in the present work, we assume that the sensor noise is uncorrelated in both space and time.

When the signal-to-noise ratio is low, the measured signal must be fed back only gently into the estimator, lest the sensor noise disrupt the estimator. When the signal-to-noise ratio is high, the measured signal may be fed back more aggressively into the estimator, as the fidelity of the measurements can be better trusted. For a given covariance of the initial conditions and external disturbances, the tuning of the assumed overall magnitude of the sensor noise in the Kalman filter design thus provides a natural "knob" to regulate the magnitude of the feedback into the estimator. Note that an intermediate amount of feedback is desired in the estimator design: if the feedback is too weak, the estimator will not converge very quickly or very accurately, and if the feedback is too strong, it may knock the estimated flow out of the small perturbation neighbourhood assumed in the linear model used in its design.

2.5. *The Kalman filter*

The forced linear equation (3) can be put in the standard state-space form since the inversion of the Laplacian is facilitated by enforcement of the homogeneous boundary conditions on Dv. Thus,

$$\dot{q} = \underbrace{-M^{-1}L}_{A} q + \underbrace{M^{-1}T}_{B} f.$$

The general state-space formulation of the flow system may thus be written

$$\begin{cases} \dot{q} = Aq + Bf, \quad q(0) = q_0, \\ y = Cq + g. \end{cases} \tag{9}$$

The measurement vector y is constructed using the measurement matrix C, defined as

$$C = \frac{\mu}{k^2} \begin{pmatrix} ik_x D^2|_{wall} & -ik_z D|_{wall} \\ ik_z D^2|_{wall} & ik_x D|_{wall} \\ D^3|_{wall} & 0 \end{pmatrix}.$$

This matrix extracts the two components of wall skin friction and the wall pressure from q.

We now build an estimator of the analogous form

$$\begin{cases} \dot{\hat{q}} = A\hat{q} - v, \quad \hat{q}(0) = 0, \\ \hat{y} = C\hat{q}, \end{cases} \tag{10}$$

with feedback

$$v = L\tilde{y} = L(y - \hat{y}). \tag{11}$$

Kalman filter theory, combined with the models outlined in §2.4 for the relevant statistics of the unknown initial conditions q_0, the unknown sensor noise g, and the unknown external forcing f, provides a convenient and mathematically-rigorous tool for computing the feedback operator L in the estimator described above such that $\hat{q}$ converges to an accurate approximation of q. Note that the volume forcing v used to apply corrections to the estimator is proportional to the "innovation process" $\tilde{y} = y - \hat{y}$, that is, the difference between the measurements of the actual system and the corresponding quantity in the estimator model.

The solution of the Kalman filter problem in the classical, finite-dimensional setting is well known (for a succinct presentation, see, e.g., Lewis & Syrmos (1995) p. 463-470). The corresponding operator equations, though more involved to derive, are completely analogous (see Balakrishnan 1976). Thus, we will not rederive these equations here. The main results, in both the finite-dimensional and infinite-dimensional settings, are:

1. the covariance $S(t) = R_{qq}$ of the flow state q is governed by the Lyapunov equation

$$\dot{S}(t) = AS(t) + S(t)A^* + BRB^*, \quad S(0) = S_0, \tag{12}$$

2. for a given L, the covariance $P(t) = R_{\tilde{q}\tilde{q}}$ of the state estimation error $\tilde{q} = q - \hat{q}$ is governed by the Lyapunov equation

$$\dot{P}(t) = A_0 P(t) + P(t)A_0^* + BRB^* + LGL^*, \quad P(0) = S_0, \tag{13}$$

where $A_0 = A + LC$, and

3. the value of L which minimizes the expected energy of the state estimation error (that is, which minimizes the trace of $P(t)$) is given by the solution of the differential Riccati equation (DRE)

$$\dot{P}(t) = AP(t) + P(t)A^* + BRB^* - P(t)C^*G^{-1}CP(t), \quad P(0) = S_0, \tag{14a}$$

$$L(t) = -P(t)C^*G^{-1}. \tag{14b}$$

Note that, for a linear, time-invariant (LTI) system (that is, for A, B, C, R, G independent of time), the covariance of the estimation error, $P(t)$, and the corresponding feedback which minimizes its trace, $L(t)$, follow a transient due to the effect of the initial condition S_0, eventually reaching a steady state in which $\dot{P}(t) = 0$ and $\dot{L}(t) = 0$. In order to minimize the magnitude of the transient of the trace of $P(t)$, it is necessary to solve the differential Riccati equation given above. If one is only interested in minimizing the trace of $P(t)$ at steady state, it is sufficient to compute time-independent feedback L by solving the algebraic Riccati equation (ARE) formed by setting $\dot{P}(t) = 0$ in (14a).

2.6. *Numerical issues*

2.6.1. *Spatial discretization*

In order to actually compute the feedback in this problem, it is necessary to discretize the control equations given in (14a)-(14b) and solve them in the finite-dimensional setting. Thus, we first need to build the discrete counterparts of the system operators A, B, C, and their respective adjoints as well as the disturbance covariances R, G, and S_0. The discrete operators are obtained through enforcement of the Orr–Sommerfeld/Squire equations at each point of the Gauss–Lobatto grid, using a Chebyshev collocation scheme

$$f_i = f(y_i), \quad y_i = \cos\frac{i\pi}{N}, \quad i = 1, \ldots, N,$$

where N is the number of gridpoints in the wall-normal direction. The discrete operators and differentiation matrices are determined using the spectral Matlab Differentiation Matrix Suite of Weideman & Reddy (2000). In particular, this suite provides fourth-order differentiation matrices invoking the clamped boundary conditions ($f(\pm 1) = f'(\pm 1) = 0$) suggested by Huang & Sloan (1993) to give an Orr–Sommerfeld matrix with satisfactory numerical properties, avoiding unstable or lightly-damped spurious eigenmodes. The spectral differentiation matrices D^1, D^2, and D^3 are combined according to the equations given previously to compute the discrete matrices A, B, and C in a straightforward fashion. The calculations reported in this paper used, where needed, the discrete definition for the adjoint of a matrix, that is, its conjugate transpose.

The integration weights $W(y_j)$ for the Chebyshev grid with the Gauss–Lobatto collocation points are computed using the algorithm from Hanifi, Schmid & Henningson (1996). These weights provide spectral accuracy in the numerical integration used to assemble the energy measure matrix Q.

2.6.2. *Solution of the DRE*

The calculation of the differential Riccati equation (DRE) is accomplished in this work using the Chandrasekhar algorithm developed by Kailath (1973). This elegant algorithm solves a factored form of the DRE at the heart of the

Kalman filter as given by the spatial discretization of the operators in (14a)-(14b). It is particularly efficient when these factors are of low rank, which happens to be the case in the present study.

The main idea in the Chandrasekhar algorithm is to solve an evolution equation for a factored form of the *time derivative* of the estimation error covariance matrix, $\dot{P}(t)$. Since it is symmetric, $\dot{P}(t)$ can be factored as

$$\dot{P} = L_1 L_1^* - L_2 L_2^* = YHY^*, \quad Y = \begin{pmatrix} L_1 & L_2 \end{pmatrix}, \quad H = \begin{pmatrix} I & 0 \\ 0 & -I \end{pmatrix}, \qquad (15)$$

where the rank of $L_1 L_1^*$ is the number of positive eigenvalues of $\dot{P}$ and the rank of $L_2 L_2^*$ is the number of negative eigenvalues of $\dot{P}$.

By differentiation of both sides of (14a) and substitution of this factorisation, it is straightforward to verify that (14a)-(14b) is equivalent to the solution of the following system:

$$\begin{cases} \dot{L}(t) = Y(t)HY^*(t)C^*G^{-1}, & L(0) = -P_0 C^* G^{-1}, \\ \dot{Y}(t) = (A + LC)Y(t), & Y(0)HY^*(0) = \dot{P}(0), \end{cases} \qquad (16)$$

where $\dot{P}(0)$ is easily determined from (13) evaluated at $t = 0$.

The key to the efficiency of this scheme is to exploit the possibility for an accurate low-rank approximation of Y. After an eigenvalue decomposition of $\dot{P}(0)$ to determine L_1 and L_2, we can perform a singular value decomposition of the matrices $L_1 L_1^*$ and $L_2 L_2^*$ and discard the singular vectors associated with small singular values, constructing an approximation of Y with the remaining singular vectors. In this paper, singular values less than 0.01% of the initial $\dot{P}$ matrix norm were discarded, resulting in a reduction of the rank of Y by approximately 75%.

In the present work, time integration is performed using a standard explicit fourth-order Runge–Kutta scheme. When only the steady state gain is needed, we can either march the DRE to steady state using the Chandrasekhar algorithm or solve directly the ARE via standard techniques based on Schur factorization (Laub (1991)).

2.6.3. *Computation of the expected energy*

In the discretized setting, the expected energy of the state q can be extracted from the discrete covariance matrix S by use of the energy measure matrix Q such that $E[\mathcal{E}(q(t))] = \text{Tr}(QS(t))$, where $\mathcal{E}(q(t))$ denotes the instantaneous energy of the state q at time t. The expected energy of the state estimation error $\tilde{q}$ can be found in a similar manner, $E[\mathcal{E}(\tilde{q}(t))] = \text{Tr}(QP(t))$.

The time evolution of the expected energy may be computed using the Chandrasekhar method. For example, the time derivative of the expected energy of the state q can be integrated forward in time from $E[\mathcal{E}(q(0))] = \text{Tr}(QS_0)$, its value at $t = 0$, via computation of $\text{Tr}(Q\dot{S}(t))$, where $\dot{S} = YHY^*$, and where the evolution equation for $Y(t)$ is simply $\dot{Y}(t) = AY(t)$, with $Y(0)$ determined

by the factorization $Y(0)HY^*(0) = \dot{S}(0)$ and $\dot{S}(0)$ determined by evaluation of (12) at $t = 0$. The time derivative of the expected energy of the state estimation error $\tilde{q}$ can be found in a similar manner with, for a given value of L, $Y(t)$ evolving according to $\dot{Y}(t) = (A + LC)Y(t)$ and $Y(0)$ determined from the factorization of $\dot{P}(0)$, which itself is determined by evaluation of (13) at $t = 0$.

3. Single-mode estimation results

In this section we will investigate the performance of the estimator at isolated wavenumber pairs. Unless stated otherwise, the results are computed for $R = 3000$, a subcritical Reynolds number characterized by transient growth phenomena. The design parameters for the stochastic model for the initial conditions (see §2.4.1) are chosen to be $\lambda_2 = 0.5$, $v_\lambda = 1$, and $s_\lambda = 0.3$. The design parameters for the stochastic model for the external disturbances (see §2.4.2) are chosen to be $v_f = 0.1$, $s_x = s_z = 0.2$, and $s_y = 0.1$. The design parameters for the stochastic model for the sensor noise (see §2.4.3) are chosen to be $\alpha_1 = \alpha_2 = 0.5$ (for the shear-stress measurements) and $\alpha_3 = 0.05$ (for the pressure measurements).

The initial conditions used for the tests at isolated wavenumber pairs are the "worst-case" initial conditions at these wavenumber pairs, i.e., the initial conditions that, leveraging the non-normality of the dynamic operator A to the maximum extent possible, lead to the largest possible transient energy growth. Such initial conditions are of particular concern in a flow transition scenario. Its description can be found in, e.g., Schmid & Henningson (2001).

The plots in this section show the evolution of the expected value of the energy of both the flow state and the state estimation error for initial conditions, sensor noise, and external disturbances distributed as described in the stochastic models presented in §2.4. Thus, these plots can be interpreted as an average over a large number of realizations of these stochastic inputs. They illustrate the effectiveness of the estimator feedback in the presence of the types of disturbances for which the estimator feedback was designed, namely, uncorrelated, zero-mean, random Gaussian distributions of the same covariance as specified in the estimator design.

3.1. *Evolution of the expected energy of the flow state and the state estimation error*

Figure 1 shows the evolution of both the expected energy of the flow state and the expected energy of the state estimation error using time-varying feedback gains for three cases, each of one includes the effect of sensor noise:

1)*Nonzero initial conditions with zero external disturbances* (dash-dotted curves): the expected energy of the state estimation error follows an initial transient, eventually tending exponentially to zero at the decay rate of the least-stable eigenmode of $A + LC$ since there is no additional excitation. In all flows considered, the expected energy of the state estimation error is rapidly reduced to over two orders of magnitude below the expected energy of the flow state.
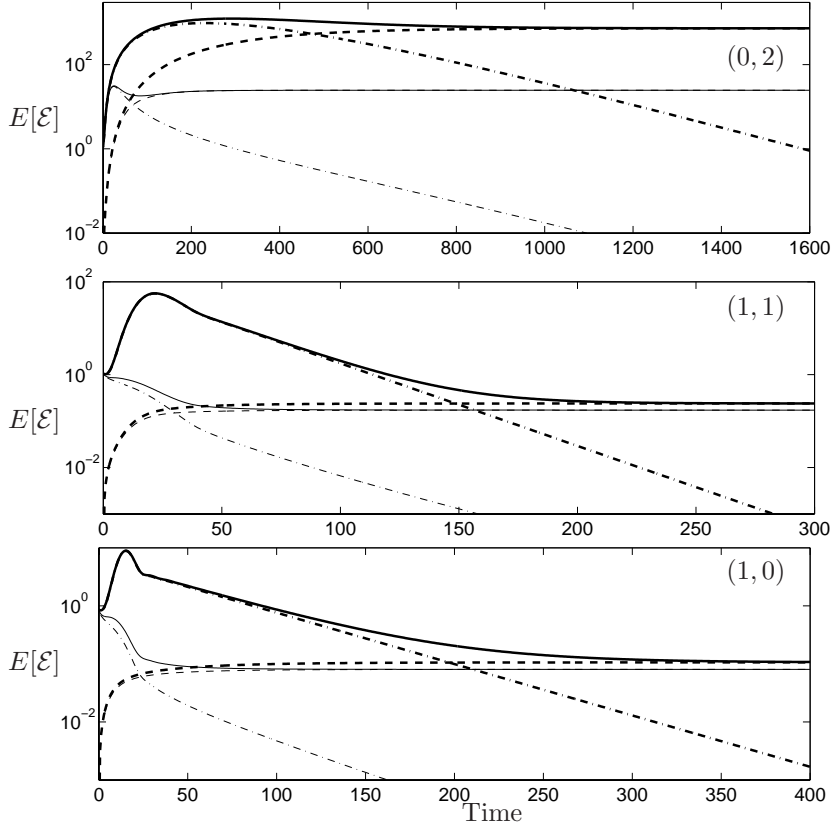
FIGURE 1. Evolution of the expected energy versus time for three flows of interest at three representative wavenumber pairs: (*top*) (0,2), (*center*) (1,1), and (*bottom*) (1,0). The stochastic inputs driving each simulation are: (solid) initial conditions plus external disturbances, (dashed) external disturbances only, (dash-dot) initial conditions only. Thick lines represent the expected energy of the flow disturbance and thin lines represent the expected energy of the estimation error.

2)*Nonzero external disturbances with zero initial conditions* (dashed curves): the expected energy of the estimation error monotonically increases towards a statistical steady state. In the flow considered at wavenumber pair (0,2), the expected energy of the state estimation error rapidly approaches a value close to two orders of magnitude below the expected energy of the flow state, indicating effective estimator convergence. In the flows considered at wavenumber pairs (1,1) and (1,0), however, the expected energy of the state estimation error is nearly as large as the expected energy of the flow state itself, indicating poor convergence of the estimator in these particular flows.
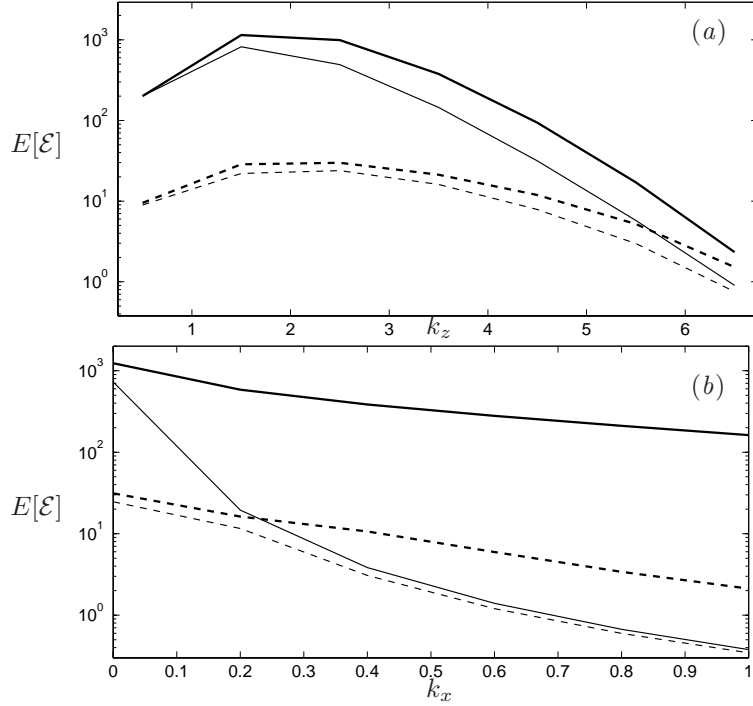
FIGURE 2. Maximum (thick lines) and steady state expected energy (thin lines) for the flow (solid) and the estimation error (dash) over a range of wavenumber pairs. (a) for $k_x = 0$ and varying k_z. (b) for $k_z = 1$ and varying k_x.

3)*Both nonzero initial conditions and nonzero external disturbances* (solid curves): as expected, due to the linearity of the system and the additive effects of the stochastic inputs on the expected energy of the system, this case is given precisely by the sum of cases (a) and (b).

It is also worth noting that the transient in the expected energy of the state estimation error is not only of lower amplitude, but is typically much faster than the transient in the expected energy of the flow state.

Figure 2 shows how the peak and statistical steady state of the expected energy of the flow state and state estimation error depend on the wavenumber pair, quantifying the effects seen in Figure 1 for a range of different wavenumbers.

3.2. *The difficulty of detecting structures in the centre of the channel with wall sensors*

The reason the estimator discussed in the previous section fails to converge effectively in the flows at wavenumber pairs $(1,1)$ and $(1,0)$ when external disturbances are present is interesting. Bewley & Liu (1998), hereafter referred

to as BL98, studied extensively the Kalman filter problem in the present flow system for the following two cases:

case (i): $Re = 10000$, $(k_x, k_z) = (1, 0)$,

case (ii): $Re = 5000$, $(k_x, k_z) = (0, 2)$.

As shown in Figure 1b of BL98, the leading eigenvectors of A in the $(1, 0)$ case include several "center" modes with nearly zero support near the wall[1]. These modes, which are absent in the $(0, 2)$ case, would be continously excited by the external disturbances, and are nearly impossible to detect with wall measurements even if the sensor noise is very low. To quanitfy this notion, the corresponding "modal observation residuals" g_κ are tabulated for both cases in Tables 1 and 2 of BL98.

Because of the presense of these nearly-unobservable center modes, the estimation problem is inherently difficult at certain wavenumber pairs when both external disturbances and sensor noise are present. Thus, the failure of the Kalman filter developed here to converge accurately for the externally-disturbed flows in the $(1, 0)$ case and the $(1, 1)$ case, which is characterized by similar unobservable center modes, is a reflection of the fundamental difficulty of this estimation problem when only wall measurements are employed, and is not a shortcoming of the estimation strategy applied in the present work.

To investigate the excitation of the center modes by the external disturbance, we may augment the definition of $\mathcal{M}^y$ in (8), which models the wall-normal distribution of the covariance of the external disturbances f, as

$$\mathcal{M}^y_{augmented} = C(p) y^{2p} \, \mathcal{M}^y.$$

The parameter p may be chosen to tune the profile of the external disturbances, with uniform intensity in y if $p = 0$ or with intensity increasing near the walls if $p > 0$, as shown in Figure 3. The constant $C(p)$ is selected such that all distributions yield of flow with expected energy of 1000 for the various values of p considered.

The effect of the location of the external disturbances may be seen in Figure 4. For the three wavenumber pairs we show the wall normal distribution of the expected energy for the flow and the estimation error at the steady state. The flow is forced both with the external disturbance with $p = 0$ (solid lines) and $p = 5$ (dashed lines). For (0,2) the location of the external disturbance has nearly no effect. Most of the energy is located in the region of high shear, as explained by the lift-up effect. For (1,0) though, the absence of forcing in the center of the domain has a strong influence on where the expected energy is located. When the excitation is present in the center, it can be seen that the flow energy as well as the estimation error energy is strongly located close to $y = 0$, far from the sensors. This leads to a low estimator performance. For the $p = 5$ case, the flow structures related to the center modes are not being excited , the estimation performance is thus good, as can be seen by the thin

---

[1]Note that the shapes of these modes are only weak functions of Reynolds number, so the same general comments hold true for the $Re = 3000$ case studied here.
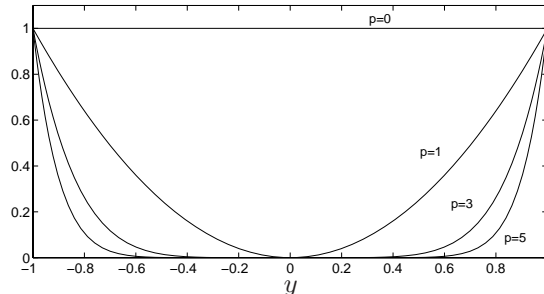
FIGURE 3. The wall normal distribution for variance of the external disturbances. Four cases are shown, corresponding to $p = 0, 1, 3, 5$.

(k_x, k_z)	(0,2)	(1,1)	(0,1)
$p = 0$	29.9	290.8	549.0
$p = 1$	26.2	112.9	178.9
$p = 3$	16.7	38.8	44.1
$p = 5$	11.9	18.3	16.9

TABLE 1. The expected value of the steady state estimation error for three wavenumber pairs and four wall normal distributions of the amplitude of the external disturbances. For each case, the magnitude of the external disturbance is scaled so that the flow expected energy is 1000.

dashed curve. The (1,1) case is an intermediate case, showing the features of both the two previous cases.

Those results are further illustrated in Table 1, where the expected energy of the estimation error is shown for $p = 0$, 1, 3, and 5. When the external disturbance is equally distributed (case $p = 0$) the estimation performance is lower for (1,0) than for (0,2) as was allready seen in Figure 1. As the excitation is closer to the wall, that is, as p increases, the performance increases for each of the shown wavenumber pairs, until they reach approximately the same value for $p = 5$. Clearly, when structure in the center of the channel are not excited, the estimator has equally good performance for all of those wavenumber pairs.

In any event, the flow structures that typically play the dominant role in the transition process (and, thus, the flow structures which we are most interested in estimating accurately) are elongated in the streamwise direction. That is, the modes of maximum interest have small k_x and large k_z, without the problematical center modes. It is also significant to point out that, to model the effects of wall roughness, it is relevant to tune the external disturbance model to have increased intensity near the wall, as done in the above discussion. For turbulent flow, however, the present results imply difficulties in estimation
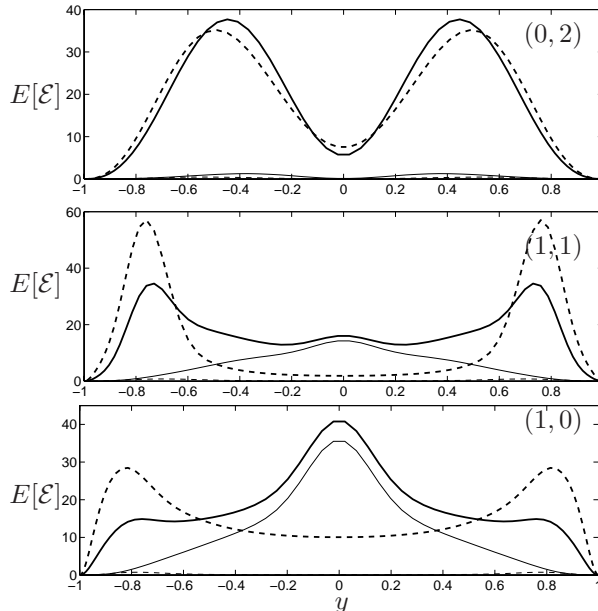
FIGURE 4. The steady state expected energy distribution along the wall normal direction for the the flow (thick lines) and the estimation error (thin lines) for three wavenumber pairs: (*top*) (0,2), (*center*) (1,1), and (*bottom*) (1,0). and for two wall normal distribution of the external perturbation: $p = 0$ (solid) and $p = 5$ (dash).

possibilities away from the walls. This has been reported by Bewley & Protas (2003) and Chevalier *et al.* (2003).

3.3. *The utility of time-varying gains in the estimator*

The feedback gains L determined by the Kalman filter, computed according to (14a)-(14b), are inherently a function of time. Thus, as stated previously, in order to minimize the trace of $P(t)$ during the transient which ensues after the estimator is turned on, it is necessary to use time-varying feedback gains. However, for large times, $P(t)$ and $L(t)$ eventually approach statistical steady state. Thus, if one is not interested in minimizing this transient, one can simply apply constant feedback gains designed to minimize the expected energy of the state estimation error at statistical steady state.

It is interesting to compare the possible utility of time-varying gains for the control and estimation problems. Consider first the problems of optimal control and optimal estimation over the finite time horizon $[0, T]$. As already seen, the optimal estimation (Kalman filter) problem is solved by a DRE that marches *forward* in time from $t = 0$ to $t = T$. On the other hand, the optimal control problem is solved by a (closely-related) DRE that marches *backward* in
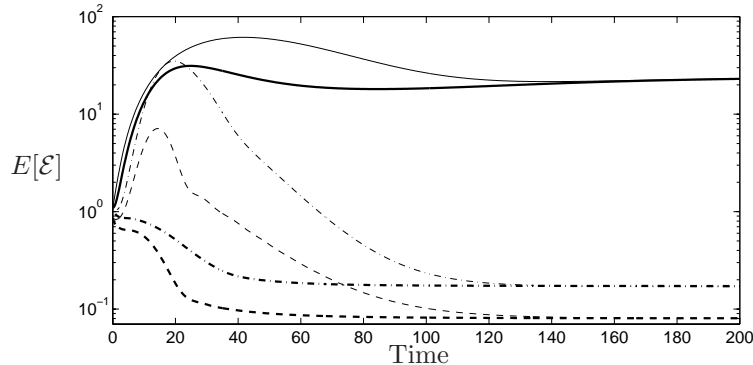
FIGURE 5. Comparison of estimation error expected energy using the time varying gain (thick lines) and steady state gain (thin lines) for three wavenumber pairs: (0,2) solid, (1,1) dash-dot and (1,0) dash.

time, from $t = T$ to $t = 0$. For time invariant systems over a long time horizon (that is, for large T), the resulting feedback gains for the estimation problem exhibit a transient near $t = 0$ and approach a constant for the remainder of the march towards $t = T$, whereas the resulting feedback gains for the control problem exhibit a transient near $t = T$ and approach a constant for the remainder of the march towards $t = 0$. In the limit that $T \to \infty$, the transient in the gains in the control problem becomes unimportant; however, the transient in the gains in the estimation problem is still significant, especially if one is concerned with how rapidly the estimator converges after the control is turned on. Failure to appreciate this point can lead to the implementation of constant-gain estimators which do not converge as rapidly as one might desire.

In our previous research on dynamic compensation (Högberg *et al.* (2003)), steady state feedback gains for both the control and estimation problems were used, taking no account of the transient due to the initial condition. The full-state feedback control problem was found to be solved successfully with this approach for a large number of relevant flow cases. However, the state estimation problem was not found to be solved effectively by this approach, and was left as an important open problem.

It is now clear that we cannot expect good estimation performance during the initial transient using the steady state estimation gain if the initial condition has strong effect on the flow. This can be seen in Figure 5 where the expected energy evolution of the estimation error is plotted for the steady state gain (thin lines) and the time varying one (thick lines). Both the steady state and the time varying gain give small errors in the steady state regime, but the error peak that is seen for short times when using the steady state gain is reduced when the time varying one is applied. By taking the covariance of the initial condition into account, we have a direct means to input knowledge about the flow case of interest. The amplitudes and the shape of the gains vary in time
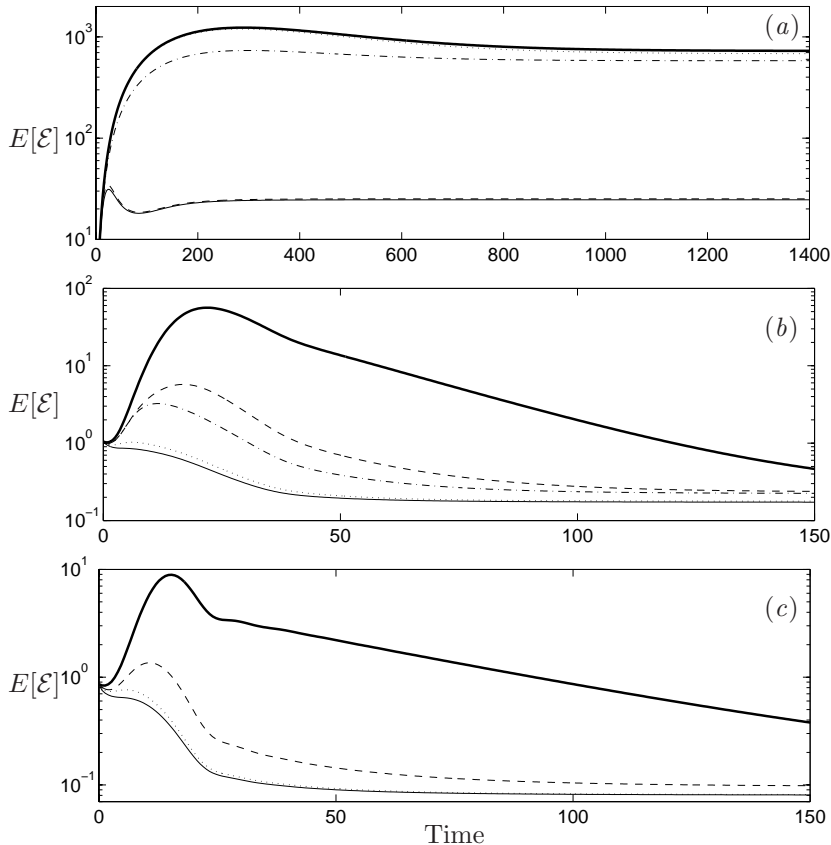
FIGURE 6. Expected energy of estimation error for individual measurements for three wavenumber pairs: (*a*) (0,2), (*b*) (1,1), and (*c*) (1,0). Solid thick line is flow expected energy, solid thin is estimation error expected energy using all measurements. Estimation error with only pressure (dot), only τ_x (dash) , only τ_z (dash-dot).

since the flow disturbance originates from an initial condition that is different from the external disturbance. Thus the gains differ for small and large times.

3.4. *Study of the individual measurement*

The improvement due to the new description of the external disturbance in §2.4.2 allowed us to use several measurements. We show here that this flexibility is necessary for good performance to be obtained over a wide range of wavenumber pairs.

Figure 6 shows the impact of the measurements on the estimation for our three wavenumber pairs. The measurement τ_x is responsible for most of the
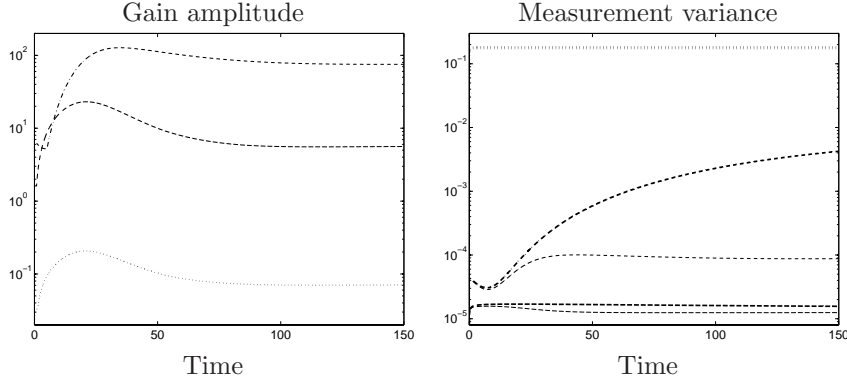
FIGURE 7. Time evolution of the gain amplitudes and measurement signal variance for the wavenumber pair (0,2). (*a*) Gain maximum absolute value for the three measurements: τ_x (dash-dot), τ_z (dash) and pressure (dot). (*b*) variance of measurement signal (thick) and measurement error (thin) with same line convention than for the gains.

estimation performance for low k_x wavenumber pairs, i.e., for elongated structures in the streamwise direction. Physically, the estimator can utilize the strong skin friction footprint associated with the streamwise streaks created be the lift-up of low momentum fluid by low amplitude streamwise vortices. On the other hand the pressure measurement is responsible for the convergence of the two wavenumber pairs with nonzero k_x.

The evolution of the gain amplitudes can be seen in Figure 7 as well as the time evolution of the variance of the measurement signals for the wavenumber pair $(0, 2)$, i.e. the expected value of the measurement signal squared. Clearly the growth of the streaks affects the streamwise skin friction measurement. The variance of the pressure measurement is constant during the process. Note that both the measurement signals and the measurement error reach a steady state, and that the measurement error is of lower amplitude.

3.5. *The application of frozen time varying gains*

Use of the full time history of the gain requires a large amount of computer memory and computational time. Here we show the performance of frozen gains picked from the time varying sequence, in order to give an insight into how a small selection of the full time history of the gain can be used in the estimation process.

In Figure 8 the expected energy of the estimation error is shown. It can be seen that when gains from the early time evolution are used, they lead to good estimation at the beginning of the transient, but yield increased error when the effect of the initial condition vanishes. As the gain is picked from later times,
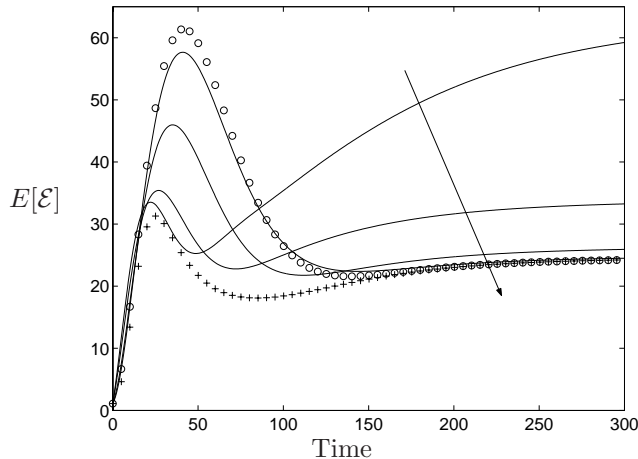
FIGURE 8. Estimation error expected energy for gains selected from the time varying scheme and applied constantly, here for the wavenumber pair (0,2). Tested gains are from times 20, 40, 60, and 80 (solid lines) increasing time shown by the arrow, compared to the steady state gain (∘) and the time varying gain (+).

the reduction of the transient error is degraded, but the steady state error is closer to the optimal. The estimation using the steady state gain itself shows a high initial transient but converges as expected to the performance of the time varying gain for later times. This shows that depending on the time interval for which the estimation is crucial, different gains from the time varying sequence are preferred.

These results will be used in the next section as a guide when only a few of the gains from the time dependent sequence are used in the estimation of the time evolution of a full 3D localised disturbance.

4. Estimation of localised disturbances

The estimator was tested on single wavenumber pair cases. We will now apply it to a realistic flow case and see how the gains are combined into the kernels, and assess the overall performance of the estimator.

4.1. *Description of the initial condition*

The localised disturbances studied by Henningson, Lundbladh & Johansson (1993) will be used in the tests of the estimation. We will here estimate the evolution of a low amplitude localised disturbance so that nonlinear effects can be neglected.
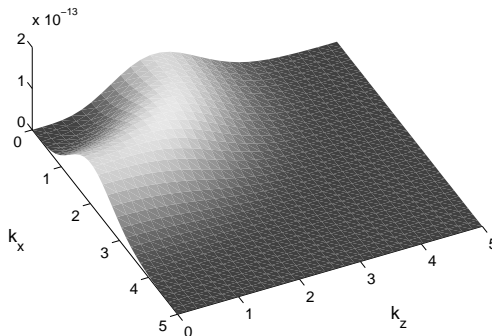
FIGURE 9. The Energy content in Fourier space of the initial condition.

The disturbance chosen consists of two counter-rotating vortices of the form

$$
\begin{cases}
\psi = \dfrac{1}{2}\varepsilon f(y) r^2 \mathrm{e}^{-(r/l)^2}, \\[2mm]
f(y) = (1+y)^2 (1-y)^2, \\[2mm]
(u,v,w) = (-\dfrac{x}{r^2}\psi_y, \dfrac{1}{r}\psi_r, -\dfrac{z}{r^2}\psi_y)\mathrm{e}^{(r/l)^2}.
\end{cases}
\tag{17}
$$

Here (x,y,z) are the streamwise, normal, and spanwise coordinates respectively, $r^2 = x^2 + z^2$, and (u,v,w) are the corresponding velocity components. The horizontal scaling was adjusted through the parameter l which is equal to 1 for the presented simulations so that the maximum energy in Fourier space is for the wavenumber pairs showing the greatest transient energy growth. The amplitude ε is 0.001.

4.2. *Kernels*

The optimisation for a single wavenumber pair produces an estimation feedback gain which is a function of the wall normal direction. By solving this problem on a large array of wavenumber pairs and performing an inverse Fourier transform in the two homogeneous directions we obtain a physical space description of the three-dimensional estimation kernel to be used in the estimation of the localised disturbance.

It was shown that the estimation gains are dependent on the expected noise and initial conditions. First we comment on the global features of both time varying and steady state kernels and illustrate how the spatial extent of the steady state kernels is affected by the size of the expected perturbating structures and the advection speed of the disturbances. For a detailed discussion of the general features of the estimation kernels, also relevant for the present results, see Högberg *et al.* (2003).

4.2.1. *Time varying kernels*

The time evolution of the kernel for the streamwise skin friction measurement is shown in Figure 10. The shape of the kernels varies rapidly for initial times, since originally all the wavenumber pairs are excited. Also their extent for short time is similar in streamwise and spanwise directions. Later, the gains for rapidly decaying wavenumber pairs decay to their steady state values, so that the ones for slowly evolving wavenumber pairs contribute the most to the kernel evolution. In addition it was shown in Figure 2 that the external disturbance excites the flow energy in the wavenumber pairs with low k_x the most. The kernels are thus eventually mostly composed of the gains for those wavenumber pairs and their streamwise extent increase as the flow evolves to its steady state.

4.2.2. *Steady state kernels*

The time varying kernels eventually converge to the steady state kernels. Figure 11 shows their shape for each measurement, and forcing on v and η. It can be seen how the isosurfaces for the τ_x measurement steady state kernel resembles the corresponding ones of Figure 10, for later times.

There is a physical argument for the localisation of the estimation kernels already discussed for the control problem in Högberg *et al.* (2003). Measurement taken at the wall are related to corresponding disturbances in the interior of the domain, and are reconstructed by a volume forcing in the estimator. Those wall footprints necessarily have to be correlated with disturbances close to the measurement, implying that the forcing in the estimator will decay with the distance from the measurement point. This decay distance is related to the correlation scale of the disturbance structure. The parameters s_x, s_y, and s_z modeling this length scale in §2.4.2 will thus affect the spatial extent of the computed kernels. Figure 12 shows for three different values of s_z the extent for the pressure kernel forcing the streamwise velocity component, integrated in the streamwise and wall-normal directions. It is clear that a disturbance which is spread out in the spanwise direction, i.e., a disturbance with greater two-point correlation length scale in the spanwise direction, has a more spread out kernel. We can also see how a more wide kernel has a lower amplitude, since the forcing is more distributed.

The streamwise extent of the kernel is less sensitive to the streamwise length scale of the disturbances, but is instead dependent on the Reynolds number. In a flow with higher Reynolds number the effect of flow advection is dominant over the diffusion effect so that information from wall sensors can be related to structures further upstream. This effect can be clearly seen in Figure 12(b) which shows the same kernel as in 12(a) but integrated in spanwise and cross-flow directions for three different Reynolds numbers.

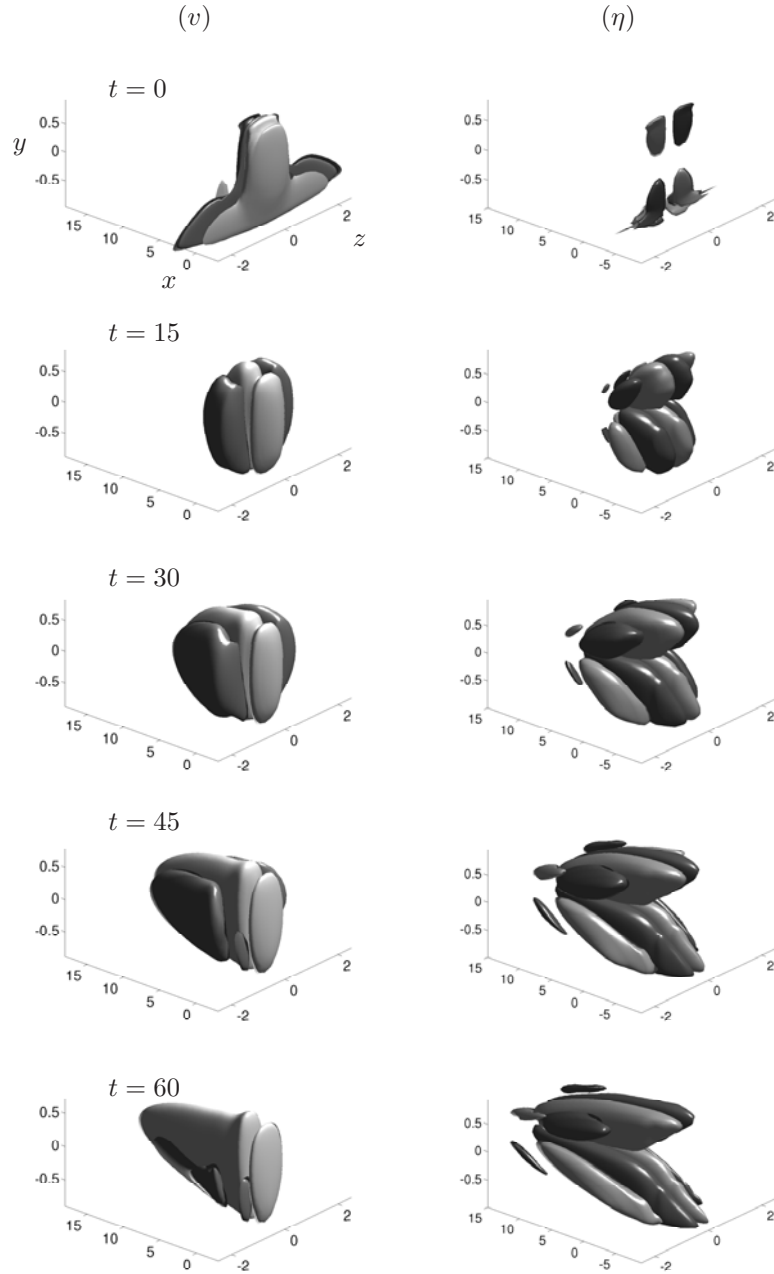(v) (η)

FIGURE 10. The time varying kernel for time 0, 15, 30, 45, and 60 relating the streamwise component of the shear stress measurement error at the point $\{x = 0,\ y = -1,\ z = 0\}$ on the wall to the estimator forcing terms on wall normal velocity (left) and wall normal vorticity (right) inside the estimator flow domain. Visualised are positive (dark) and negative (light) isosurfaces with isovalue $\pm 5\%$ of the maximum amplitude of the kernels during the shown time interval.
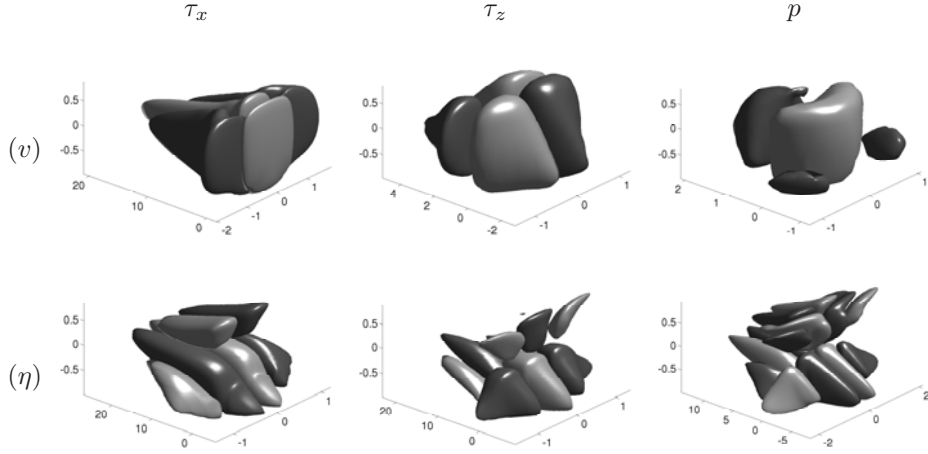
FIGURE 11. The steady state kernels relating the τ_x (*left*), τ_z (*centre*), and p (*right*) measurement at the wall to the forcing in the estimator domain for v (*top*) and η (*bottom*). Visualised are positive (dark) and negative (light) isosurfaces with isovalue $\pm 5\%$ of the maximum amplitude for each kernel.
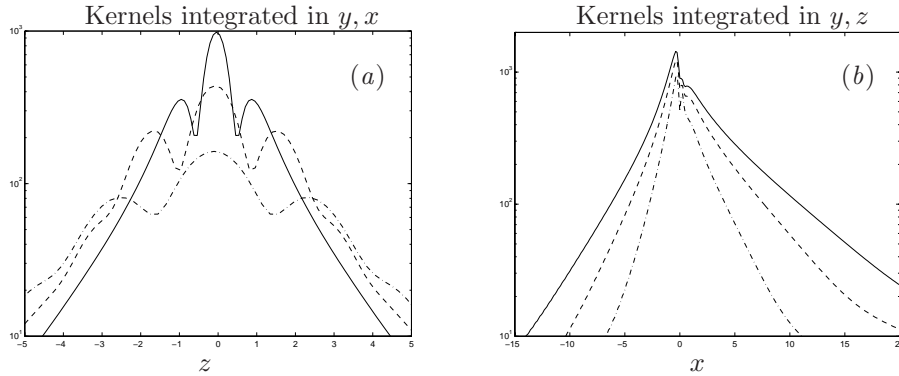

FIGURE 12. Decay of pressure kernel forcing u. (*a*) integrated in streamwise and wall normal direction, for $s_x = s_z = 0.2$ (–), 0.7 (dash), 1.3 (dash-dot). (*b*) integrated in spanwise and wall-normal directions for three Reynolds number, $Re = 3000$ (solid), 2000 (dash), 1000 (dash-dot).

4.3. *Flow evolution*

We will now test the estimator performance in a specific flow case. Note that here we perform a deterministic simulation of the evolution of a particular initial condition, not the stochastic simulation of the mean over an infinite number of initial conditions and process noise, as was presented for the single wavenumber pairs in the previous section.

We will test different models for the covariance of the initial conditions by varying the parameter λ_2 describing how good our knowledge of the statistical properties of the initial condition is. It is varied from 0 (only noise) to 1 (only the deterministic initial condition). For these simulations we use the initial condition in (17) as the "specific" component of S_0 in the computation of the kernels.

We do not use in this section the full time history of the time varying kernel. Instead we proceed to a gain scheduling, making use of the result from §3.5. The selection of only one kernel cannot efficiently address the estimation of all wavenumber pairs since many time scales are present in the energy evolution: the flow at $(k_x, k_z) = (0, 2)$ evolves much slower than wavenumber pairs with $k_z = 0$ for instance. We do a selection of three kernels as follow: the kernel from time zero is applied to the estimation on the time interval $t \in [0, 5]$ to contribute to the estimation of rapidly decaying wavenumber pairs. This kernel will barely affect slower wavenumber pairs. The kernel from time 20 is applied to the estimation on $t \in [5, 60]$ to deal with the transient of the estimation error, and the kernel from time 60 is used for $t \geq 60$, to further deal with the transient as well as the decaying tail of the flow evolution.

Recall that the actual initial condition in the estimator simulation $\tilde{q}_0$ is systematically set to zero, and that only the covariance property of the initial condition is input to the optimisation. This imply that $\lambda_2 = 1$ corresponds to the case where the shape of the initial condition in the wall normal direction is known but neither the amplitude nor the phase are known. This corresponds to a flow case where the perturbating source is identified but none of its instantaneous properties are known. The case with $\lambda_2 = 0$ would then correspond to a situation where any type of disturbance is likely to enter the domain. Models with $\lambda_2 = 0, 0.25, 0.5, 0.75, 1$ are applied to the estimation of the same initial condition in order to illustrate how knowledge of the initial condition affects the estimator's performance.

We can see on Figure 13 that the variation of λ_2 between 1 and 0.25 barely affects the performance, when compared to the flow energy or the estimation with steady state kernel, but clearly the curve for $\lambda_2 = 0$ shows that when no information is available on the initial condition, it is preferable to use the steady state kernel.

Figure 14 illustrates the evolution of the initial condition during the transient of the estimation error. Isosurfaces for the flow (left) show how the initial condition spreads in the flow domain and is advected by the mean flow. It is also clearly seen how the structures become elongated in the streamwise direction as the energy for wavenumbers with $k_x = 0$ become prominent due to their large transient growth. One can see in parallel on the right the evolution of the estimated flow using the kernels with $\lambda_2 = 0.5$. Initiated with no disturbance, structures of the flow appear progressively, the measurements at the wall being fed back through the kernels. Eventually most of the features of the flow are
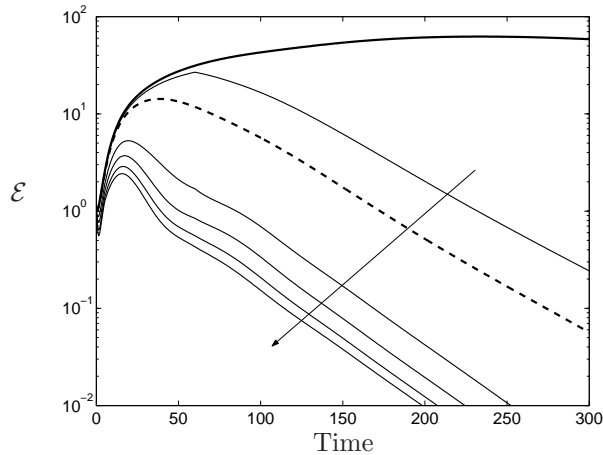
FIGURE 13. The deterministic simulation, with axisymetric localised initial condition. Flow energy (solid thick), estimation error energy using the steady state kernels (thick dash). Thin lines are the estimation error energy using a selection of three kernels from the time varying procedure with λ_2 being respectively 0, 0.25, 0.5, 0.75, and 1. The energy of the initial flow is normalized to one in this plot.

reconstructed at time 60. Recall from Figure 13 that the disturbance is at an early stage of its evolution at time 60.

5. Conclusion

We have studied the estimation by measurement feedback of a fluid flow subject to initial condition and external disturbance, i.e.,disturbance such as acoustic waves or wall roughness. The limited performance of the estimation in earlier studies as compared to the performance of the control motivated us to study the estimation by itself. We found that physical modeling for the external disturbance, as well as a model for the initial condition of the flow to be estimated, was key to the performance of the estimator.

The use of a physically relevant model for the external disturbance developed in this paper allowed us to get well resolved estimation kernels for basic wall quantities as pressure fluctuations and wall shear stresses. We showed how the model affects the physical properties of the kernels. The spanwise extent of the external disturbances are related to the spanwise extent of the kernels and we saw how the streamwise extent of the kernel was dependent on the Reynolds number. A more specific study on the model for the external disturbance related to the estimation of a turbulent channel flow is being carried in Chevalier *et al.* (2003).

The model for the initial condition was tested on the evolution of a localised disturbance, and we demonstrated that taking into account transient

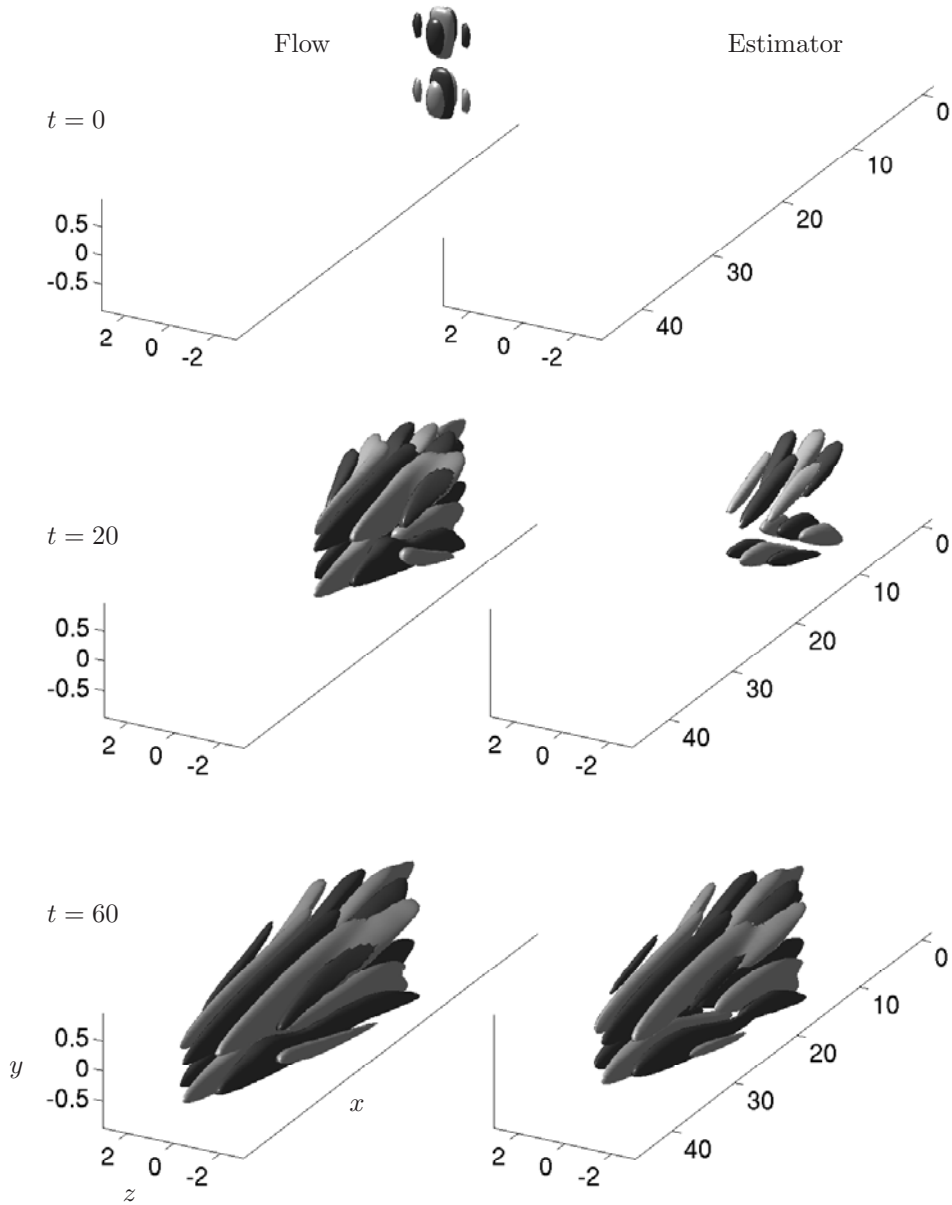FIGURE 14. Evolution of a localised disturbance to the state (*left*) and the corresponding state estimate (*right*) at time $t = 0$ (*top*), $t = 20$ (*middle*), and $t = 60$ (*bottom*), with $\lambda_2 = 0.5$. Visualised are positive (light) and negative (dark) isosurfaces of the streamwise component of the velocity. The isovalues are $\pm 10\%$ of the maximum streamwise velocity of the flow during the shown time interval.

effects by the use of time varying kernels lead to a clear improvement of the estimation performance when compared to the estimation method previously used in transitional problems. In addition we show that this improvement is dependent on the assumed stochastic disturbances. Indeed in a case where nothing is know about the flow to be estimated, steady state kernels perform better.

When the estimation procedure is applied to transitional problems a 3D model is necessary for both initial condition and external disturbance, introducing number of design parameters. In addition the time varying procedure is computationally more demanding since the full time history of the kernel evolution has to be resolved. Those problem have been tackled by the introduction of generic design parameters which can be related to physical insight on the flow to be estimated and the adaptation of the Chandrasekhar method for solving the Riccati equation on flow applications. The problem allows efficient parallelisation since it is decoupled in Fourier space. Further it was shown that a good performance of the estimator can be obtained by selecting a few kernels from the time varying procedure, illustrating that it is the idea of taking into account the stochastic properties of the initial condition that is central, and not necessarily the complete treatment of the time evolution.

The estimation gains computed have been tested on flows associated with individual wavenumber components as well as for the development of localised disturbances. The estimation performs well for all cases except when stochastic external noise is present in the centre of the channel for wavenumbers pairs with nonzero streamwise component.

It is possible to introduce in the objective function of the control problem an extra penalisation of the final state. The resulting control kernels will then also be time dependent. This is the subject for future systematic studies on objective functions. The time varying estimation and control can then be put together to a dynamic compensator and the applied to linear as well as nonlinear flow cases.

References

BALAKRISHNAN, A. V. 1976 *Applied functional analysis*. Springer.

BEWLEY, T. R. 2001 Flow control: new challenges for a new renaissance. *Progress in Aerospace Sciences* **37**, 21–58.

BEWLEY, T. R. & LIU, S. 1998 Optimal and robust control and estimation of linear paths to transition. *J. Fluid Mech.* **365**, 305–349.

BEWLEY, T. R. & PROTAS, B. 2003 Skin friction and pressure: the "footprints" of turbulence. *Physica D* In press.

CHEVALIER, M., HŒPFFNER, J., BEWLEY, T. R. & HENNINGSON, D. S. 2003 State estimation in wall-bounded flow systems. part II : turbulent flow. *To be submitted* .

GUNZBERGER, M. D. 1996 Perspectives in flow control and optimization. *SIAM* .

HANIFI, A., SCHMID, P. J. & HENNINGSON, D. S. 1996 Transient growth in compressible boundary layer flow. *Phys. Fluids* **8**, 826–836.

HENNINGSON, D. S., LUNDBLADH, A. & JOHANSSON, A. V. 1993 A mechanism for bypass transition from localized disturbances in wall-bounded shear flow. *J. Fluid Mech.* **250**, 169–207.

HENNINGSON, D. S. & SCHMID, P. J. 1992 Vector eigenfunction expansions for plane channel flows. *Stud. Appl. Maths* **87**, 15–43.

HUANG, W. & SLOAN, D. M. 1993 The pseudo-spectral method for solving differential eigenvalue problems. *J. Comp. Phys.* **111**, 399–409.

HÖGBERG, M., BEWLEY, T. R. & HENNINGSON, D. S. 2003 Linear feedback control and estimation of transition in plane channel flow. *J. Fluid Mech.* **481**, 149–175.

JOSHI, S. S., SPEYER, J. L. & KIM, J. 1999 Finite dimensional optimal control of poiseuille flow. *J. Guid. Control Dyn.* **22**, 340.

JOVANOVIÌC, M. & BAMIEH, B. 2001*a* Modeling flow statistics using the linearized Navier–Stokes equations. *Proc. 40'th IEEE Conference on decision and control, FL* .

JOVANOVIÌC, M. & BAMIEH, B. 2001*b* The spatio-temporal impulse response of the linearized Navier–Stokes equations. *Proc. American control conference* .

KAILATH, T. 1973 Some new algorithms for recursive estimation in constant linear systems. *IEEE transaction on information theory* **IT-19** (6), 750–760.

KIM, J. 2003 Control of turbulent boundary layers. *Physics of fluids* **15** (5).

KIM, J. & LIM, J. 2000 A linear process in wall-bounded turbulent shear flows. *Phys. Fluids* **12** (8), 1885–1888.

LAUB, A. 1991 *Invariant subspace methods for the numerical solution of Riccati equations*. Springer.

LEE, C., KIM, J., BABCOCK, C. & GOODMAN, R. 1997 Application of neural network to turbulence control for drag reduction. *Phys. Fluids* **9**, 1740–1747.

LEWIS, F. L. & SYRMOS, V. L. 1995 *Optimal control*. Wiley-Interscience.

SCHMID, P. J. & HENNINGSON, D. S. 2001 *Stability and transition in shear flows*. Springer.

THOMAS, A. S. W. 1990 Active wave control of boundary-layer transition. In *Viscous Drag Reduction in Boundary Layers* (eds. D. M. Bushnell & J. N. Hefner),

Progress in Astronautics and Aeronautics, vol. 123. Washington, D.C: American Institute of Aeronautics and Astronautics.

WEIDEMAN, J. A. C. & REDDY, S. C. 2000 A MATLAB differentiation matrix suite. *ACM Transaction of Mathematical Software* **26** (4), 465–519.

Paper 2

2

State estimation in wall-bounded flow systems. Part II : turbulent flow

By M. Chevalier[1,2], J. Hœpffner[2], T. R. Bewley[3] and D. S. Henningson[1,2]

[1]The Swedish Defense Research Agency (FOI), SE-172 90, Stockholm, Sweden
[2]Department of Mechanics, Royal Institute of Technology, S-100 44, Stockholm, Sweden
[3]Department of Mechanical and Aerospace Engineering, University of California San Diego, La Jolla, CA 92093, USA

This work aims at estimating a turbulent channel flow at $Re_\tau = 100$ based on a time history of noisy wall measurements of the flow. We do this by applying plain and extended Kalman filters based on the linearised Navier–Stokes equations together with a stochastic model based on statistics gathered from a direct numerical simulations (DNS) of the same turbulent flow we aim to estimate. By using relevant statistical information when constructing the stochastic model we obtain well resolved estimation gains for all measurements and an improved estimation performance compared with simpler choices of stochastic models. The performance of the Kalman and extended Kalman filter is quantified through DNS of turbulent channel flow using the incompressible Navier–Stokes equations.

1. Introduction

Flow control has received much interest in recent years due to the possible benefits. By, for example, extending the laminar flow region over a wing large savings in terms of fuel consumption could be made. In other applications a turbulent flow state is desirable, for example, when one wants to achieve enhanced mixing in combustion chambers.

Many different strategies to control and reduce the drag in turbulent flows have been proposed and attempted. Over the years the approaches have gone from more intuition based toward more systematic and automated approaches. In order to systemize the control, recent advances in modern control theory have been introduced and applied to fluid mechanical systems. Reviews of recent efforts in flow control with model-based feedback control as well as other strategies can be found in, for example, Bewley (2001), Kim (2003), Gunzberger (1996), Gad-el-Hak (1996), and also in Högberg, Bewley & Henningson (2003).

Linear model-based feedback control based on noisy measurements can be divided in two independent sub problems: the control problem and the estimation problem. The control problem requires full state information to determine an effective feedback control. Full state information however is not accessible in real applications. One can solve instead the estimation problem where time resolved measurements of the flow state with wall sensors are used in an on-line simulation where the flow state is reconstructed. The combined problem of flow control and state estimation is often referred to as a compensator. The effectiveness of the compensator depend on the performance of both sub problems. Even though promising results have been obtained with compensators, as for example in Bewley & Liu (1998) and Högberg *et al.* (2003), much remains to be done on the efficiency of the estimator problem.

An important aspect of the linear optimal estimation problem is how to describe the covariance data that represents the parts of the flow not included in the dynamical model. This is as important as the choice of objective function in the corresponding control problem.

The importance of proper disturbance modeling was understood by Jovanoviè & Bamieh (2001), where the aim was to construct a stochastic disturbance model for the linearised Navier–Stokes equations such that it created second order statistics that matched the statistics of a turbulent channel flow. Nevertheless, little has been accomplished in terms of application of appropriate disturbance models for flow estimation and control in the published literature. In Bewley & Liu (1998), Joshi, Speyer & Kim (1999), and Högberg *et al.* (2003) the covariance of the external disturbances was modeled at single wavenumber pairs by assuming a zero spatial correlation. In a study by Hœpffner *et al.* (2003) another stochastic model for the external disturbances acting on the flow system was proposed. They introduced a spatially correlated model for the external disturbances (models used in previous studies the stochastic model assumed constant variance in the wall-normal direction for the disturbances and zero correlation at different positions between the channel walls). By introducing the new stochastic model, more wall measurements could be computed. This was performed for a transitional channel flow.

In order to further study the impact of the choice of stochastic model we choose to study a turbulent channel flow. In the present paper, we base the stochastic model of the external disturbances on turbulent DNS statistics. By so doing, the stochastic model accounts for nonlinear and turbulent mean flow effects otherwise missing in the linearised Navier–Stokes equations.

1.1. *Outline*

The present work is essentially divided in three parts. In the first part we collect statistical data from direct numerical simulations of turbulent Poiseuille flow. That data is used in the second part of the study, where we compute the optimal estimation gains. The gains are applied to the estimation of a turbulent flow in the last part of this investigation.

In §2, the theory related to the estimation problem is presented. Section 3 contains the description of the computations of the statistics, and in §4, the numerical simulations are presented and discussed. Finally in §5 the results are summarised and some concluding remarks are made.

2. Estimation theory

A general state-space system can be written on the form

$$\dot{q} = Aq + Bf, \quad q(0) = q_0,$$
$$y = Cq + g, \tag{1}$$

where q is the state, A is the linear operator representing the dynamics of the system. The external disturbances f force the state through B, and q_0 is the initial condition. Operator C extracts the measurements from the state and g adds a stochastic measurement noise with given statistical properties, which leaves the actual measured quantity in y. Once we have the physical model on this form, we can apply the linear estimation theory, see for example Lewis & Syrmos (1995).

The aim with this study is to construct the covariance R of the random forcing f, such that it in a statistical sense, represents as much as possible of the physics neglected in the linearised model and subsequently to quantify what impact it will have on the estimation process.

Throughout this work we have chosen to study the incompressible plane channel flow. In order to fit the Navier–Stokes equations into the dynamical model we linearise about the turbulent mean flow profile at a Reynolds number, $Re_\tau = 100$.

2.1. *System dynamics*

In order to construct the operator A, we assume a periodic flow in the streamwise and spanwise directions. This allow a Fourier decomposition into wavenumber pairs (k_x, k_z). This, together with the linearisation of the Navier–Stokes equations and reformulation to the (v, η) form where v is the wall normal velocity and η is the wall normal vorticity, yield the Orr–Sommerfeld/Squire equations

$$\begin{pmatrix} \Delta \dot{\hat{v}} \\ \dot{\hat{\eta}} \end{pmatrix} = \begin{pmatrix} \mathcal{L}_{OS} & 0 \\ \mathcal{L}_C & \mathcal{L}_{SQ} \end{pmatrix} \begin{pmatrix} \hat{v} \\ \hat{\eta} \end{pmatrix}, \tag{2}$$

where

$$\mathcal{L}_{OS} = -ik_x U \Delta + ik_x U'' + \Delta^2/Re,$$
$$\mathcal{L}_{SQ} = -ik_x U + \Delta/Re, \tag{3}$$
$$\mathcal{L}_C = -ik_z U'.$$

Here Re is the Reynolds number based on the centreline velocity and the channel half-width. In terms of equation (1) the state q is defined as

$$q = \begin{pmatrix} \hat{v} \\ \hat{\eta} \end{pmatrix}, \tag{4}$$

The operator A is constructed as

$$A = \begin{pmatrix} \Delta & 0 \\ 0 & I \end{pmatrix}^{-1} \begin{pmatrix} \mathcal{L}_{OS} & 0 \\ \mathcal{L}_C & \mathcal{L}_{SQ} \end{pmatrix}. \tag{5}$$

Above, hats accents ($\hat{\ }$) indicate Fourier transformed quantities but will be left out in the rest of the paper. The Laplacian operator is denoted $\Delta = D^2 - k^2$, where D is the wall-normal derivative and $k^2 = k_x^2 + k_z^2$. For details on this derivation see, for example, Schmid & Henningson (2001).

2.2. *Stochastic forcing*

A simple assumption is to let f be a zero-mean white noise Gaussian process that is uncorrelated in space. But by computing the statistical properties of the turbulent flow, we can improve the dynamical stochastic system to better match the Navier–Stokes equations.

By linearising the incomprehensible Navier–Stokes equations about a turbulent mean flow velocity profile U and decomposing the flow in two parts as

$$u = \tilde{u} + U,$$

where $\tilde{u}$, $\tilde{v}$, $\tilde{w}$, and $\tilde{p}$ are the fluctuating parts of the flow, we get the following nonlinear equations

$$\begin{aligned} \frac{\partial \tilde{u}}{\partial t} + U\frac{\partial \tilde{u}}{\partial x} + \tilde{v}\frac{\partial U}{\partial y} &= -\frac{\partial \tilde{p}}{\partial x} + \frac{1}{Re}\Delta\tilde{u} + f_1, \\ \frac{\partial \tilde{v}}{\partial t} + U\frac{\partial \tilde{v}}{\partial x} &= -\frac{\partial \tilde{p}}{\partial y} + \frac{1}{Re}\Delta\tilde{v} + f_2, \\ \frac{\partial \tilde{w}}{\partial t} + U\frac{\partial \tilde{w}}{\partial x} &= -\frac{\partial \tilde{p}}{\partial z} + \frac{1}{Re}\Delta\tilde{w} + f_3, \end{aligned} \tag{6}$$

where the vector $f = (f_1, f_2, f_3)^T$ constitutes a volume forcing including the terms left out in the linearised equations. This yields the following definition of f,

$$\begin{aligned} f_1 &= -\tilde{u}\frac{\partial \tilde{u}}{\partial x} - \tilde{v}\frac{\partial \tilde{u}}{\partial y} - \tilde{w}\frac{\partial \tilde{u}}{\partial z} - \frac{\partial P}{\partial x} + \frac{1}{Re}\frac{\partial^2 U}{\partial y^2}, \\ f_2 &= -\tilde{u}\frac{\partial \tilde{v}}{\partial x} - \tilde{v}\frac{\partial \tilde{v}}{\partial y} - \tilde{w}\frac{\partial \tilde{v}}{\partial z}, \\ f_3 &= -\tilde{u}\frac{\partial \tilde{w}}{\partial x} - \tilde{v}\frac{\partial \tilde{w}}{\partial y} - \tilde{w}\frac{\partial \tilde{w}}{\partial z}. \end{aligned} \tag{7}$$

Note that since we linearise about a turbulent mean flow profile and not the laminar flow profile we get the additional last two terms in f_1. To transform (6) to v, η form we take the divergence of each equation and add them together which yield an expression for the Laplacian of the pressure perturbation

$$\nabla^2\tilde{p} = -2\frac{\partial U}{\partial y}\frac{\partial \tilde{v}}{\partial x} + \nabla \cdot f. \tag{8}$$

By taking the wall-normal derivative of (8) and applying Δ on equation (6) we eliminate the disturbance pressure and get an equation in v only. We can thus identify the forcing term f_v and f_η as

$$f_v = -\frac{\partial}{\partial y}(\nabla \cdot f) + \Delta f_2 = -\frac{\partial^2 f_1}{\partial y \partial x} + \frac{\partial^2 f_2}{\partial x^2} + \frac{\partial^2 f_2}{\partial z^2} - \frac{\partial^2 f_3}{\partial y \partial z},$$

$$f_\eta = \frac{\partial f_1}{\partial z} - \frac{\partial f_3}{\partial x},$$

(9)

Note that the evolution model is the same independently of what profile we linearise about as long as $U = U(y)$ and $P = P(x)$ since

$$\frac{\partial^2}{\partial y \partial x}\left(-\frac{\partial P}{\partial x} + \frac{1}{Re}\frac{\partial^2 U}{\partial y^2}\right) = 0.$$

(10)

This derivation yields the final form for operator B in the state-space system (1) as

$$B = \begin{pmatrix} \Delta & 0 \\ 0 & I \end{pmatrix}^{-1} \begin{pmatrix} ik_x D & k^2 & ik_z D \\ ik_z & 0 & -ik_x. \end{pmatrix}.$$

(11)

2.3. *Measurements*

We want to extract as much information as possible about the flow from the measurements. The actual measured quantities can be chosen in many different ways but in this study we have chosen to look at the wall-normal derivative of the wall-normal vorticity η_y, the second wall-normal derivative of the wall-normal velocity v_{yy}, and the pressure in the linearised system. This particular choice was convenient since we work with the wall-normal velocity and wall-normal vorticity when we compute the estimation gains. The current choice of measurements gives the following measurement matrix

$$C = \frac{1}{Re}\begin{pmatrix} 0 & D \\ D^2 & 0 \\ D^3/k^2 & 0 \end{pmatrix}.$$

(12)

Each measurement is assumed to be affected by a zero-mean stationary white noise process. The parameters are collected in the 3×3 matrix G, defined as

$$G = \begin{pmatrix} \alpha_\eta & 0 & 0 \\ 0 & \alpha_v & 0 \\ 0 & 0 & \alpha_p \end{pmatrix},$$

(13)

where α_η, α_v, and α_p represent the α-value for the measurements η_y, v_{yy}, and p respectively. The α-values reflect the balance between the magnitude of measurement noise and the magnitude of the model disturbances. A relatively low α-value indicates that the signal-to-noise ratio is high and that we trust the measurement. This in turn will render a strong gain.

If the measured quantity and the model describing the physics were free from modeling error and noise, we could set α close too zero. However, in a DNS, a too strong volume forcing would require shorter time steps.

2.4. *Estimation error*

We build an estimator analogous to the stochastic dynamical system (1) as

$$\dot{\hat{q}} = A\hat{q} - v, \quad \hat{q}(0) = \hat{q}_0,$$
$$\hat{y} = C\hat{q}, \tag{14}$$

where $\hat{q}$ is the estimated state and $\hat{y}$ is the measurement of the estimated flow. The volume forcing v, defined as

$$v = L(y - \hat{y}) = L\tilde{y}, \tag{15}$$

is the feedback of the measurement error $\tilde{y}$ through the estimation feedback gain L. As the error between the plant and the estimator approaches zero the volume forcing also tends to zero. The choice of L is crucial for fast convergence of the estimated system toward the real system. In this study we use an optimal L based on Kalman filter theory and the resulting estimator is known as a Kalman filter (Kalman & Bucy (1960)).

To derive the optimal estimator gain L we first need to define the estimation error system

$$\dot{\tilde{q}} = (A + LC)\tilde{q} + Bf + Lg, \quad \tilde{q}(0) = q_0 - \hat{q}_0, \tag{16}$$

where $\tilde{q} = q - \hat{q}$ is the state estimation error. Thus the error is governed by the dynamics A, the feedback LC and both the process and measurement noise f and g. By taking the mean of equation (16) we get a deterministic system

$$E[\dot{\tilde{q}}] = A_0 E[\tilde{q}] + B E[f] + L E[g], \quad E[\tilde{q}_0] = 0, \tag{17}$$

where the noise terms disappear since we assume that they have zero mean. The corresponding equation for the second-order moment of the estimation error, $P(t) = E[\tilde{q}\tilde{q}^*]$, is the following Lyapunov equation

$$\dot{P}(t) = A_0 P(t) + P(t)A_0^* + \text{cov}(Bf + Lg), \quad P(0) = P_0, \tag{18}$$

where P_0 is the covariance of the initial state estimation error. For details on the derivation see, for example, Balakrishnan (1976).

Better gains will make the expected covariance come closer to zero. To render the computational problem more tractable, we are solving for the stationary infinite time horizon solution which makes the time derivative in the Lyapunov equation (18) disappear. To find the gain L we minimise the expected variance of the estimation error, which can be expressed as the trace of P. This is done for all wavenumber pairs separately.

The error covariance P, with the optimal gain L applied, can be computed by solving an operator Riccati equation

$$AP + PA^* + BRB^* - PC^*G^{-1}CP = 0, \tag{19}$$

and once it is solved we can compute the optimal gain L as follows

$$L = -PC^*G^{-1}. \tag{20}$$

Note that we are going to extract the covariance of f, denoted R, in equation (19) to render a more efficient L, see §3.1 for details.

Estimation gains for single wavenumber pairs for the Orr–Sommerfeld/Squire operator pairs were considered in, for example, Bewley & Liu (1998) and Hœpffner *et al.* (2003). For details on discretization of the operators and implementation issues see, for example, Högberg *et al.* (2003).

3. Statistics

The performance of the estimator can be improved by computing statistical properties of the forcing term f instead of assuming the stochastic model be spatially uncorrelated. A step in that direction is to compute the second order moments of f in a DNS and use that information when solving the estimation problem. To fit the moments into the standard state-space system (1), we model f as a stationary white noise process. Furthermore we assume that we have zero-mean forcing,

$$E[f_i(x, y, z, t)] = 0, \quad i = 1, 2, 3.$$

These assumptions are only a first attempt to evaluate the importance of a better statistical modeling. Extending the state-space model to incorporate both statistics of the dominant frequencies as well as non zero-mean forcing is possible but in this study we have chosen to focus on the spatial behaviour.

The mean quantities that we are interested in are obtained from the expectation operator $E[\cdot]$ defined as the average over all possible realizations of f.

3.1. *Two-point correlation*

In physical space, the covariance of f is defined as

$$\mathrm{cov}(f_i, f_j) = E[f_i(x, y, z, t)f_j(x + r_x, y', z + r_z, t')] = \delta(t - t')R_{ij}(r_x, y, y', r_z),$$

where $\delta(\cdot)$ is Dirac's δ-function and where

$$R_{ij}(r_x, y, y', r_z) = E[f_i(x, y, z)f_j(x + r_x, y', z + r_z)]. \tag{21}$$

Indices $i = 1, 2, 3$ and $j = 1, 2, 3$ represent the covariance components between the corresponding components of f. Note that we treat the individual wavenumber pairs as uncorrelated from each other.

It is more convenient to compute and use the Fourier transform of the two-point correlation R_{ij} rather than using R_{ij} itself since the estimation problem is formulated and implemented in Fourier space. The computation of the covariance is also simpler since the convolution sum over x and z becomes a multiplication over k_x and k_z.

After a Fourier transform of R_{ij} we obtain the two-point spectral density function Θ_{ij} defined as

$$\Theta_{ij}(k_x, y, y', k_z) = \frac{1}{4\pi} \int \int \mathrm{e}^{-ik_x r_x - ik_z r_z} R_{ij}(r_x, y, y', r_z) \, \mathrm{d}r_x \mathrm{d}r_z, \tag{22}$$

and

$$\Theta_{ij}(k_x, y, y', k_z) = E[\hat{f}_i(k_x, y, k_z)\hat{f}_j^*(k_x, y', k_z)], \qquad (23)$$

where again hat accents ($\hat{\,}$) denote Fourier transformed quantities left out in the rest of the paper. Since R_{ij} is a real-valued function, Θ_{ij} will be Hermitian,

$$\Theta_{ij}(k_x, y, y', k_z) = \Theta_{ij}^*(-k_x, y, y', -k_z). \qquad (24)$$

By definition of the two-point spectral density we also have the following symmetry

$$\Theta_{ij}(k_x, y, y', k_z) = \Theta_{ji}^*(k_x, y', y, k_z). \qquad (25)$$

In addition we also have the following two symmetries due to the Navier–Stokes equations and the boundary conditions for channel flow

$$\Theta_{ij}(k_x, y, y', k_z) = \pm\Theta_{ij}^*(k_x, -y, -y', k_z) \qquad (26a)$$

$$\Theta_{ij}(k_x, y, y', k_z) = \pm\Theta_{ij}^*(k_x, y, y', -k_z) \qquad (26b)$$

where the minus sign is used for $i = 2$ or $j = 2$ but not both in equation (26a) and for $i = 3$ or $j = 3$ but not both in equation (26b). See, for example, Moin & Moser (1989) for similar computations. Finally, for later use, Θ is defined as

$$\Theta = \begin{pmatrix} \Theta_{11} & \Theta_{12} & \Theta_{13} \\ \Theta_{21} & \Theta_{22} & \Theta_{23} \\ \Theta_{31} & \Theta_{32} & \Theta_{33} \end{pmatrix},$$

for each wavenumber pair.

4. Numerical results

As described in the previous section the work is divided in three parts. The first part is to gather statistics of the unmodeled physics in the linearised Navier–Stokes equations through the forcing term f. That data is used in the next part when the optimal estimation gains are computed. In the last part the gains are applied when we estimate a fully turbulent flow with both plain and extended Kalman filters. An extended filter differs from the plain filter in that the estimator simulation is governed by the nonlinear Navier–Stokes equations and forced by the estimator forcing v derived from the linearised model of the complete system.

In both the first and third part of this work, direct numerical simulations have been performed of turbulent channel flow at $Re_\tau = 100$. For all DNS calculations the code of Bewley, Moin & Temam (2001) was used. It is a pseudospectral code with 3/2 dealiasing in the streamwise and spanwise directions. In the wall-normal direction, an energy-conserving second-order finite difference technique is applied. The marching in time is performed with a hybrid second-order Crank–Nicolson and third order Runge–Kutta method developed by Aksevoll & Moin (1995). In this scheme, the wall-normal derivatives are treated implicitly to improve the stability properties of the code when using blowing and suction boundary conditions at the walls. The pressure is updated
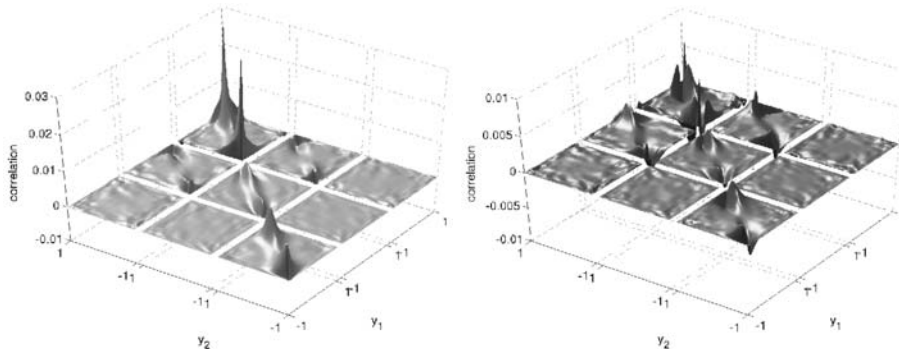
FIGURE 1. The covariance data is taken for wavenumber pair $(k_x = 1.5, k_z = 6.0)$. The nine "squares" correspond to the correlation between the different components of the forcing vector. From top to bottom the components are f_1, f_2, and f_3 on each axis. The side of each square represents the channel flow width. The variance is plotted along the diagonal of each square.

through a fractional step method which also ensures the incompressibility condition.

All simulations are performed for constant mass-flux flow in a computational box of size $4\pi \times 2 \times 4\pi/3$ in $x \times y \times z$ respectively. The resolution is $42 \times 64 \times 42$ Fourier, finite difference, Fourier modes.

4.1. *Steady state statistics of the forcing term*

The covariance of the forcing term $f = (f_1, f_2, f_3)^T$ is sampled during a DNS calculation long enough to obtain converged second-order statistics. In the simulation, the full covariance matrices are computed and all symmetries mentioned in §3.1 are used only in a post processing step to increase the convergence of the data.

In Figure 1 the real (left) and imaginary part (right) of the covariance of f for wavenumber $(k_x = 1.5, k_z = 6.0)$ is plotted. The variance (the diagonal of each square) of the forcing terms is stronger toward the walls as expected due to the stronger shear in that region and the covariance quickly decreases as the wall-normal distance between points increases. Note also that there is a pronounced cross-correlation between f_1 and f_2 but that other cross-correlations between different forcing components are close to zero. This data is qualitatively representative for all wavenumber pairs even though the intensity levels and relative amplitudes differ.

The size of the covariance data is $N_x \times N_z \times N_y^2$ for each correlation component of the forcing vector without exploiting any symmetries, where N_x, N_y, and N_z denote the resolution in the corresponding directions.

Case	α_η	α_v	α_p	R	$J^{1/2}$
1	0.1200	–	–	I	52
2	0.0037	–	–	Θ_{11}	52
3	0.0030	0.0030	0.0075	Θ	53

TABLE 1. The estimation simulations. For the cases when using one measurement, only the corresponding α is relevant since the other measurements are excluded from the C-matrix.

4.2. *Estimation kernels*

As described in section 2.3, in the present formulation there is one parameter to tune for each measurement. This parameter will affect both the strength and the shape of the gain. In order to make a fair comparison between the different stochastic models we construct the following measure

$$J = \int_{-1}^{1} \int_{0}^{L_x} \int_{0}^{L_z} L_{\eta_y}^2 \, \mathrm{d}x \, \mathrm{d}y \, \mathrm{d}z,$$

where L_{η_y}, the gain corresponding to the η_y measurement, is integrated in all three spatial directions. In case 2 and 3 the α_η parameter is tuned so that the integrated strength J is approximately the same and in case 3 all three α parameters are tuned together to render the same strength of J (each α value affects all the gains), see table 1. The reason for only matching the strength of the η_y gain, even in case 3 where we have three gains, is to make the comparison as fair as possible. Each measurement captures different physics in the flow field and we want to see what additional information we get when the two new measurements are added rather than investigating how the strength is distributed over estimator gains and how this affects the estimation process.

In case 3 the total strength of the two other measurements is about 20% stronger than the η_y measurement alone. Note also that α_p is higher than α_η and α_v which means that the pressure gains are relatively weakened. The reason being that, for the same α-value, the pressure measurements are stronger and feeding them back with too strong gains will cause problems in the DNS calculation.

The resulting strength of the gains require no adjustment of the time step in the extended Kalman filter DNS to run properly. For the estimation simulations discussed in section 4.3 we have used gains based on the parameters listed in table 1.

4.3. *Extended Kalman filter simulations*

Two simulations are run in parallel, one representing the "real" flow and the other the estimated flow. The real flow is initiated by a fully turbulent flow field and the estimated flow is initiated by a turbulent mean flow field with no disturbances. In the estimator, the volume forcing v computed from the measurements from both the real and estimated flow and the optimal gains, is

added, and it forces the estimated flow to converge toward the real flow. For both systems the nonlinear Navier–Stokes equations are solved. An estimator that is based on linearized equations and then applied to the full nonlinear system is called an extended Kalman filter.

To evaluate the performance of the estimator we have computed the correlation between the real flow and the estimated flow throughout the domain at each instant of time,

$$\text{corr}_y(q, \hat{q}) = \frac{\int_0^{L_x} \int_0^{L_z} q\hat{q} \, \mathrm{d}x\mathrm{d}z}{\left(\int_0^{L_x} \int_0^{L_z} q^2 \, \mathrm{d}x\mathrm{d}z\right)^{1/2} \left(\int_0^{L_x} \int_0^{L_z} \hat{q}^2 \, \mathrm{d}x\mathrm{d}z\right)^{1/2}}, \tag{27}$$

where q and $\hat{q}$ represent either u, v, w, or p from the real and estimated flow, respectively. This quantity is averaged in time where the short initial transient in the correlation is omitted. The transient, as can be seen for the streamwise velocity u in Figure 5, is quickly passed and the correlation levels out and stabilises with small fluctuations around some value depending on how far from the walls we look.

Another useful quantity to study is the error between the real and estimated flow, also here computed for each flow variable separately,

$$\text{errn}_y(q, \hat{q}) = \frac{\left(\int_0^{L_x} \int_0^{L_z} (\hat{q} - q)^2 \, \mathrm{d}x\mathrm{d}z\right)^{1/2}}{\left(\int_0^{L_x} \int_0^{L_z} q^2 \, \mathrm{d}x\mathrm{d}z\right)^{1/2}}. \tag{28}$$

In another study (Bewley & Protas (2003)), a turbulent channel flow at $Re_\tau = 180$ is estimated from limited measurements with two different methods. The first method uses Taylor series expansions of the measurements and it is shown that the flow state can be uniquely determined from the wall measurements if no noise is present. However, this requires that one can compute higher and higher derivatives of the measurements without loss of accuracy to converge toward the proper flow from these generally noisy measurements. The other method is an adjoint approach where one tries to find the initial condition for the flow that at a certain time gives the best match for all wall measurements during all time. The adjoint method is computationally demanding but should instead give a very good estimate of the flow at a certain time. Since the present results are computed for a lower Reynolds number we can compare the performance only qualitatively, but the general behaviour is the similar.

4.3.1. *One measurement - η_y with old and new covariance data*

The old covariance data refers to previous studies where the covariance R was chosen as the identity matrix $R = I$, as for example in Högberg *et al.* (2003) and new covariance data refers to using Θ in (22) for the statistics of f. From Figure 2 and Figure 3 one can see that only a marginal improvement in terms of correlation and error is achieved. However, the important result is that we are now able to compute well resolved estimation gains for all three measurements
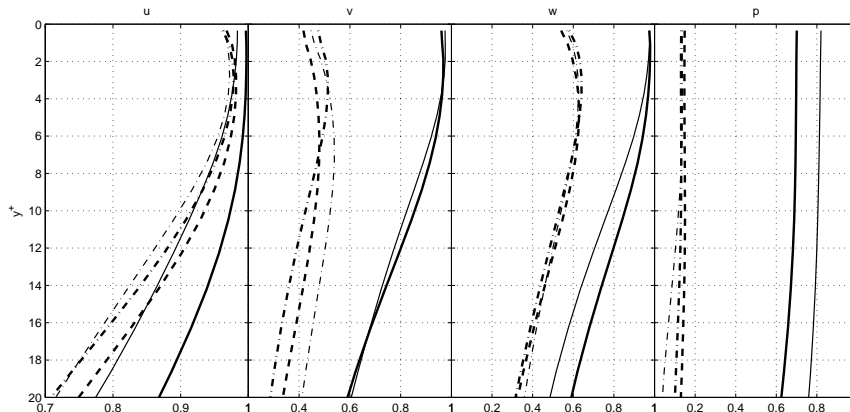
FIGURE 2. From left to right, the figure shows the correlation, defined as in equation (27), along the y-axis for the primitive quantities u, v, w, and pressure. The solid line denotes estimation performed with all three measurements and gains based on turbulence statistics. The dashed line denotes the estimator performance using only the η_y measurement with gains based on the same statistics. The dash-dotted line is the correlation when using the identity matrix as stochastic model instead. The thick lines represent the extended Kalman filter correlation, whereas the thin lines represent the plain Kalman filter correlation.

which was not the case before. The correlation for the u-velocity component is close to one (perfect correlation) while the other components show only weak correlation. This is due to the fact that the streamwise disturbance velocity holds more energy than the other components and that with only the η_y measurement we are missing a lot of information about what happens in the flow.

For both cases and all primitive variables the correlation drops off once we get beyond $y^+ \approx 10$.

4.3.2. *Three measurements*

With the new stochastic model it is now possible to compute well resolved gains for all three measurements which was not possible before with the numerical scheme that we have used. For details on how that scheme has been applied to our estimation problem see, for example, Högberg *et al.* (2003).

In Figure 2 we can clearly see that the correlation between the real and estimated flow for v, w, and p is greatly improved when the additional measurements are included. Also the correlation for u is improved. However, the strongest improvement in terms of correlation appears for the pressure which
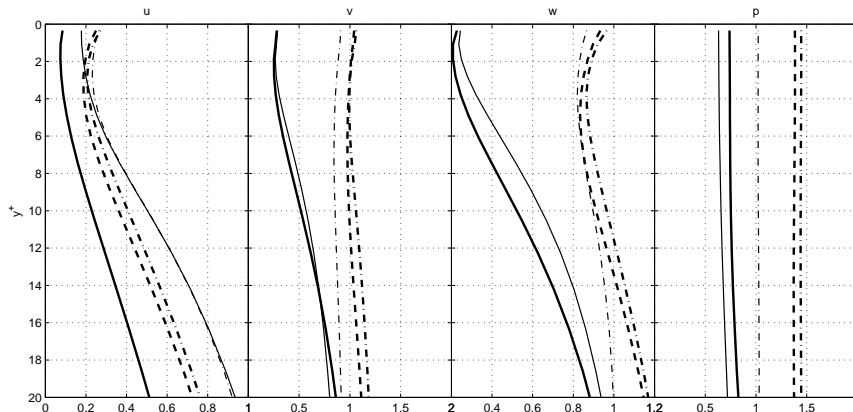
FIGURE 3. The same setup as in Figure 2 but here the relative estimation error, defined as in equation (28), is plotted instead of the correlation.

is clearly due to the additional pressure measurement. For the v and w correlation we get smaller improvements but they contain less energy and since we minimise the expected energy of the estimation error their importance is relatively lower.

4.4. *Plain Kalman filter simulations*

The procedure for the plain Kalman filter is the same as for the extended Kalman filter simulations as described in section 4.3. Here, however we enforce the turbulent mean flow profile that we linearised about in the estimator initially and allow no nonlinear interactions to take place. The plain Kalman filter results are shown in Figure 2 and Figure 3 with thin lines. For the u and w correlation there is a clear difference between the linear and nonlinear filter which is expected, but surprisingly the pressure correlation in the plain filter is even better than the correlation from the nonlinear filter. This might have to do with the fact that in the plain filter, we actually apply the filter to the system of equations it is actually constructed for.

In Figure 4, an instantaneous plot of the v velocity component is shown at $y^+ = 10$ for the flow field and the two different filters, all based on three measurements. Similar main structures are present in all three flows. At some instants of time the plain Kalman filter even has a better match compared to the extended Kalman filter with the real flow but Figure 4 represents the general picture. The plain Kalman filter performance also drops more quickly as the wall normal distance is increased.
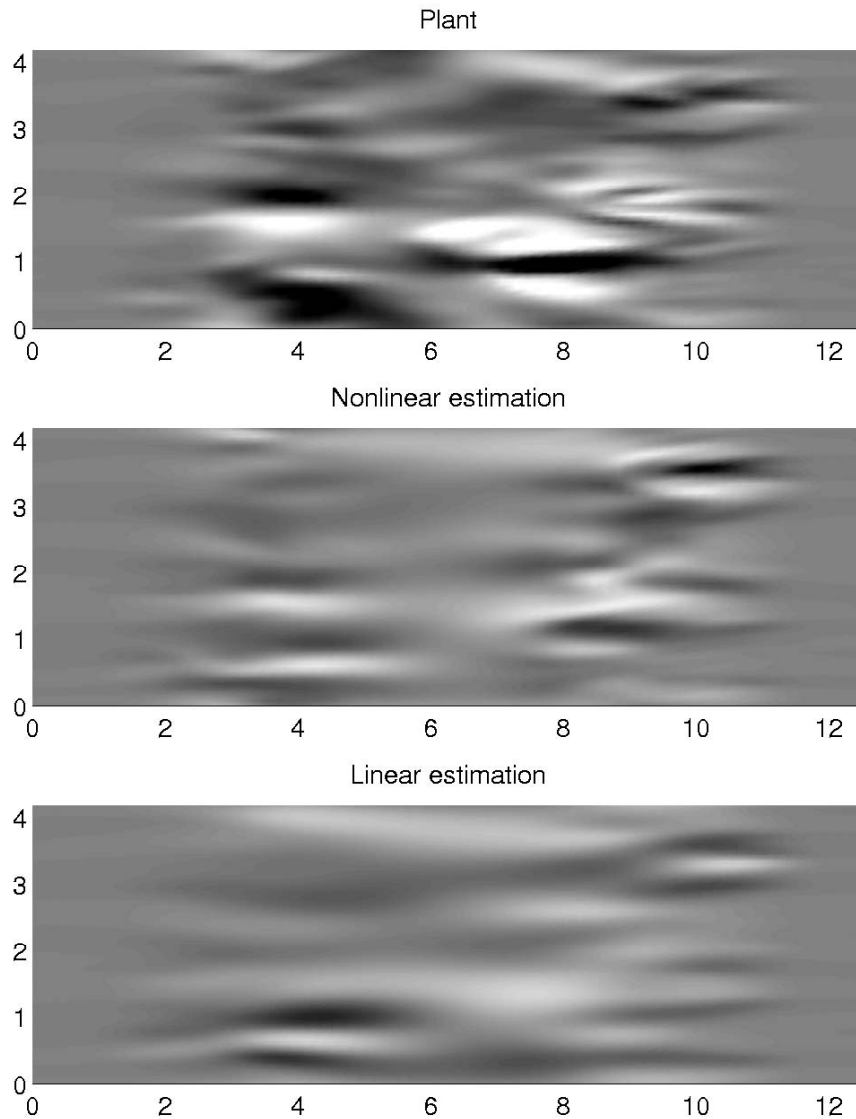
Plant

Nonlinear estimation

Linear estimation

FIGURE 4. Wall normal velocity component v plotted at $y^+ = 10$. In the top figure the flow is plotted. The middle plot shows the velocity field reproduced by the extended Kalman filter and the bottom plot shows the velocity field reproduced by the plain Kalman filter. The contour levels range from -1 to 1 where black and white represent the lower and upper bound respectively.
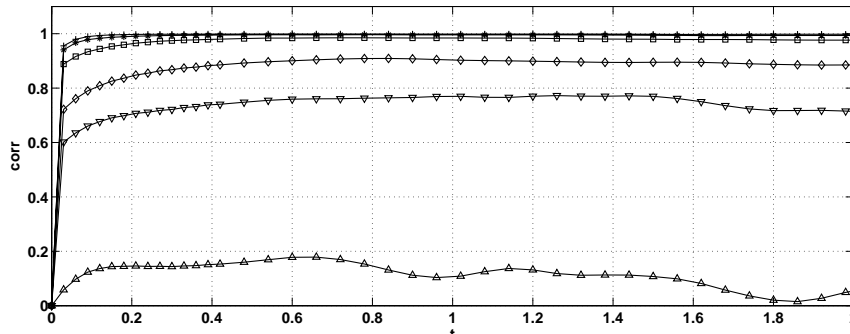
FIGURE 5. The transient of the for the streamwise velocity u at $y^+ = 1.5$, $y^+ = 5.5$, $y^+ = 9.7$, $y^+ = 19.8$, $y^+ = 31.5$, and along the channel centreline for case 3 in table 1.

5. Conclusions

We have shown that by using the available statistical information about the full nonlinear system, and including that information into the estimation gain computation, we can compute gains for other measurements than just η_y and get a better correlation between the real and estimated flow, both measured in maximum correlation as well as how far into the channel the correlation reaches compared to using a spatially uncorrelated stochastic model. Also, the estimation gains can be transformed to physical space to form localised kernels.

In another study, Hœpffner *et al.* (2003), estimation of a transitional flow is investigated and it is shown that a spatial Gaussian distribution model for the covariance is enough to get well-resolved estimation gains. That fact together with the result from the present study indicates that the choice of the disturbance model is important but that a detailed modeling may be less important.

The plain Kalman filter compared to the extended Kalman filter is performing surprisingly well. The estimated state from the plain filter degrades faster with the wall-normal distance but the main structures are captured close to the wall even though the strength of the structures in general is weaker. The extended Kalman filter manages to capture the structures further into the domain and also with a more correct strength.

To further improve the covariance modeling of the forcing f, we can take into account dominant frequencies of the "shape" functions that we can extract from the covariance data for each wavenumber pair and by so doing incorporate also temporal information about the turbulent flow. One other limiting assumption in the present work is that we assume that the forcing term f has zero mean. In theory, it is straightforward to extend the model to include both these effects.

References

AKSEVOLL, K. & MOIN, P. 1995 Large eddy simulations of turbulent confined coannular jets and turbulent flow over a backward facing step. Technical Report Report TF-63. Thermosciences Division, Dept. of Mech. Eng., Stanford University.

BALAKRISHNAN, A. V. 1976 *Applied functional analysis*. Springer.

BEWLEY, T. R. 2001 Flow control: new challenges for a new renaissance. *Progress in Aerospace Sciences* **37**, 21–58.

BEWLEY, T. R. & LIU, S. 1998 Optimal and robust control and estimation of linear paths to transition. *J. Fluid Mech.* **365**, 305–349.

BEWLEY, T. R., MOIN, P. & TEMAM, R. 2001 DNS-based predictive control of turbulence: an optimal benchmark for feedback algorithms. *J. Fluid Mech.* **447**, 179–225.

BEWLEY, T. R. & PROTAS, B. 2003 Skin friction and pressure: the "footprints" of turbulence. *Physica D* In press.

GAD-EL-HAK, M. 1996 Modern developments in flow control. *Appl. Mech. Rev.* **49** (7), 364–379.

GUNZBERGER, M. D. 1996 Perspectives in flow control and optimization. *SIAM* .

HŒPFFNER, J., CHEVALIER, M., BEWLEY, T. R. & HENNINGSON, D. S. 2003 State estimation in wall-bounded flow systems. part I : laminar flow. *J. Fluid Mech.* Submitted.

HÖGBERG, M., BEWLEY, T. R. & HENNINGSON, D. S. 2003*a* Linear feedback control and estimation of transition in plane channel flow. *J. Fluid Mech.* **481**, 149–175.

HÖGBERG, M., CHEVALIER, M. & HENNINGSON, D. S. 2003*b* Linear compensator control of a pointsource induced perturbation in a falker–skan–cooke boundary layer. *Phys. Fluids* Accepted.

JOSHI, S. S., SPEYER, J. L. & KIM, J. 1999 Finite dimensional optimal control of poiseuille flow. *J. Guid. Control Dyn.* **22**, 340.

JOVANOVIÇ, M. & BAMIEH, B. 2001 Modeling flow statistics using the linearized Navier–Stokes equations. *Proc. 40'th IEEE Conference on decision and control, FL* .

KALMAN, R. & BUCY, R. 1960 New results in linear filtering and prediction theory. *ASME Transactions, Series D: Journal of basic Engineering* **83**, 95–108.

KIM, J. 2003 Control of turbulent boundary layers. *Physics of fluids* **15** (5).

LEWIS, F. L. & SYRMOS, V. L. 1995 *Optimal control*. Wiley-Interscience.

MOIN, P. & MOSER, R. D. 1989 Characteristic-eddy decomposition of turbulence in a channel. *J. Fluid Mech.* **200**, 471–509.

SCHMID, P. J. & HENNINGSON, D. S. 2001 *Stability and transition in shear flows*. Springer.

Paper 3

3

Model reduction applied to control of wall-bounded flow systems

By J. Hœpffner[1] & D. S. Henningson[1,2]

[1]Department of Mechanics, Royal Institute of Technology, S-100 44, Stockholm, Sweden

[2]The Swedish Defense Research Agency (FOI), SE-172 90, Stockholm, Sweden

Many complex flows exhibit low-dimensionality. The central dynamical mechanisms can thus be targeted in a low-dimensional model. Linear system theory provides us with numerous techniques to achieve the reduction of dynamic models. We investigate in this paper the control of small disturbances in the plane channel flow, and apply modal truncation to the high-order controller designed using optimal control theory. It is found that a controller with moderate strength can be highly truncated with little degradation of the control performance.

1. Introduction

The apparent low-dimensionality of many commonly studied flows can be seen by proper orthogonal decomposition (POD) i.e. by extracting the most energetic coherent structures of the flow. Most of the energy content of the flow is typically contained in a small number of the extracted modes. In addition, it is sometimes not necessary to know the evolution of the complete flow state. For instance, small scales of the motion are not resolved in turbulence modeling. An other example is the dynamical system whose input-output response only plays a role. In this case, states immaterial to the system response can be removed with little deterioration.

Need for low-order models is widespread. A simple model exhibit the fundamental mechanism of the system studied and enlighten the underlying physics. The need also comes from engineering, and in particular in the domain of control. Recent advances of control theory lead to controllers with size of the same order than the model for the system or even higher. This limits drastically the implementability since the on-line computation required by the controller have to be fast enough to catch up with the evolution of the real systems.

Flow control is recently subject of much research effort. All types of control objectives can be considered as for instance preventing the growth of small disturbances to a basic flow, avoiding separation, relaminarizing turbulent flows, or even locking instationnary processes. Particularly, flow feedback control based

on linear control theory has been studied in many aspects (see e.g. Bewley (2001)). Such systems are typically of large order and with physical processes relatively rapid. Real implementation would greatly benefit from an efficient model reduction.

Control theory provides well developed tools for controller reduction for linear systems. Extensive description can be found in Obinata & Anderson (2001). To obtain a low order controller, one can either design directly a low order controller for a high order system (direct method). Such method are often computationally chalenging and do not rely on standard controller design method as LQG, or $\mathcal{H}_\infty$. One can alternatively design a low order controller by a standard method, either by first reducing the order of the system to be controlled, and then designing the controller, or by designing a high order controller and reduce it afterward. Techniques for the later are becoming available, that not only take the controller into account, but also the system that is controlled. That way, one can seek to maintain the closed loop performance or retain stability through the reduction. Note that it is more attractive to first design a high order controller using the high order model of the system and then reduce it, since one wants to introduce the reduction error as late as possible. This should be done only if the cost for the controller computation precludes from designing it using the full order system.

Nevertheless, this paper is a preliminary study. We apply here a simple model reduction technique, i.e. we apply model reduction to the controller instead of controller reduction. That way, we have no formal guarantee for maintained closed loop performance. The most widely used procedures for model reduction rely on projection of the system on a reduced linear subspace, assuming then the states discarded in the projection to be zero as in the truncation method, or fixing them to their steady state as in the singular perturbation method. For those method, the critical step is the determination of a subspace within which most of the dynamics takes place. This can as a first choice be done by selection of a subset of eigenmodes of the system, since they carry a physical meaning. For example highly damped modes may contribute little to the dynamics. In a numerical setting, spurious modes originating from the discretization of an infinite dimensional system may be removed.

The selection of this subspace can also be justified from an input-output point of view, for example, the system to be reduced can be a controller: its input is the measurements from the flow system (for instance the wall shear stress), and its output is the control to be performed in the flow (for instance blowing and suction at the walls). Its states that are not affected by the input i.e uncontrollable, and are not detectable at the output i.e. unobservable, play no role in the performance of the closed loop system. They may thus be discarded. That way, states that are little controllable or little observable can be progressively removed. A measure of the individual controllability and observability of the states is provided by the modal residuals as will be exemplified in this paper.

In the present paper, we investigate the model reduction for the control of small disturbances in the plane channel flow. The technique used is the modal truncation, i.e. truncation of states in the basis of the eigenmodes. After introducing two useful result of linear filtering in §1, we describe the flow system and the standard LQG control procedure in §2, introducing as well the stochastic model for the incoming stochastic disturbances and the definition of the measurement and actuation. The full order controller will then be reduced in section §3 and applied to the full order flow system in section §4.

2. Two useful results from linear filtering

The flow system studied here is subject to stochastic disturbances. These disturbance will excite the state of the system. The state and quantities extracted from the state (e.g. the measurement or the energy) will thus be stochastic quantities that we can describe by their mean and covariance. We introduce here two useful results of linear filtering. More details can be found in Söderström (2002).

For a linear dynamic system forced by a stochastic process f with covariance R_{ff} and uncorrelated in time

$$\dot{x} = Ax + Bf,$$

the covariance R_{xx} of the state x is the solution of a Lyapunov equation

$$AR_{xx} + R_{xx}A^+ + R_{ff} = 0. \tag{1}$$

Where the superscript+ stands for the associated adjoint operator (hermitian transpose for discrete operators). The diagonal elements of the covariance operator are the variances of the associated state variables, and the total flow energy can be extracted from these diagonal elements. We will use this equation for example to compute the flow energy due to a chosen external disturbances, and assess the control performance.

With B a linear operator, the covariance R_{ll} of $l = Bf$ is

$$R_{ll} = BR_{ff}B^+. \tag{2}$$

We will use this relation for instance to compute the variance of the sensor signal in the flow to be controlled, knowing the covariance of the flow state from (1).

3. Flow and control formulation

Here we briefly recall the flow configuration and the control formulation that we later use for the reduction. For more details on the flow, the numerical method, and the estimation part, see Hœpffner *et al.* (2003). For the formulation of the controller, including the lifting technique, see Högberg *et al.* (2003). For more on the control see e.g. Green & Limebeer (1995).

3.1. *Flow configuration*

We consider here the 3D flow between two infinite flat plates (at $y = \pm 1$) driven by a pressure gradient in the streamwise (x) direction. we model the flow as being periodic in the streamwise and spanwise directions x and z, using a computational domain of sufficient extent in these directions. This approach allows all variables with spatial variation to be expanded in Fourier series. We assume low amplitude perturbations, so that nonlinear effects can be disregarded. We thus use the linearised Navier–Stokes equations, Fourier transformed in x and z, i.e. the Orr–Sommerfeld/Squire equations. We can write the dynamic system in state space form

$$\dot{q} = A_h q + B_1 f$$

with flow state q, dynamic operator A_h, and forcing due to external sources f.

3.1.1. *Sensors*

We assume that we can measure the continuous distribution of streamwise and spanwise skin friction, and pressure on the wall. We will use this information to estimate the instantaneous flow state. Each of the three measurements is assumed to be corrupted by sensor noise, modeled as independent white random processes, the amplitude of which is determined by the assumed quality of the sensors. To decide the sensor noise variance, we first compute the covariance of the flow state when excited by the external disturbance, using (1). From this covariance we can obtain the variance of the individual sensor signals with use of (2). We thus set the variance of the individual sensor noises as a proportion of the signal variance. That way we specify the individual sensor quality by its signal to noise ratio.

3.1.2. *External disturbances*

We will assume the external disturbance forcing f to be a stationary white Gaussian process with zero mean. Our model for the covariance of f assumes that the disturbance has a localised structure, i.e., the two-point correlation of the disturbance decays exponentially with distance, and the correlations between forcing terms on different velocity components are zero. Furthermore, we assume stronger disturbances close to the wall, where wall roughness is likely to disturb the velocity field. We thus have the (two point) covariance for the disturbance

$$R_{f_i f_j}(y, y') = a \; r(y) \delta_{ij} e^{-\frac{(y-y')^2}{2s_y}} \tag{3}$$

where f_1, f_2 and f_3 are the external forcing on the streamwise, wall-normal, and spanwise velocity component u, v, and w. The amplitude factor a is used to scale the forcing to have a unit flow expected energy. The function r specifies the variation of the forcing variance with the wall normal coordinate. In this study, we use $r(y) = y^{10}$ to have a relatively stronger forcing in the near-wall region. The parameter s_y determines the extent of the two point correlation between the walls. We use $s_y = 0.1$ throughout this paper.

3.1.3. *Actuation*

The actuation is blowing and suction at the wall (wall transpiration) The forcing thus introduced in the system by the boundary condition ϕ on the wall-normal velocity is lifted from the wall to a volume forcing by a splitting of the state $q(t)$ into homogeneous $q(t)_h$ and inhomogeneous parts $\phi(t)q_p$ such that $q = q_h + \phi q_p$. We then follow the evolution of the system through the homogeneous part and force it with the blowing and suction by mean of the function q_p . The inhomogeneous part q_p satisfies the non-zero boundary condition on the wall normal velocity. The dynamic equation thus reads

$$\dot{q}_h = A_h q_h + \phi A_h q_p - \dot{\phi} q_p.$$

It appears that we force the dynamics of the homogeneous part of the state with the time derivative of the blowing and suction $\dot{\phi}$. Note that we have blowing and actuation at both walls, so that ϕ is a vector with two components. Similarly, q_p is composed of a function satisfying the non homogeneous boundary conditions at the top wall, and a function satisfying the non homogeneous boundary condition at the bottom wall $q_p = \left(\ q_p^t, q_p^b \ \right)$. The augmented state $x = (q_h, \phi)^T$ obeys the forcing problem:

$$\dot{x} = Ax + B_1 f + B_2 u \tag{4}$$

where

$$A = \left(\begin{array}{cc} A_h & A_h q_p \\ 0 & 0 \end{array} \right), B_2 = \left(\begin{array}{c} -q_p \\ I \end{array} \right), u = \dot{\phi}. \tag{5}$$

The function q_p may then as well be chosen to satisfy a numerically convenient equation on the interior of the domain. In the present case we define the lifting with the proper boundary conditions via the equation $A_h q_p = 0$ so that q_p is a stationary solution of the forced problem with unit blowing at the walls.

3.1.4. *Control objective*

Our control objective is to minimise the kinetic energy of the fluctuation about the laminar mean profile. Hindering the growth of small perturbation thus prevent secondary instabilities and further transition to turbulence. This objective can be expressed in a quadratic norm

$$\mathcal{J}(q, u) = E[||q|| + \ell^2 ||u||_2] \tag{6}$$

where $E[\cdot]$ is the expectation operator and $||q||$ denotes the instantaneous flow energy. Note that the control signal is the time derivative of the blowing and suction, so that we both penalise the blowing and suction amplitude through the flow energy term, and the time derivative of the blowing and suction, enforcing thus a smooth actuation.

3.2. *Control formulation*

We recall the LQG control formulation, see e.g. Green & Limebeer (1995). The systems can be written in state space form

$$\begin{cases} \dot{q} = Aq + B_1 f + B_2 u \\ y = Cq + g. \end{cases} \tag{7}$$

$$\begin{cases} \dot{\hat{q}} = A\hat{q} + B_2 u - v \\ \hat{y} = C\hat{q}. \end{cases} \tag{8}$$

$$v = L\tilde{y} = L(y - \hat{y}), \quad u = K\hat{q}. \tag{9}$$

In (7), the flow state q follow the evolution due to the linear dynamic operator A, and is affected by disturbances on the form of a stochastic forcing f through B_1, and can be controlled by the actuation u through B_2. The measurement vector y is extracted from the state, using the measurement matrix C, and corrupted by the sensor noise g. The estimator is build with analogous form in (8). The estimator state $\hat{q}$ follow the same dynamics as the flow states q and is forced by a feedback v of the measurement through the estimation gain L in (9). The flow and estimator states q and $\hat{q}$ are in turn forced as a feedback u of the estimated state through the control gain K. The optimal feedback gains L and K can be computed independently for each wave number pair by solving two Riccati equations, see e.g. Glover *et al.* (1989).

The operators for the augmented state are decomposed into homogeneous part (subscript h) and inhomogeneous part (subscript ϕ).

$$B_2 u = \begin{pmatrix} B_h \\ I \end{pmatrix} u, \quad B_1 f = \begin{pmatrix} B_{h1} \\ 0 \end{pmatrix} f,$$

$$y = Cx = \begin{pmatrix} C_h, C_\phi \end{pmatrix} \begin{pmatrix} q \\ \phi \end{pmatrix}, \quad u = \begin{pmatrix} K_h, K_\phi \end{pmatrix} \begin{pmatrix} \hat{q} \\ \phi \end{pmatrix}$$

Combining the estimator and the controller, and introducing the feedback laws L and K, we obtain a state space formulation for the complete closed loop system

$$\begin{pmatrix} \dot{q} \\ \dot{\phi} \\ \dot{\hat{q}} \end{pmatrix} = \begin{pmatrix} A_h & B_h K_\phi & B_h K_h \\ 0 & K_\phi & K_h \\ -L_h C_h & B_h K_\phi & A_h + B_h K_h + L_h C_h \end{pmatrix} \begin{pmatrix} q \\ \phi \\ \hat{q} \end{pmatrix} + \begin{pmatrix} B_{h1} f \\ 0 \\ -L_h g \end{pmatrix}.$$

We can rewrite this system in a more compact form

$$\begin{pmatrix} \dot{x} \\ \dot{\hat{q}} \end{pmatrix} = \begin{pmatrix} A & B_s C_0 \\ B_0 C_s & A_0 \end{pmatrix} \begin{pmatrix} x \\ \hat{q} \end{pmatrix} + \begin{pmatrix} f_s \\ f_0 \end{pmatrix}$$

with

$$A_0 = A_h + B_h K_h + L_h C_h,$$

$$B_0 = \begin{pmatrix} -Lh, B_h \end{pmatrix}, \quad C_0 = K_h, \quad f_0 = -Lhg$$

$$B_s = \begin{pmatrix} B_h \\ I \end{pmatrix}, \quad C_s = \begin{pmatrix} C_h & 0 \\ 0 & K_\phi \end{pmatrix}, \quad f_s = \begin{pmatrix} B_{h1} f \\ 0 \end{pmatrix}.$$

In this form, we can identify the system to be controlled

$$\begin{cases} \dot{x} = Aq_h + B_s u + f_s \\ y = C_s x \end{cases} \tag{10}$$

and the controller

$$\begin{cases} \dot{\hat{q}}_h = A_0 \hat{q}_h + B_0 y + f_0 \\ u = C_0 \hat{q}_h \end{cases} \tag{11}$$

Note that the measurement is the output from the system to be controlled, and is the input of the controller. Similarly, the control signal is the output of the controller, but is the input of the system to be controlled. The connection of those two system is the closed loop control system.

3.3. *Numerics*

To compute the feedback in this problem, we discretize the control equations and solve them in the finite-dimensional setting. The discrete operators are obtained through enforcement of the Orr–Sommerfeld/Squire equations at each point of the Gauss–Lobatto grid, using a Chebyshev collocation scheme (see e.g. Weideman & Reddy (2000)). For all presented cases, the system was discretized using 152 Chebychev polynomials in the wall normal direction.

4. Reduction of the controller

The controller system has as input the measurement from the flow and as output the optimal control signal. We can discard from the dynamics of the controller the states that contributes little to its input-output response. We will first project a state space representation of the controller in the basis of its eigenmodes, and then truncate eigenmodes that are little controllable, little observable and highly damped, i.e. that are little affected by the input, and that affect little the output. The reduction will be performed on the controller system in (11).

4.1. *Projection*

The projection can be performed by means of a set of vector biorthonormal to the basis of the eigenvector of the controller dynamics A_0. A good choice are the eigenvector of the adjoint of the controller dynamics, A_0^+. The adjoint is defined through the choice of an inner-product. We chose here the energy inner-product. given arbitrary test functions q_1 and q_2 in the proper space we define

$$< A_0 q_1, q_2 > = < q_1, A_0^+ q_2 > + \text{boundary terms}$$

and the boundary terms here vanish since the controller state on which A_0 operates, is homogeneous. We have the biorthonormality relation

$$< q_i, q_j^+ > = \delta_{ij}$$

if q_i and q_j^+ are the properly scaled eigenvectors of respectively A_0 and its adjoint.

In the case of the reduction of the controller, there is no available analytical expression of the adjoint (on the contrary to the adjoint of the Orr–Sommerfeld/Squire equation for instance) since the feedback is optimised numerically. We thus use the discrete controller dynamics A_0 and its discrete adjoint A_0^+

$$A_0^+ = Q^{-1} A_0^H Q$$

where the superscript H stands for the hermitian transpose, and where Q is the energy measure matrix. We can now define the discrete energy inner-product

$$< q_1, q_2 >= q_2^H Q q_1.$$

Note that Q is positive definite, so that its inverse is well behaved.

It is now straightforward to project the controller state q, the dynamics A_0, and the input and output operators B_0 and C_0

$$\begin{cases} \dot{k} = A_0^M k + B_0^M y \\ u = C_0^M k \end{cases}$$

with

$$k_i =< q, q_i^+ >, \quad A_0^M(i,j) =< A_0, q_i^+ > q_j,$$
$$B_0^M(i) =< B_0, q_i^+ >, \quad C_0^M(j) = C_0 q_j$$

where the superscript M stands for "modal", i.e. expanded in the basis of the eigenmodes. Naturally, A_0^M is the diagonal matrix of the eigenvalues λ_i of A_0 and k_i are the expantion coeficient of the state on the basis of the eigenvectors. Recall that we have 6 measurement (two components of the skin friction and pressure at both walls) and 2 actuation variables (wall normal velocity at both walls) so that B_0 and C_0 are matrices. The projected system thus writes

$$\begin{cases} \begin{pmatrix} \dot{k}_1 \\ \dot{k}_2 \\ \vdots \\ \dot{k}_N \end{pmatrix} = \begin{pmatrix} \lambda_1 & 0 & \dots & 0 \\ 0 & \lambda_2 & \dots & 0 \\ \vdots & \vdots & \ddots & \vdots \\ 0 & 0 & \dots & \lambda_N \end{pmatrix} \begin{pmatrix} k_1 \\ k_2 \\ \vdots \\ k_N \end{pmatrix} + \begin{pmatrix} < B_0, q_1^+ > \\ < B_0, q_2^+ > \\ \vdots \\ < B_0, q_N^+ > \end{pmatrix} \begin{pmatrix} y_1 \\ \vdots \\ y_6 \end{pmatrix} \\ \begin{pmatrix} u_1 \\ u_2 \end{pmatrix} = \begin{pmatrix} C_0 q_1, C_0 q_2, \dots, C_0 q_N \end{pmatrix} \begin{pmatrix} k_1 \\ k_2 \\ \vdots \\ k_N \end{pmatrix} \end{cases}$$

$$(12)$$

4.2. Modal residuals and truncation

The dynamical system is now expressed in a convenient basis for truncation, since the states are decoupled from each other. We can now proceed to the truncation. We will introduce the modal residuals as a truncation criterion.

The measurement vector y will affect the eigenmode i through the input $f_i = || < B_0, q_i^+ > ||_\infty$. We call this coefficient the control modal residual. Similarly $g_i = ||C_0 q_i||_\infty$ is the observability modal residual for eigenmode i. It

is clear from 12 that a zero f_i will forbid any input to excite the associated k_i as well as a zero g_i would make the evolution of the corresponding mode k_i undetectable at the output. The exponential decay rate of a single mode affects as well its role in the system response. A highly damped mode can be discarded. The truncation criterion thus writes

$$c_i = \frac{f_i g_i}{-\Re(\lambda_i)}.$$

It was found in Hœpffner & Henningson (2004) that the controller system A_0 can be unstable, even though the full order controller by construction stabilises the flow. The possibly unstable eigenmodes were retained in this study.

5. Results on modal truncation

In this section, we will show the performance of the controller, and see how this performance is affected by the reduction. We test the controller on three isolated wavenumber pairs $(k_x, k_z) =$(0,2), (1,1), and (1,0). Those three wavenumber pair present typical behaviour in flow transition. (0,2) correspond to streamwise elongated structures. This is where there is highest potential for initial transient energy growth (see e.g. Schmid & Henningson (2001)). The Fourier mode (1,1) correspond to oblique waves. There is less potential for transient growth, but oblique Fourier components are essential in transition to turbulence, i.e. where secondary instability processes take place. The Fourier mode (1,0) correspond to two dimensional waves, propagating in the direction of the flow. This is the region of Fourier space where the first linear instability appears when the Reynolds number is increased.

5.1. *Test case*

Each of those wavenumber pairs is forced with the same stochastic volume forcing, normalised such that the resulting flow has unit expected energy. The forcing is chosen to be stronger close to the walls. It was noted in Hœpffner *et al.* (2003) that oblique and 2D modes have eigenmodes that are difficult to detect, because they have no support at the wall. We thus restrict the flow case to a forcing that would not excite those centre modes. We assume moderate quality sensors, for which the ratio of the signal variance to the noise variance is 2. We will then play with the control penalty, allowing stronger or weaker control, and we will see how this affect the performance of the controller, and the performance degradation with truncation.

We found that the stronger the controller is, the best the performance, but also the faster the performance drops when it is truncated. If the controller is excessively truncated, it may even destabilise the flow. On the other hand, a milder controller will have lesser performance, but can be highly truncated with little performance loss. In the result shown here, we chose the control penalty and measurement noise to obtain little performance degradation with truncation and still maintain a good full order performance.
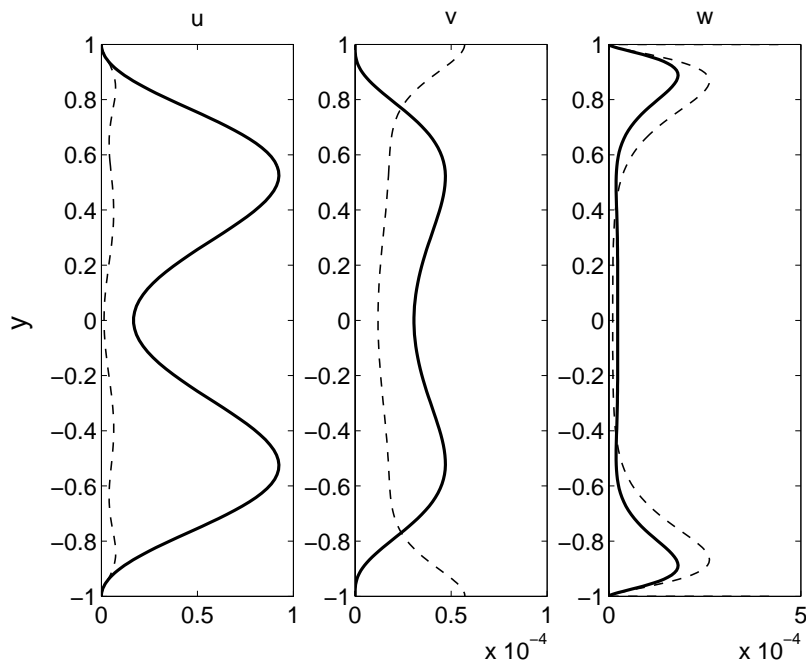
FIGURE 1. Variance of the individual components of the velocity for the wavenumber pair (0,2), for no control (solid) and full order control (dashed). One clearly sees that most of the flow energy is located in the streamwise component of the velocity (left). The actuation at both walls is visible by the nonzero variance of the wall normal velocity component at both walls (centre). One also sees on the spanwise component of the velocity (right) that some energy is input to the system by the actuation.

5.1.1. *Amplitude of the forcing*

The energy of the controlled flow is not zero at the walls, due to the blowing and suction. This effect can be clearly seen when plotting the variance of each velocity component separately, as figure 1, since the wall normal velocity contributes less to the total energy but is directly affected by the actuation. It is known that streamwise elongated vortices of the order $1/Re$ can generate streamwise streaks of order one by interaction with the mean flow. It is clearly the case here, for the wavenumber pair (0,2). The actuation with an energy of low magnitude ($\mathcal{O}(10^{-4})$) act directly on the streamwise vortices, and have thus an effect of order one on the flow energy.
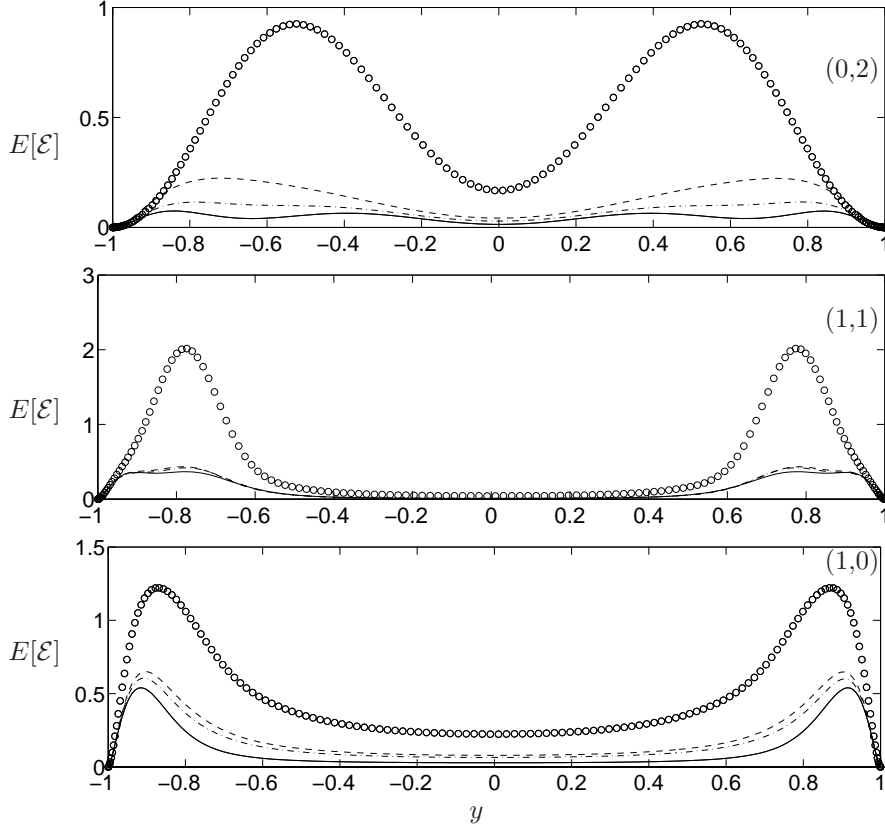
FIGURE 2. Expected energy of the flow perturbation when excited by a stochastic forcing, as a function of the wall normal coordinate for three wavenumber pairs (0,2) (top), (1,1) (middle) and (1,0) (bottom). The flow ($\circ$) is normalised to unit energy. The energy of the flow controlled with full order controller (solid) can be compared to the energy resulting from the reduced controller truncated to 10 modes (dash-dotted), and 5 modes (dashed).

5.2. *Description of the results*

See figure 2 for the variation with the wall normal coordinate of the expected energy for the flow and controlled flow. We use the full order controller as a reference, and show the performance for the controller truncated to 10 and 5 eigenmodes. The flow and controlled flow expected energy is located close to the wall, due to the stronger forcing there, and due to the strong shear.
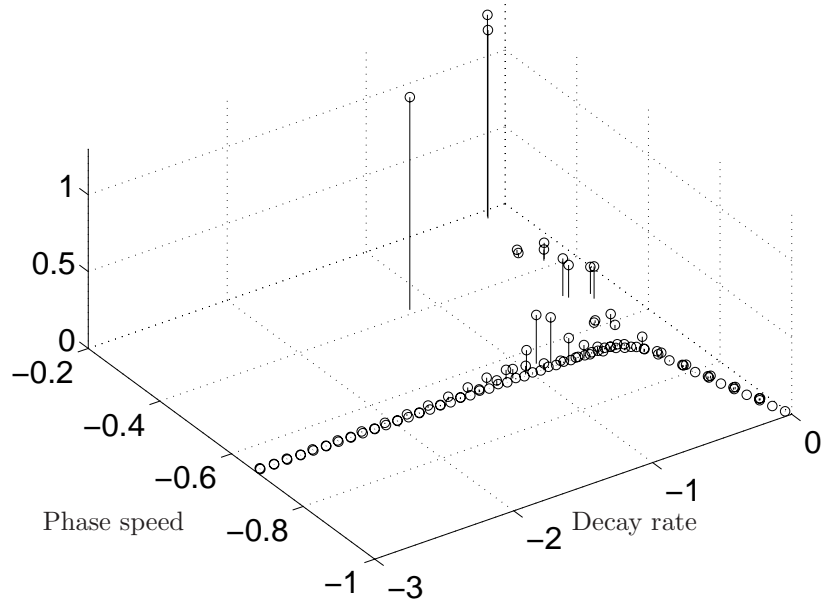
FIGURE 3. The truncation criterion plotted over the spectra of the controller in complex plane. The criterion takes into account observability, controllability and decay rate of the individual eigenmodes. Eigenmodes with a low criterion are discarded first.

5.2.1. *The modal residuals*

The selection of eigenmodes of the controller is done using the modal residuals as a criterion. If only a small number of modes are jointly observable and controllable, the controller can be efficiently truncated. Figure 3 presents the truncation criterion for the wavenumber (1,1) plotted over its spectra in the complex plane. We could not observe clear difference between the truncation criterion for strong and mild controller.

6. Conclusion

Recent research effort shows that many complex flows can be described by low-dimensional representations. Linear system theory provides powerful tools to achieve reduction of linear models. We applied in this paper a modal truncation method on a controller for a channel flow with small disturbances. The controller uses wall shear stress and pressure measurement to estimate the flow state and wall transpiration to affect the growth of the disturbances. To reduce the full order controller, we projected the controller system on the basis of its eigenvectors. This projection could be achieved by use of the biorthogonality between the eigenvectors and adjoint eigenvectors. We then discarded the states corresponding to eigenmodes that are highly damped, poorly controllable and

poorly observable. The performance of the reduction was then assessed against the performance of the full order controller for spatially correlated stochastic forcing, on three individual wavenumber pairs.

The performance of the reduced controller was found to be little affected by the truncation if the controller has moderate strength. Truncating a controller designed with a low control penalty and a low measurement noise lead to rapid loss of performance when truncating, and may even render the system unstable. Indeed there is no guarantee of maintained stability for this controller reduction technique. Nevertheless, if the controller is properly designed, with an efficient actuation and sensing, as well as proper disturbance model and objective function, good performance can be achieved with a mild controller. This controller can in turn be efficiently reduced.

It should be noted that the system that is to be controlled is infinite dimensional. There are thus two successive model reduction techniques performed in this paper. The first one is the projection of the linearised Navier–Stokes equation on Fourier modes and Chebyshev polynomials, and truncation to an affordable computational resolution. The controller optimisation is performed on this discretised version of the system. The second reduction is then the projection of the controller on the basis of its eigenmodes and then truncation. We decided in this work to build an accurate discretised version of the system (where most of the important physical mechanism are included) that we then highly truncate after the optimisation.

This work is a preliminary study of model reduction applied to controller in flow control. A simple truncation criterion and projection basis was used. Numerous techniques are available to perform controller and model reduction in a more systematic way, that should be tried on similar flow cases. It would be interesting to obtain controllers for more general flow cases, for instance flow with curvature, finite amount of sensors and actuators properly located, secondary instability, etc... Appropriate dynamic models for such flow cases may generate unwieldy computational tasks. Properly performed model reduction can thus open a rich domain of application for the standard control technique used in this paper.

References

BEWLEY, T. R. 2001 Flow control: new challenges for a new renaissance. *Progress in Aerospace Sciences* **37**, 21–58.

GLOVER, J. C. D. K., KHARGONEGAR, P. P. & FRANCIS, B. A. 1989 State space solutions to standard $\mathcal{H}_2$ and $\mathcal{H}_\infty$ control problems. *IEEE transactions on automatic control* **34** (8).

GREEN, M. & LIMEBEER, D. J. N. 1995 *Linear robust control*. Prentice Hall.

HŒPFFNER, J., CHEVALIER, M., BEWLEY, T. R. & HENNINGSON, D. S. 2003 State estimation in wall-bounded flow systems. part I : laminar flow. *J. Fluid Mech.* Submitted.

HŒPFFNER, J. & HENNINGSON, D. 2004 Coupling sensor to actuators in flow control. *Internal report* .

HÖGBERG, M., BEWLEY, T. R. & HENNINGSON, D. S. 2003 Linear feedback control and estimation of transition in plane channel flow. *J. Fluid Mech.* **481**, 149–175.

OBINATA, G. & ANDERSON, B. D. 2001 *Model reduction for control system design*. Springer.

SCHMID, P. J. & HENNINGSON, D. S. 2001 *Stability and transition in shear flows*. Springer.

SÖDERSTRÖM, T. 2002 *Discrete-time stochastic systems*. Springer.

WEIDEMAN, J. A. C. & REDDY, S. C. 2000 A MATLAB differentiation matrix suite. *ACM Transaction of Mathematical Software* **26** (4), 465–519.

Paper 4

4

Coupling sensors to actuators in flow control

By J. Hœpffner[1] & D. S. Henningson[1,2]

[1]Department of Mechanics, Royal Institute of Technology, S-100 44, Stockholm, Sweden
[2]The Swedish Defense Research Agency (FOI), SE-172 90, Stockholm, Sweden

Feedback control uses the signals from the sensors to decide the proper reaction toward a control objective. We show that a transfer function representation is a relevant tool for analysis and implementation of the controller for physical systems with spatially distributed sensing and actuating. We found that the transfer function may be unstable even though the closed loop system is stable by construction. We identified the cause of this instability as the dependence of the transfer function input on its output when the control loop is closed. We redefined the input of the transfer function to include this dependence, and studied the properties of the controller through the transfer function representation. The method is exemplified on control of wave packets in a laminar Poiseuille flow.

1. Introduction

In many applications like aeroplane wings, pipes, turbine blades, etc ... growth of small perturbations can lead to transition to turbulence and thus to increase of friction drag. It appears crucial to affect the flow for the engineering application at hand. Control is being increasingly applied to fluid flow as the theories and devices are being developed. A powerful theory for linear feedback control is available and can be applied to flow control, assuming a linear dynamics for the flow (small amplitude disturbances), with a quadratic objective function, and a Gaussian distribution for the disturbances. This method known as LQG or L_2 control (Green & Limebeer (1995)) is used in this paper.

The optimal linear feedback design can be decomposed into two sub-problems. First the flow state is to be estimated from sensor information. This is a stochastic problem where the disturbances affecting the system are described by their covariance over the flow domain. The second part is to apply control in the flow using the state information gathered in the estimation. The separation principle (see e.g. Green & Limebeer (1995)) formally prove that those two problems are decoupled. This leads to great conceptual simplifications when it comes to understand and tune separately the two steps of the controller design. However this decomposition may be an obstacle for a physical understanding of the complete feedback process. Feedback is about the relation between sensors and actuators.

We have a tool to represent this relation between sensors and actuators. The transfer function is a natural representation, and is of common use for linear system, see e.g. Kailath (1980). It can also be used for example to represent the energy response of the systems to excitations (Jovanovìc & Bamieh (2001)) or the controller performance (Bewley & Liu (1998)). In the case of the control of a channel flow, a transfer function can tie information from the wall to actuation at the wall, thus reducing the space in which to study the feedback. Furthermore, this transfer function will have spatial properties that are of physical relevance: localisation of the feedback (which sensors are actually used by a specific actuator), how the convection speed of flow structures affects the relation between sensors and actuators, time scales and spatial scales of this relation.

A common formulation for stability studies in shear flows is the temporal formulation. Assuming a periodic domain in streamwise and spanwise direction, one can look at the temporal evolution of isolated Fourier modes. The control problem is then decoupled in Fourier space. The control nevertheless retains a spatial structure after inverse Fourier transform, as does the flow, which is of significance in transition control. The transfer function give explicit information on the spatio-temporal structure of the controller, which provides a useful tool for analysis.

2. Control and estimation

We recall the LQG control formulation, see e.g. Green & Limebeer (1995). The systems can be written in state space

$$\begin{cases} \dot{q} = Aq + B_1 f + B_2 u \\ y = Cq + g. \end{cases} \tag{1}$$

$$\begin{cases} \dot{\hat{q}} = A\hat{q} + B_2 u - v \\ \hat{y} = C\hat{q}. \end{cases} \tag{2}$$

$$v = L\tilde{y} = L(y - \hat{y}), \quad u = K\hat{q}. \tag{3}$$

In (1), the flow state q follow the evolution due to the linear dynamic operator A, and is affected by disturbances on the form of a stochastic forcing f through the input B_1, and can be controlled by the actuation u through B_2. The measurement vector y is extracted from the state, using the measurement matrix C, and corrupted by the sensor noise g. The estimator is built with analogous form in (2). The estimator state $\hat{q}$ follow the same dynamics as the flow state q and is forced by a feedback v of the measurement through the estimation gain L in (3). The flow and estimator states q and $\hat{q}$ are in turn forced as a feedback u of the estimated state through the control gain K. The optimal feedback gains L and K can be computed independently for each wave number pair by solving two Riccati equations, see e.g. Glover *et al.* (1989).

For the dynamic operator A, we use the linearised Navier–Stokes equations transformed to Fourier space, i.e. the Orr-Sommerfeld/Squire equations.

When dealing with transitional cases, one possible objective is to minimise the kinetic energy of the fluctuation about a laminar mean profile. Hindering the growth of small perturbation thus prevent secondary instabilities and further transition to turbulence. This objective can be expressed in a quadratic norm (Högberg *et al.* (2003)). The second central input to the optimisation concerns the estimation problem, and is the description of the external disturbances to the flow. Indeed the best the knowledge about what can possibly disrupt the system, the more specific the estimator can be, and specificity means good performance (Hœpffner *et al.* (2003)).

The information from the flow is measured at the wall, typical quantities are the two components of the skin friction, and the pressure. They give independent information and each relate to a particular type of flow structure (Bewley & Protas (2003)). The actuation is done by wall transpiration i.e. low amplitude zero-net mass flux blowing and suction through the walls. A small component of wall normal velocity can linearly interact with the mean flow and introduce large energy changes, thus leading to an inexpensive control effort. The purpose of this paper is to introduce a transfer function representation of the feedback in order to be able to analyse how the measurements and the actuation are optimally related.

The introduction of the control and estimation feedbacks (3) in (2) gives the state space compensator

$$\begin{cases} \dot{\hat{q}} = A_0\hat{q} - Ly \quad , \quad A_0 = A + LC + B_2K \\ u = K\hat{q}. \end{cases} \tag{4}$$

which maps the measurement signal y and the actuation signal u.

3. Transfer functions

The inverse Fourier transform of the gains L and K will give convolution kernels in physical space, and those kernels have usually been used as representing the properties of the control process (Högberg & Bewley (2001)). Their localisation is an important physical property. This property was found to be retained despite the decomposition in Fourier modes and the independent optimisation, when the objective function and the noise model are of physical relevance (Bamieh (1997)). But the kernels fail in providing with a global understanding of the action of the controller, that is intrinsically the relation between sensors and actuator at the wall. Furthermore those kernels do not provide information about the time properties of the control, since the time dependency is implicitly handled by the estimator dynamics in (4). In order to describe this we can introduce the transfer function, i.e. the mapping between the sensor signal y and the actuator signal u,

$$u(t) = \int_0^\infty \underbrace{-Ke^{A_0\tau}L}_{G(\tau)}\, y(t-\tau)\mathrm{d}\tau. \tag{5}$$
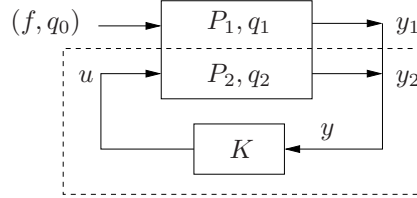
FIGURE 1. Definition of the input of the transfer function

The actuation at time t thus depends on the history of past measurement $y(t - \tau)$ for time lags τ ranging from zero to infinity. The transfer function convolution kernel G is a function of the time lag τ and is composed of the operator A_0 originating from the estimator dynamics, as well as the estimation and control gains L and K. After inverse Fourier transform, this transfer function can be interpreted in two ways. First as a convolution operator (or Green's function) that weights the input from the measurement history for all positive time lags τ and all wall location (x, z) to give the actuation at time t for a single actuator at the wall location (0,0). It can also be seen as the response of the actuators on the entire wall to an impulse at the single sensor location (0,0) at initial time.

The closed loop system is stable by construction, but it appears that the controller itself, with dynamics $A + B_2 K + LC$ is not guaranteed to be stable. This tells us that y in the controller transfer function is not an arbitrary signal, but is dependent on the control. We can thus split the measurement in two parts, one from the disturbance $y_1(f, q_0)$ and one from the effect of the control $y_2(u)$. The transfer function from y_1 to u is stable by construction and represent how the controller reacts to an arbitrary disturbance. See figure 1 and equation (6) how the plant P is split into P_1, whose state q_1 is the uncontrolled disturbance, and P_2 whose state q_2 is the flow created by the control. Let

$$\begin{cases} \begin{pmatrix} \dot{q}_1 \\ \dot{q}_2 \end{pmatrix} = \begin{pmatrix} A & 0 \\ 0 & A \end{pmatrix} \begin{pmatrix} q_1 \\ q_2 \end{pmatrix} + \begin{pmatrix} B_1 f \\ B_2 u \end{pmatrix} \\ \begin{pmatrix} y_1 \\ y_2 \end{pmatrix} = \begin{pmatrix} C & 0 \\ 0 & C \end{pmatrix} \begin{pmatrix} q_1 \\ q_2 \end{pmatrix} + \begin{pmatrix} g \\ 0 \end{pmatrix} \end{cases} \tag{6}$$

$$\begin{cases} \dot{\hat{q}} = A_0 \hat{q} - L(y_1 + y_2) \\ u = K\hat{q}. \end{cases} \tag{7}$$

By linearity $q = q_1 + q_2$ and $y = y_1 + y_2$. The transfer function output u is the optimal control for the given disturbances. The relation between u and y_1 can

be written in state space form, by including the dynamics of q_2 in the controller

$$
\begin{cases}
\begin{pmatrix} \dot{q}_2 \\ \dot{\hat{q}} \end{pmatrix} = \underbrace{\begin{pmatrix} A & B_2 K \\ -LC & A_0 \end{pmatrix}}_{\mathcal{A}_0} \begin{pmatrix} q_2 \\ \hat{q} \end{pmatrix} - \underbrace{\begin{pmatrix} 0 \\ L \end{pmatrix}}_{\mathcal{L}} y_1 \\
u = \underbrace{\begin{pmatrix} 0, K \end{pmatrix}}_{\mathcal{K}} \begin{pmatrix} q_2 \\ \hat{q} \end{pmatrix}
\end{cases}
\tag{8}
$$

The new transfer function that maps y_1 and u can thus be written

$$
u(t) = \int_0^\infty \underbrace{-\mathcal{K}\mathrm{e}^{\mathcal{A}_0 \tau}\mathcal{L}}_{\mathcal{G}(\tau)} \, y_1(t - \tau)\mathrm{d}\tau.
\tag{9}
$$

All the following analysis and plots relate to this modified definition of the input to the transfer function.

4. Controller behaviour and performance

The control procedure described above is now applied to the control of a wave packet. The initial disturbance is taken from Henningson *et al.* (1993) where a series of test is made on the transient growth of localised disturbances. The chosen disturbance would correspond to experimentally induced perturbations caused by the motion of a membrane at the wall. Low amplitude are used here so that nonlinear effect can be disregarded.

See figure 2 for the representation of the transfer function between the streamwise skin friction and the blowing and suction at the lower wall for three time lags $\tau =$1, 20 and 40. For the short time lag, the weighting is mainly on measurement signal closely upstream of the actuator, whereas it is further upstream for longer time lag. Relevant wall information is measured further upstream as the time lag increases, since the disturbances are travelling with the mean flow. For each time lag, the controller uses measurements from only a localised region at the wall.

Figure 3 shows contours of the transfer functions for individuals measurements integrated in the spanwise z (rigth column) and streamwise x (left column) directions. There is a relatively strong weighting of the measurement for short time lag. These measurements are important for the controller. Then, for increasing time lag, measurements upstream are increasingly weighted. The flow structures are convected downstream with the mean flow, so that the controller will use further upstream information for the flow structure as the sensor information is older. In addition, the transfer functions are more elongated in the streamwise direction than in the spanwise direction. Since structures travelling in the cross-flow direction are not prevalent, a sensor do not provide relevant information for an actuator remote in the spanwise direction.

The different measurements give information about different types of flow structures. Mainly the streamwise skin friction tells about streamwise elongated structures. Streamwise elongated vortices create streaks of streamwise
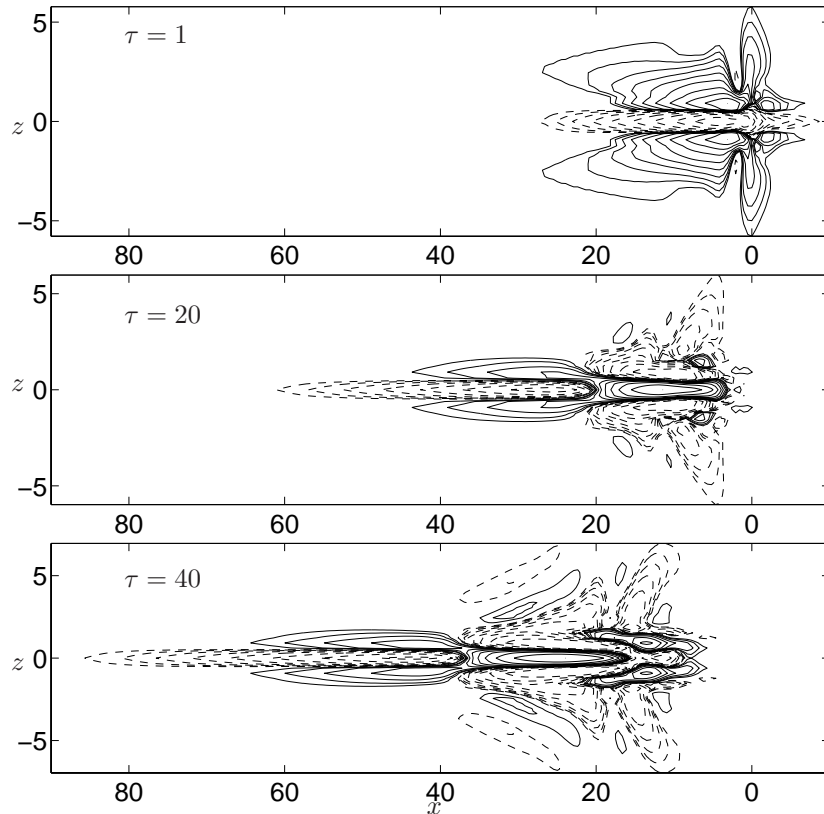
FIGURE 2. Contour for three time lags $\tau =1$ (top), 20 (middle), and 40 (bottom) of the transfer function relating the streamwise skin friction measurement to the actuation at the bottom wall. The contour are logarithmically spaced, for positive (solid) and negative (dashed) values of the transfer function.

velocity, elongated in the streamwise direction, that have a strong footprint of streamwise skin friction at the wall. Those structures are omnipresent, and are an effect of the nonnormality of the dynamic operator. Similarly, the spanwise skin friction measurement tells about structures elongated in the spanwise direction. Such structures are less prevalent in shear flows, so that this measurement do not contribute as much to the controller performance. The pressure measurement do not favour elongated structure, instead is a footprint of structures away from the wall. Indeed, even disturbances with velocity component in the centre of the channel will affect the pressure field close to the walls.

The transfer function for the streamwise skin friction measurement has the particularity that even for short time lag, the actuator uses information from

sensors far upstream, whereas for the two other measurements, the controller uses for short time lags sensor information rather centered around the actuator. We can understand this by the streamwise elongation of the flow structures that this measurement detects. The streamwise skin friction measurement is mostly affected by structures elongated in the streamwise direction. The strong coherence of such structure is prominent over the convection with the mean flow.

On the other hand, the convection effect is prominent for the structures detected by the spanwise skin friction and pressure, that are not necessarily elongated in the streamwise direction (mostly present at wavenumber pairs with nonzero k_x).

Nevertheless, you can see that for the type of disturbances studied, the optimal controller uses sensor information close to the actuator itself (strong weighting of the sensor signal for short time lags and small x). This means that in an optimal setting, the sensors should be located close to the actuators.

Figure 4 shows the control applied to a single initial disturbance. The flow energy initially grows and eventually decays exponentially towards rest. Two curves depict the evolution of the flow when the controller is turned on at initial time and time 20.

The structure of the weighting in space and time of the transfer function can lead to simplification of the final implementation of the controller. For each time lag, the weighting is localised in space, so that only a limited number of sensors are relevant to provide the needed information. As time lag increases, this localised forcing function travels upstream of the actuator so that sensors further upstream should be used. This procedure has a natural extension to spatially developing flows where disturbances are typically generated upstream and convect downstream with the mean flow. The controller designed upon local flow parameters should be applied locally. This localisation is explicitly enforced through the localisation of the weighting function.

5. Conclusion

In this paper, we discussed a transfer function representation for feedback control in a system with spatially distributed sensing and actuation. This formulation recast the reactive control in a global framework where the two steps of control and estimation are re-unified. The transfer function from an arbitrary wall measurement to the actuation was found to be possibly unstable even though the overall closed loop system is stable by construction. The transfer function could still be studied by incorporating the dependency of the measurement on the actuation when the control loop is closed, thus changing the definition for its input. We commented the localisation properties of the transfer function, and how the controller uses wall information from further upstream for increasing time lag, thus naturally accounting for the downstream propagation of disturbances.

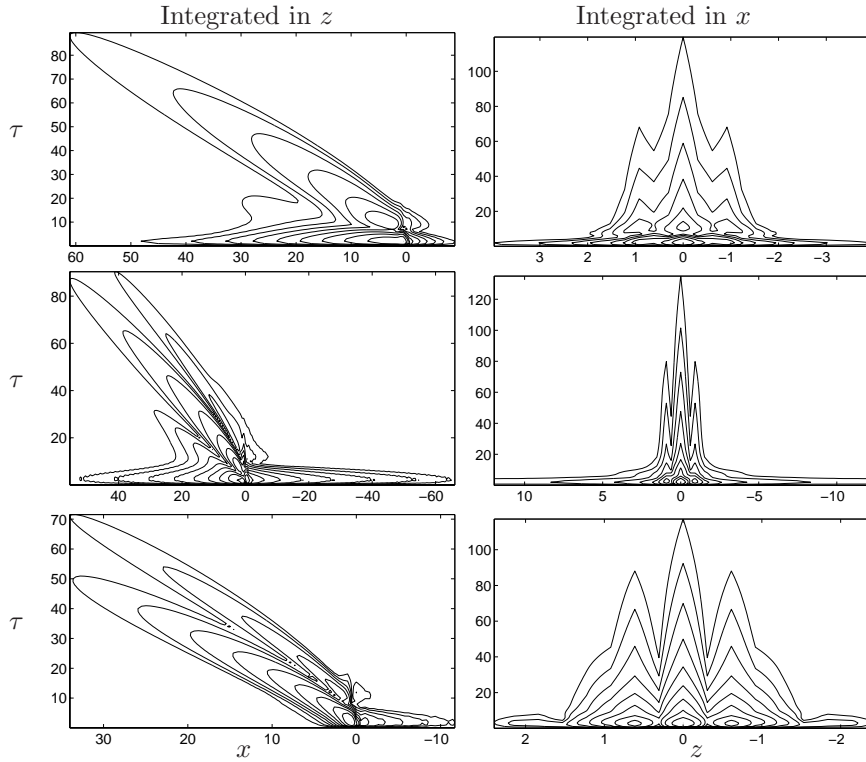Integrated in z Integrated in x

FIGURE 3. The transfer function in time, integrated in the streamwise direction (left column) and spanwise direction (right column) for the three measurement, streamwise skin friction (top), spanwise skin friction (middle) and pressure (bottom).

Further study should be carried in order to enforce the stability of the controller system. The transfer function, once stable, could be used for implementation of the controller in a flow experiment, where the actuation would be obtained as a convolution of the measurement history for a limited number of sensors and actuators.
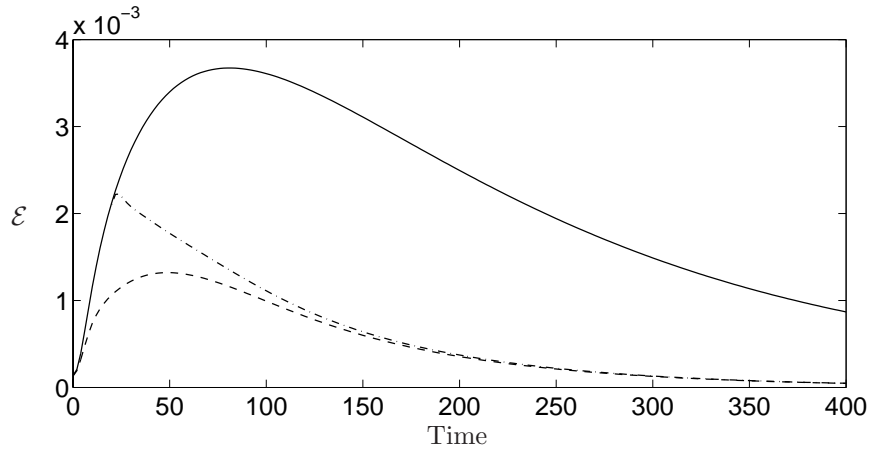
FIGURE 4. Energy evolution of the localised initial condition, without control (solid) and with the controller turned on at initial time (dashed) and time 20 (dash-dotted).

References

BAMIEH, B. 1997 The structure of the optimal controller of spatially invariant ditributed parameter systems. In *Proc. 36th IEEE Conf. on Decision and Control*.

BEWLEY, T. R. & LIU, S. 1998 Optimal and robust control and estimation of linear paths to transition. *J. Fluid Mech.* **365**, 305–349.

BEWLEY, T. R. & PROTAS, B. 2003 Skin friction and pressure: the "footprints" of turbulence. *Physica D* In press.

GLOVER, J. C. D. K., KHARGONEGAR, P. P. & FRANCIS, B. A. 1989 State space solutions to standard $\mathcal{H}_2$ and $\mathcal{H}_\infty$ control problems. *IEEE transactions on automatic control* **34** (8).

GREEN, M. & LIMEBEER, D. J. N. 1995 *Linear robust control*. Prentice Hall.

HENNINGSON, D. S., LUNDBLADH, A. & JOHANSSON, A. V. 1993 A mechanism for bypass transition from localized disturbances in wall-bounded shear flow. *J. Fluid Mech.* **250**, 169–207.

HŒPFFNER, J., CHEVALIER, M., BEWLEY, T. R. & HENNINGSON, D. S. 2003 State estimation in wall-bounded flow systems. part I : laminar flow. *J. Fluid Mech.* Submitted.

HÖGBERG, M. & BEWLEY, T. R. 2001 Spatially-localized convolution kernels for decentralized control and estimation of transition of plane channel flow. *Automatica* Submitted.

HÖGBERG, M., BEWLEY, T. R. & HENNINGSON, D. S. 2003 Linear feedback control and estimation of transition in plane channel flow. *J. Fluid Mech.* **481**, 149–175.

JOVANOVIC̀, M. & BAMIEH, B. 2001 The spatio-temporal impulse response of the linearized Navier–Stokes equations. *Proc. American control conference* .

KAILATH, T. 1980 *Linear systems*. Prentice hall.